Chair of Materials Science and Testing of Polymers

Master's Thesis

Residual stress measurement study on injection molded Polyoxymethylene specimens

Theresia Schrank, BSc

Leoben, February 2019

EIDESSTATTLICHE ERKLÄRUNG

Ich erkläre an Eides statt, dass ich diese Arbeit selbständig verfasst, andere als die angegebenen Quellen und Hilfsmittel nicht benutzt, und mich auch sonst keiner unerlaubten Hilfsmittel bedient habe.

Ich erkläre, dass ich die Richtlinien des Senats der Montanuniversität Leoben zu "Gute wissenschaftliche Praxis" gelesen, verstanden und befolgt habe.

Weiters erkläre ich, dass die elektronische und gedruckte Version der eingereichten wissenschaftlichen Abschlussarbeit formal und inhaltlich identisch sind.

Datum 22.02.2019

Theresia Schrank

Unterschrift Verfasser/in
Theresia, Schrank
Matrikelnummer: 01235194

EIDESSTATTLICHE ERKLÄRUNG

Ich erkläre an Eides statt, dass ich diese Arbeit selbstständig verfasst, andere als die angegebenen Quellen und Hilfsmittel nicht benutzt und mich auch sonst keiner unerlaubter Hilfsmittel bedient habe.

AFFIDAVIT

I declare in lieu of oath, that I wrote this thesis and performed the associated research myself, using only literature cited in this volume.

LEOBEN, February 2019 **(Theresia Schrank)**

ACKNOWLEDGEMENT

The research work of this paper was performed at the Polymer Competence Center Leoben GmbH (PCCL, Austria) within the framework of the “BRIDGE” program of the Federal Ministry for Transport, Innovation and Technology and the Federal Ministry of Digital and Economic Affairs with contributions by Materials Science and Testing of Polymers / Montanuniversitaet Leoben and Department of Industrial Engineering / University of Salerno. The PCCL is funded by the Austrian Government and the State Governments of Styria, Lower Austria and Upper Austria.

My thank goes to my supervisor Dipl.-Ing. Dr.mont. Michael Berer for his guidance throughout this thesis and the time he took for discussions and problem solving even in stressful times.

For the appraisal of this thesis, my thanks go to Univ.-Prof. Dipl. Ing. Dr.mont. Gerald Pinter.

Also, I would like to thank Dipl.-Ing. Dr.mont. Michael Feuchter, who shared his knowledge on X-ray measurements and data evaluation with me and also brought in ideas for further research in this field.

I really want to thank Gerald Meier, who spent a lot of time with me milling the specimens.

A very special thank goes out to my family in particular to my parents for their support throughout the whole studying time.

At last, I want to thank Lukas. His support means everything to me.

ABSTRACT

Polyoxymethylene is an engineering thermoplastic, which can reach a high degree of crystallinity and shows good mechanical properties. These mechanical properties are on the one hand dependent on the polymer's morphology and on the other hand on residual stresses. Residual stresses develop as a consequence of non-uniform cooling conditions and deformations during the processing.

In this thesis, injection molded tensile specimens were examined regarding their residual stress distribution throughout their thickness. These specimens were produced in March 2017 within the framework of a former study. A Design of Experiments was carried out at that time: the holding pressure, the temperature profile along the barrel and the mold temperature were varied. Previously, the specimens were analyzed by tensile tests, fracture tests, differential scanning calorimetry (DSC), microscopy and X-ray diffraction. Now, within this thesis, three different methods for the evaluation of the residual stresses and stress profiles were conducted: layer removal technique (LRT), wide angle X-ray diffraction (WAXD) and nanoindentation. One aim was to obtain residual stress distributions in dependence of the injection molding conditions and to compare them to each other. For this, layer removal technique was chosen, as this method has been widely used in polymer science. Furthermore, basic feasibility studies on WAXD and nanoindentation for their capability in the determination of residual stress profiles were of interest.

With layer removal technique, plausible results regarding residual stress distributions were obtained. Compressive stresses were found in the near surface regions and tensile stresses in the core. The influence of the different processing parameters also met the expectations. Nevertheless, high standard deviations in the near surface stress values were observed, which arose as a consequence of the milling process and the curvature determination at big bending radii. Therefore, no exact statements could be made on this areas. WAXD also gave plausible stress distributions, which were in good accordance with the ones obtained by LRT. However, due to assumptions made on the stress free state and the so-called X-ray elastic constants during stress calculation, no quantitative comparison with other methods could be made. For nanoindentation, two models for the stress calculation based on

literature were used. Samples were not milled as in the two other methods, but the surfaces of the tensile specimens were analyzed. This was conducted along the thickness, width and the cross-section. Neither of the two models led to satisfying results. Geometrical issues as well as rough surfaces made it difficult to conduct valid measurements. In general, LRT is considered to give the best results, but WAXD measurements do also yield potential. Nanoindentation is at the present considered to be not suitable for the residual stress determination of Polyoxymethylene.

KURZFASSUNG

Polyoxymethylene ist ein technischer Thermoplast, der hohe Kristallinitätsgrade erreichen kann und gute mechanische Eigenschaften besitzt. Diese mechanischen Eigenschaften sind sowohl von der Morphologie des Kunststoffs als auch von den Eigenspannungen abhängig. Eigenspannungen entwickeln sich zufolge ungleichmäßiger Abkühlbedingungen und Deformationen meist während des Verarbeitungsprozesses.

In dieser Arbeit wurden spritzgegossene Zugprüfstäbe hinsichtlich ihres Eigenspannungsprofils über die Dicke untersucht. Die Stäbe wurden im März 2017 im Rahmen einer früheren Arbeit hergestellt. Dabei wurde ein Versuchsplan („Design of Experiments“) durchgeführt, bei dem Nachdruck, Temperaturprofil über den Zylinder und die Werkzeugtemperatur variiert wurden. Des Weiteren wurden damals bereits Zugversuche, bruchmechanische Versuche, Differential Scanning Calorimetry (DSC), Mikroskopie und Röntgenmessungen durchgeführt. Im Rahmen dieser Arbeit wurden nun drei unterschiedliche Methoden zur Analyse von Eigenspannungen angewandt: die Layer Removal Technik (LRT), Wide-Angle X-Ray Diffraction (WAXD) und Nanoindentation. Ziel war es einerseits, Eigenspannungsprofile für die unterschiedlichen Verarbeitungsbedingungen zu erhalten und zu vergleichen. Dafür wurde die Layer Removal Technik gewählt, die bereits früher für Polymere angewandt wurde. Des Weiteren sollten WAXD und Nanoindentation auf ihre Anwendbarkeit zur Bestimmung von Spannungsprofilen und -werten überprüft werden.

Mit der Layer Removal Technik wurden durchwegs plausible Eigenspannungsprofile erzielt. Druckspannungen in den äußeren Schichten sowie Zugspannungen im Inneren der Stäbe traten auf. Auch der Einfluss der Verarbeitungsparameter entsprach den Erwartungen. Allerdings konnte aufgrund des Einflusses des Abfräsprozesses und der Bestimmung der Krümmung bei großen Biegeradien keine eindeutige Aussage über Änderungen in den oberflächlichen Schichten getroffen werden. Mit den WAXD-Messungen wurden ebenfalls plausible Spannungsverläufe erhalten. Jedoch mussten bei der Auswertung verschiedene Annahmen bezüglich des spannungsfreien Zustands und der sogenannten elastischen Konstanten getroffen werden, die einen quantitativen Vergleich mit anderen Methoden erschweren. Bei der Nanoindentation wurden zwei unterschiedliche Auswertungsmodelle

aus der Literatur verwendet. Die Proben wurden nicht schichtweise untersucht wie bei den vorhergegangenen Methoden, sondern auf den Oberflächen über die Dicke und die Breite sowie über den Querschnitt der Zugprüfstäbe. Keines der beiden Modelle lieferte zufriedenstellende Resultate. Geometrische Probleme und die Rauigkeit der Oberfläche machten es schwierig, sinnvolle Versuche durchzuführen. Grundsätzlich ist zu sagen, dass die Layer Removal Technik die plausibelsten Ergebnisse lieferte und WAXD-Messungen großes Potential besitzen. Nanoindentation wird in der Form und zum jetzigen Zeitpunkt als ungeeignet angesehen.

TABLE OF CONTENT

SYMBOLS AND ABBREVIATIONS

POM	Polyoxymethylene
DSC	Differential scanning calorimetry
LRT	Layer removal technique
WAXD	Wide angle X-ray diffraction
SAXS	Small angle X-ray scattering
IM	Injection molding
CM	Compression molding
DOE	Design of experiments
PC	Polycarbonate
PVC	Polyvinylchloride
ABS	Acrylonitrile butadiene styrene
PPO	Poly(p-phenylene oxide)
θ	Radial angle in SAXS and WAXD
X	Azimuthal angle in SAXS and WAXD
FCC	Folded chain crystal
ECC	Extended chain crystal

LIST OF FIGURES

1 INTRODUCTION

Polyoxymethylene (POM) is a highly crystalline thermoplastic, which is widely used in engineering applications. Its excellent mechanical properties, amongst others a high fatigue resistance, in combination with its outstanding tribological performance make it interesting especially for machine parts in rolling applications e.g. polymeric bearing elements or gear wheels (Berer and Major 2010, 2012; Rösler 2005; Heym and Beitz 1995). However, for polymeric materials the mechanical behavior strongly depends on the processing history and the resulting morphology. Hence, in the past the fracture mechanical behavior of POM in dependence on its morphology was examined excessively (Berer et al., 2018; Halb, 2016; Berer et al., 2014).

Additionally, processing of polymers by injection molding (IM) also gives rise to residual stresses. These stresses are present without any external loading and, like the polymer morphology, are known to have significant influence on the mechanical behavior. Furthermore, residual stresses are dependent on various processing parameters of the injection molding process. Hence, they are like the morphology highly dependent on the processing conditions. Unfortunately, their quantitative or even qualitative determination is not trivial, since they cannot be measured directly. This rises the need for proper analysis techniques.

This diploma thesis is embedded within the project PENELOPE (Processing, structure and performance evolution of Polyoxymethylene), in which the correlation between processing conditions, resulting morphology and final (fracture) mechanical behavior of POM specimens is systematically investigated. In this context, tensile specimens were produced in the beginning of this project, which were injection molded by following a design of experiments (DOE). The DOE included a variation in holding pressure, melt temperature profile and mold temperature. While mechanical behavior and morphology were analyzed in detail previously, the information about the residual stress levels and distributions was still missing. Hence, the aim of this thesis was to examine different methods for residual stress determination, to compare these techniques and to provide residual stress distributions of selected injection molded specimens. Additionally, the effect of annealing on the residual stresses was selectively studied using this techniques.

As illustrated in Fig. 1.1, three methods were chosen for the residual stress measurements. The first was the layer removal technique (LRT). This method was proposed by (Treuting and Read, 1951) for flat metal plates and has already been used in polymer science. For this reason, it was considered as benchmark method, which was used to quantify the residual stress levels and distributions for all processing conditions. The second method was wide angle X-ray diffraction (WAXD), which can be applied on crystalline and semi-crystalline materials. The last method, nanoindentation, is not yet very common for polymers. For this technique, two different evaluation approaches were analyzed. For both, WAXD and nanoindentation the aim was to conduct basic feasibility studies on their application potential for a residual stress determination in POM.

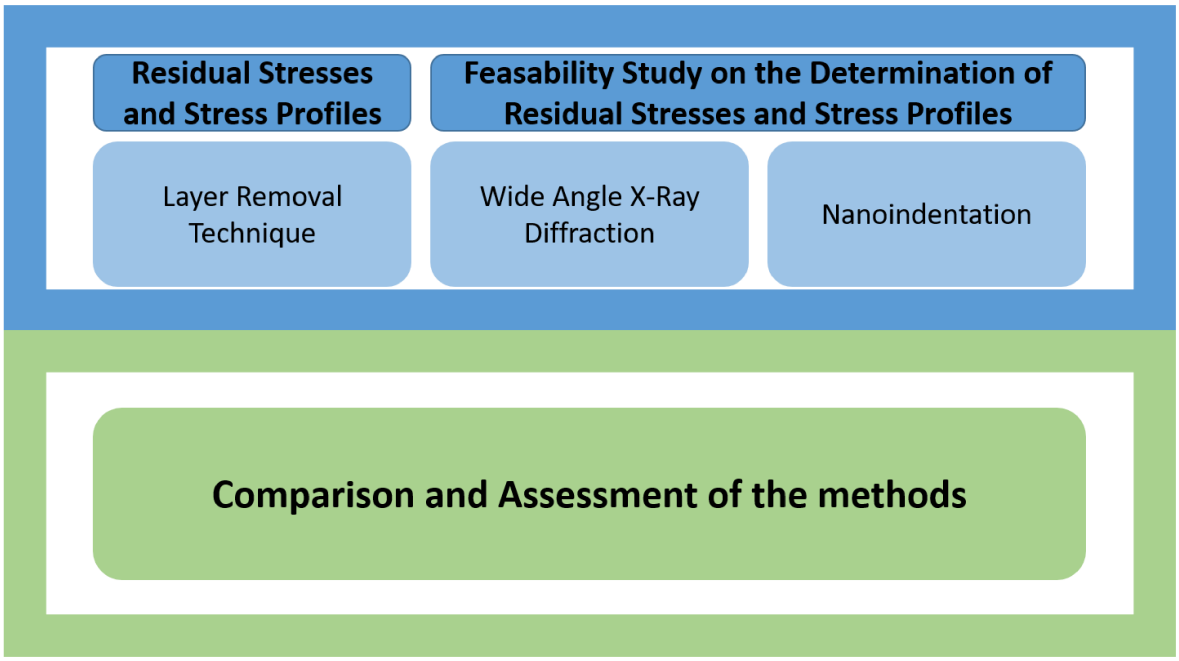

Fig. 1.1: Illustration showing the structure of this thesis.

2 THEORETIC BACKGROUND

2.1 Development of residual stresses

Residual stresses are present in most polymeric parts. These stresses exist independently of an external stress or strain applied to the material and can, depending on their value, lead to premature failure of the part during its application. Therefore, it is important to investigate the distribution of residual stresses in particular in injection molded parts, since within this processing method residual stresses are practically unavoidable. In amorphous and semi-crystalline polymers, these stresses mainly occur due to a combination of large temperature gradients and non-uniform deformation. Especially in semi-crystalline polymers they strongly depend on the crystallization conditions. In injection molding, the outer layers of the part have less time to form crystals as they are cooled very fast. The inner layers are cooled slower due to the low thermal conductivity of polymers. This leads to density differences and therefore, deformation.

In general, residual stresses can be classified as macro or micro residual stresses on the one hand and they can be divided into thermally induced and flow induced residual stresses on the other hand. Residual macro and micro stresses arise from differences between different regions and phases (Withers and Bhadeshia, 2001). Residual macro stresses for example are caused by peening, cold hole expansion, bending and welding, whereas residual micro stresses arise from thermal stresses, loading stresses, transformational stresses and intergranular stresses as shown in Fig. 2.1. Residual macro stresses are present on a scale larger than the grain size. They vary over the thickness of the part and depending on the processing conditions also in plane. They are often referred to as Type I stresses. Residual micro stresses can further be divided into two types regarding to the scale on which they develop. Type II stresses develop in the range of a single grain. In single phase materials they exist due to anisotropy, in multi-phase materials due to different properties of the phases. Type III are stresses present in a single grain as a result of dislocation and crystalline defects (Withers and Bhadeshia, 2001). This is illustrated in Fig. 2.2 for a multi-phase material. M and R in this illustration denote matrix and reinforcement.

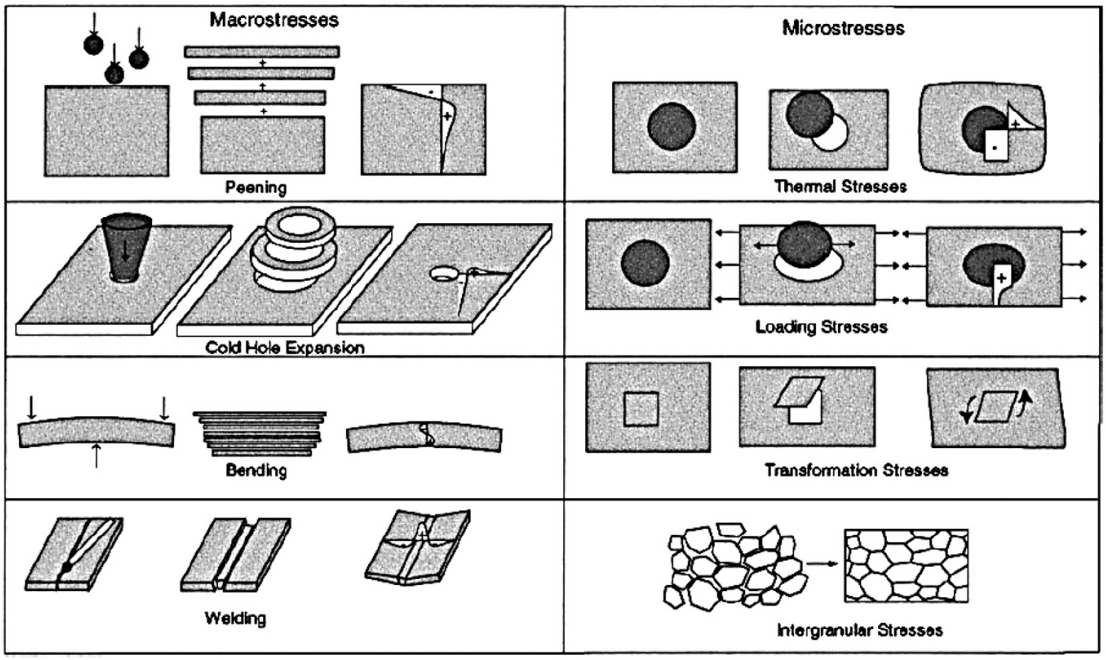

Fig. 2.1: Origins of residual macro and micro stresses (Withers and Bhadeshia, 2001).

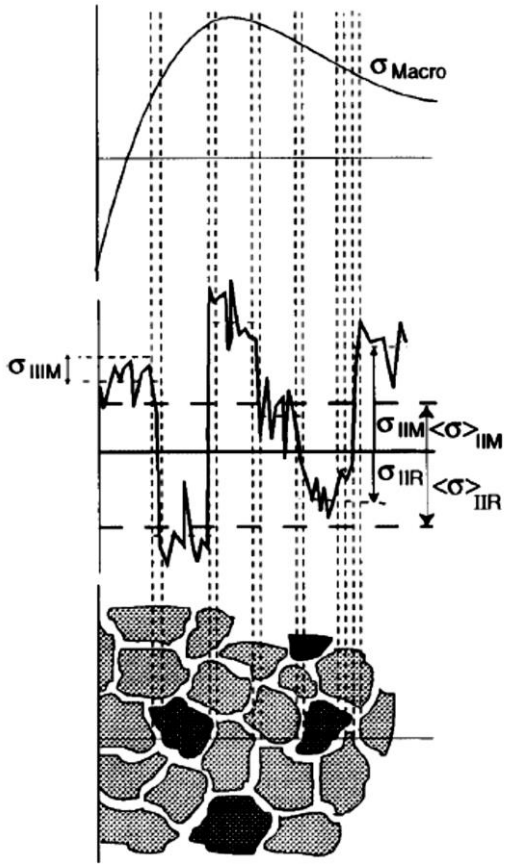

Fig. 2.2: Residual macro and micro stresses on different length scales in a material (Withers and Bhadeshia, 2001).

Flow induced residual stresses result from orientation of the molecules during the filling and holding stage in the injection molding process. Due to high cooling rates, the oriented chains are not allowed to relax and therefore are frozen in the bulk. According to (Guevara-Morales and Figueroa-López, 2014), the stress profile over the cross-section of the part changes during the manufacturing process. During filling, the molecules are oriented in the flow direction especially in the outer layers. With successive cooling the relaxation of these more oriented chains is restrained by the less aligned chains in the inner layers. As a result, tensile stresses develop in the outer and compressive stresses in the inner layers (Fig. 2.3).

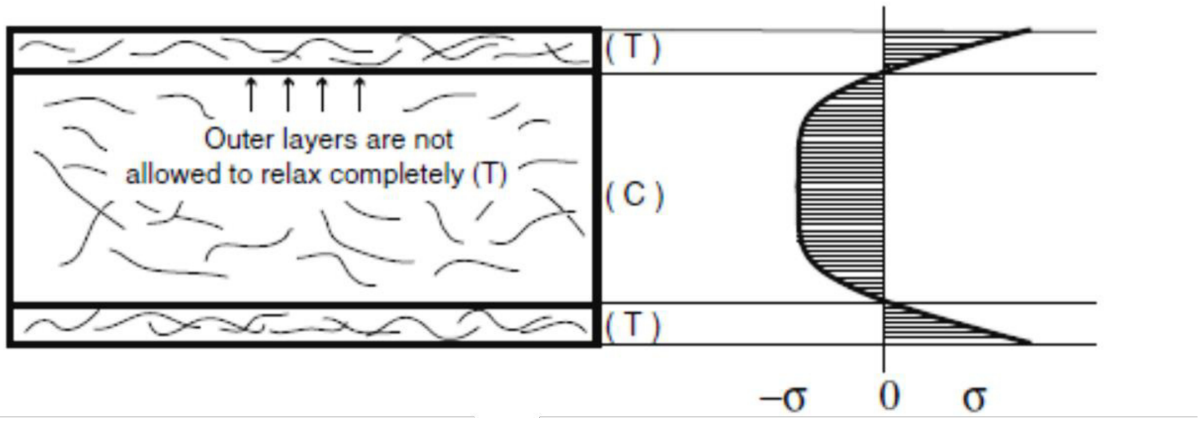

Fig. 2.3: Flow induced residual stress profile developing in the filling stage of the injection molding process (Guevara-Morales and Figueroa-López, 2014).

In the following holding stage the pressure level is supposed to have significant influence on the stress profile. When a rather low holding pressure is applied, the pressure in the core is assumed to reach zero, while the thickness of the skin region is rather small. During further cooling, the volume of the core is reduced due to an increase in density upon crystallization and as a consequence the skin layers are compressed. Tensile stresses in the bulk and compressive stresses in the skin develop (Fig. 2.4). This residual stress profile is also observed, when parts are quenched (although the origin is here, as described below, slightly different). At high holding pressure levels the liquid core is compressed and tension in the skin occurs (Fig. 2.4). When a holding pressure profile is applied, where at first a high pressure level acts on the bulk followed by a lower level, this results in a more complex stress distribution, where a tensile skin is followed by a compressed sub-skin region and a tensile core (Guevara-Morales and Figueroa-López, 2014).

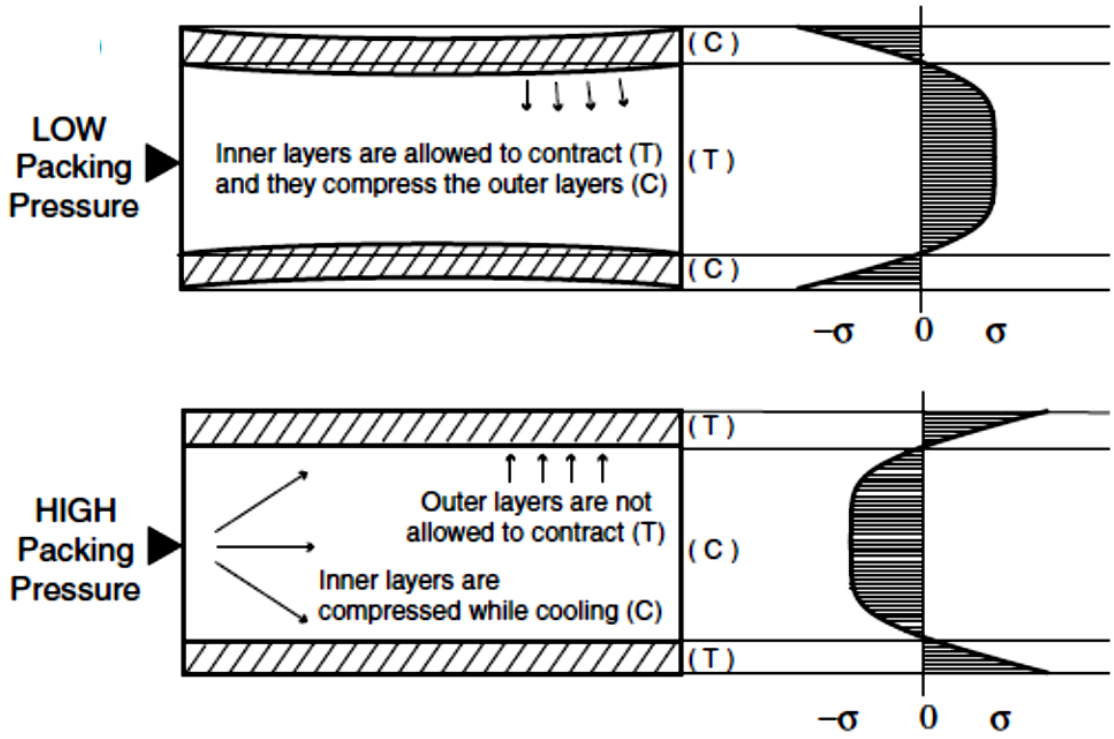

Fig. 2.4: Flow induced residual stress profile developing in the packing stage of the injection molding process – effect of low and high holding pressure (Guevara-Morales and Figueroa-López, 2014).

(Jansen, 2015) molded plates at different holding pressures and observed that at low pressure levels, the plates warped towards the hotter side, whilst when increasing the pressure they observed warpage towards the cooler side. As residual stresses are strongly linked to shrinkage and warpage, this also indicates a significant impact of the applied packing pressure. It has also to be kept in mind that as the pressure usually decreases over the flow path, the stress profile will vary over the length of a part.

Thermally induced residual stresses are a consequence of non-uniform cooling of the material. The outer layers that are in contact with the mold are cooled very quickly, while the core region needs more time to cool and solidify. Here, the skin layers are able to contract freely and are considered to be rather stress free whilst the core is still liquid. During further cooling the contraction of the core is constrained by the solid skin which results in compressive stresses in the skin and tension in the core as observed in free quenching (Guevara-Morales and Figueroa-López, 2014). In the injection molding process the thermally induced residual stress profile depends on various parameters such as the

absolute temperatures, the temperature difference, the holding pressure, the adhesion to the mold, the geometry, the temperature of the mold, the injection pressure and the injection rate. The schematic formation of the residual stress profile for high holding pressure levels is illustrated in detail in Fig. 2.5. At the very beginning of the IM process, the temperature of the material in the mold is considered to be uniform and no pressure is present. According to (Guevara-Morales and Figueroa-López, 2014), at the end of the filling stage small tensile stresses have developed in the skin layers, which are a result of the non-slip condition between the mold and the already solid skin (Fig. 2.5a). In the next step the holding pressure is applied on the melt and also on the solid outer layer. This introduces compression in all layers. Further cooling increases the thickness of the solid layer and also prevents its contraction, which decreases the compression in this region (Fig. 2.5b and Fig. 2.5c). When the gate is frozen, the compressive holding pressure no longer acts on the part (Fig. 2.5d), which reduced the compressive stress level significantly. The IM process is finished and the part is ejected from the compressed mold. An equilibrium with tensile stresses in the skin layers, followed by compressive stresses in a sub skin region and again tensile stresses in the core develop (Fig. 2.5e) (Guevara-Morales and Figueroa-López, 2014).

Many investigations on the influences of different injection molding parameters and conditions on the residual stress profile were made in the past. (Kubat and Rigdahl, 1976) significantly reduced the residual stresses in a part with adding small amounts of metal fillers. The better thermal conductivity resulted in a smaller temperature gradient and therefore in a lower stress level. (Siegmann et al., 1982a) investigated the effect of thermal history on internal stresses. They studied the influence of different temperature gradients relative to the melting temperature of the material. It was found that the residual stresses on the surface were very sensitive to the thermal conditions, while the stresses in the core region were not. In another publication, (Siegmann et al., 1982b) examined the influences of melt temperature, mold temperature, injection rate and injection pressure on the stress profile. They identified an influence of the melt temperature on the profile as well as on the stress level. The mold temperature did not highly affect the surface stresses but the core stresses, whereas the injection rate had a high influence on the surface stresses. Surface stresses were also found to increase with increasing injection pressure up to a

certain point and a decrease afterwards. Stresses in inner layers were only affected by the injection pressure in regions near the gate.

Finally, the resulting residual stress profile of a part is a combination of both flow induced and thermally induced stresses. In general, compressive stresses are expected in the near surface regions, whereas tensile stresses are expected in the core (Siegmann et al., 1981, 1982b; Turnbull et al., 1999).

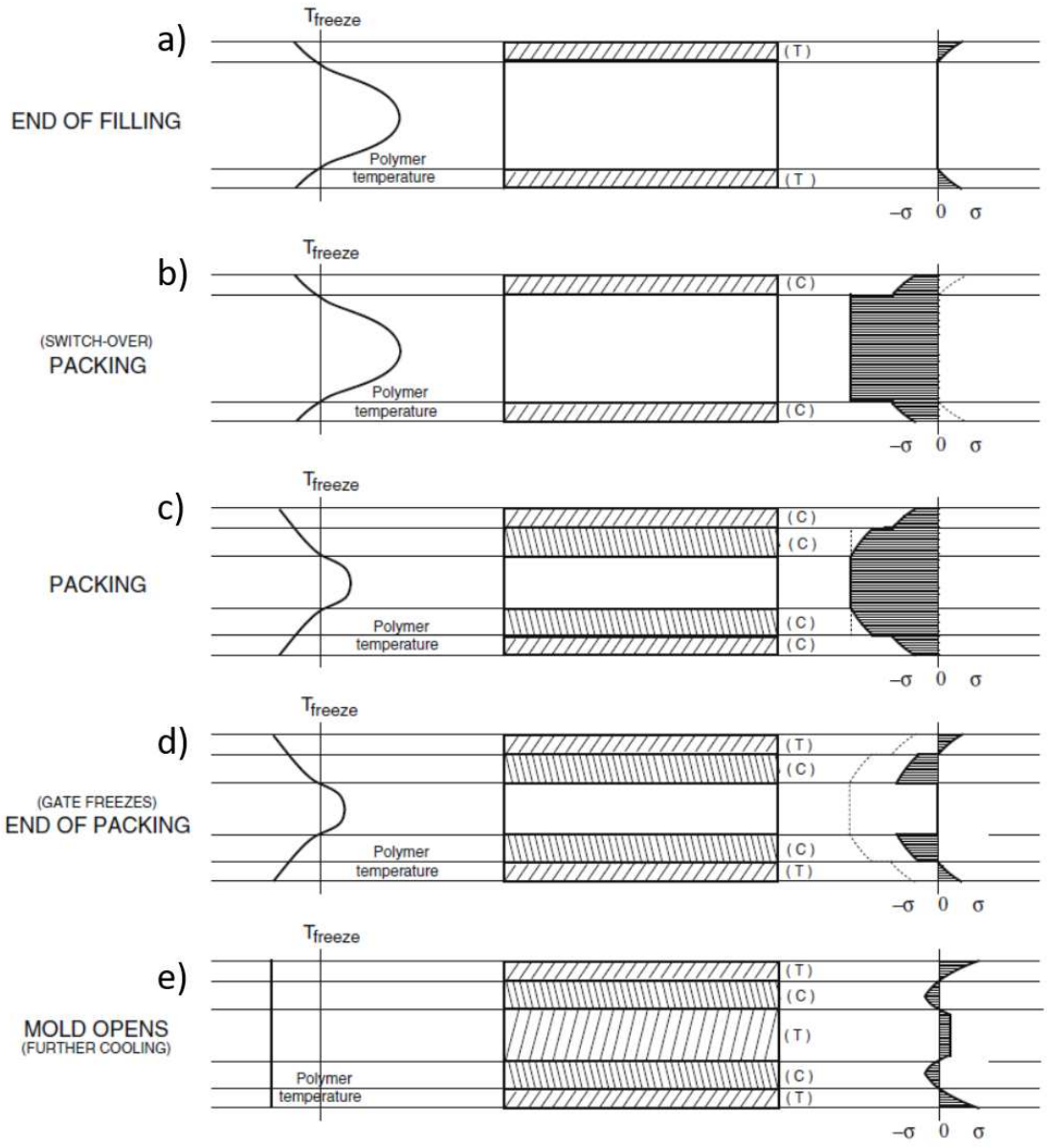

Fig. 2.5: Thermally induced residual stress profiles during different stages of the injection molding process a) in the filling stage, b)-d) in the packing stage and e) after demolding of the part (Guevara-Morales and Figueroa-López, 2014).

2.2 Influence of residual stresses on mechanical properties

Since residual stresses are present in a part without any external load applied, they also influence the performance of the part under loading. The desired behavior of the part can be distorted by shape changes such as warpage, when the residual stress profile is not symmetric over the cross-section of the part. Also mechanical properties are influenced by internal stresses both negative and positive. (So and Broutman, 1976) stated that for Polycarbonate (PC) the notched IZOD impact strength is increased, when compressive stresses are present in the surface. As this was not found for Polyvinylchloride (PVC) and Acrylonitrile butadiene styrene (ABS), it was assumed that this effect is limited to polymers with a highly localized failure initiation. (Chen and Tyler, 2004) found that the photochemical degradation of polymers is accelerated by tensile stresses and retarded by compressive ones. (Siegmann et al., 1981) studied the effect of residual stresses on the mechanical behavior of quenched Poly(p-phenylene oxide) (PPO) specimens. They conducted tensile tests on quenched specimens, whilst successively removing layers. An increase of the ultimate tensile stress, the elastic modulus and of the ultimate elongation was found with successive removal of layers. Furthermore, when investigating injection molded specimens they found that the maximum residual stresses were not located at the surface as for example observed for quenched specimens, but a little below (Fig. 2.6). The tensile modulus of the unmilled injection molded specimen exhibited the same increase with successively removed layers as the quenched samples. The ultimate tensile stress and the ultimate elongation exhibited a minimum at the position of the maximum residual stress.

The changes of residual stresses and crystallinity during the ageing of quenched POM specimens was studied by (Siegmann and Kenig, 1986). They found that upon further ageing the surface crystallinity as well as the surface residual stresses increased. After 120 days, the crystallinity at the surface remained rather constant, while the specimens showed a significant drop of the surface stresses (Fig. 2.7). It was stated that the development of stresses at the surface was caused by secondary crystallization at low temperatures. When surface crystallinity reached its maximum, the residual stresses started to relax.

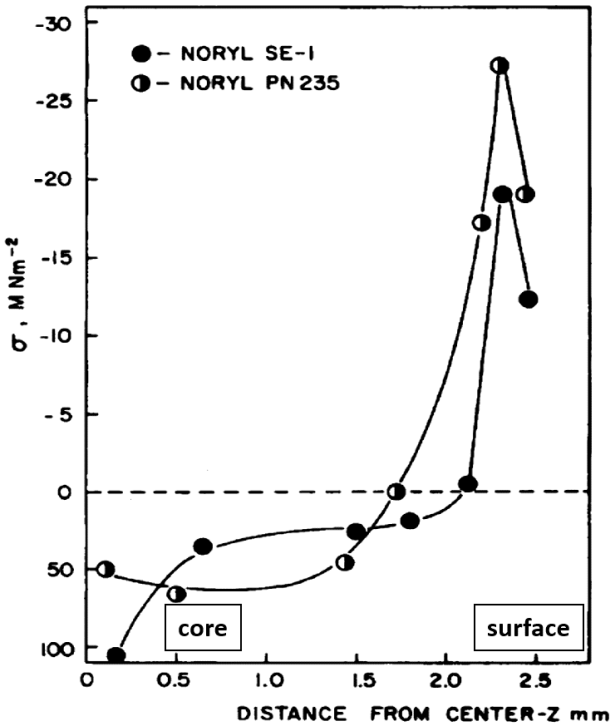

Fig. 2.6: Residual stresses in injection molded Noryl plates (Siegmann et al., 1981).

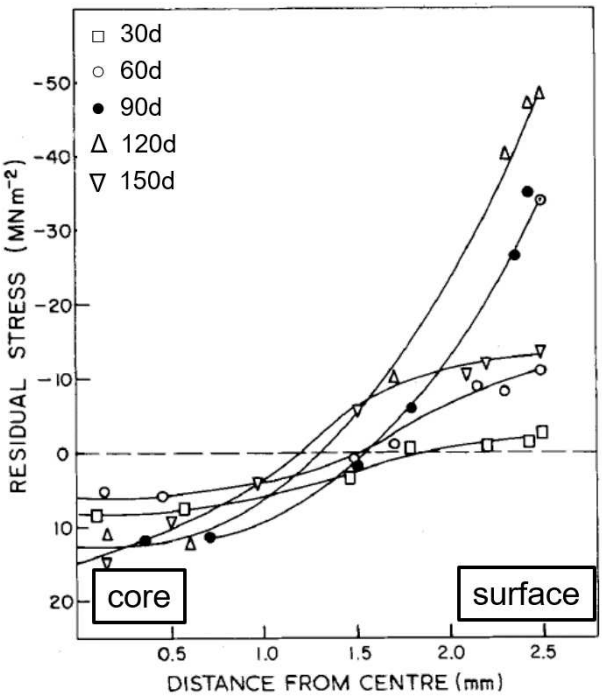

Fig. 2.7: Residual stress distribution of quenched Polyoxymethylene aged for a different period of time (Siegmann and Kenig, 1986).

2.3 Measurement techniques

In general, several methods are available for the analysis of residual stresses and residual stress profiles. In this work, the layer removal technique, wide angle x-ray diffraction and nanoindentation will be used to obtain stress levels and distributions. Layer removal and wide angel X-ray diffraction are methods generally used in polymer science. Nanoindentation is getting more pronounced, since measurements also yield additional information on mechanical properties. In general, macro residual stresses are accessed by these methods, micro and phase residual stresses can be calculated (Hauk and Behnken, 2006). Aside from the three methods that were conducted in this thesis, there are further approaches for the determination of residual stresses described in literature. These include for example the hole-drilling method, the chemical probe technique, neutron diffraction, ultrasonic methods and optical refraction methods (Withers and Bhadeshia, 2001; Kandil et al., 2001; Turnbull et al., 1998). However, these techniques were not part of the residual stress determination in this thesis.

2.3.1 Layer removal technique

This destructive method is based on the successive removal of thin layers from an initially straight specimen. Before a layer is removed, the internal stresses in the sample are equilibrated. When now part of the specimen is removed, this equilibrium no longer exists. Therefore, the sample will bend to reestablish the equilibrium (Fig. 2.8).

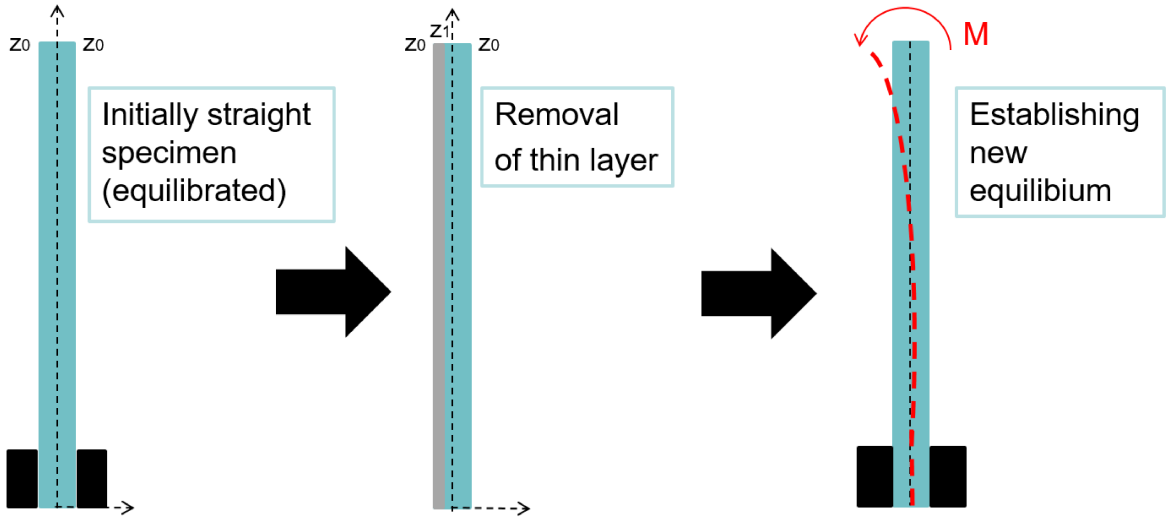

Fig. 2.8: Illustration of the principle of the layer removal technique.

The forces and moments that are necessary to prevent this bending are linked to the residual stresses in the removed plane. In Fig. 2.9 the cross-section of a specimen with residual stresses in x- and y-direction is shown (Treuting and Read, 1951). Here, $\pm z_0$ are the initial distances from the mid plane to the surface and z_1 is the distance from the initial mid plane to the new surface after layer removal. F_x and M_x are the force and the bending moment that are required to prevent deformation of the sample after a layer was removed. When they are not constrained the sample will bend. The residual stresses are now estimated by measuring the curvature of the specimen. They are calculated by Eq. (2.1), which was derived by (Treuting and Read, 1951). The stresses are determined for successively removed layers and a stress profile over the thickness of the sample can be measured in this way.

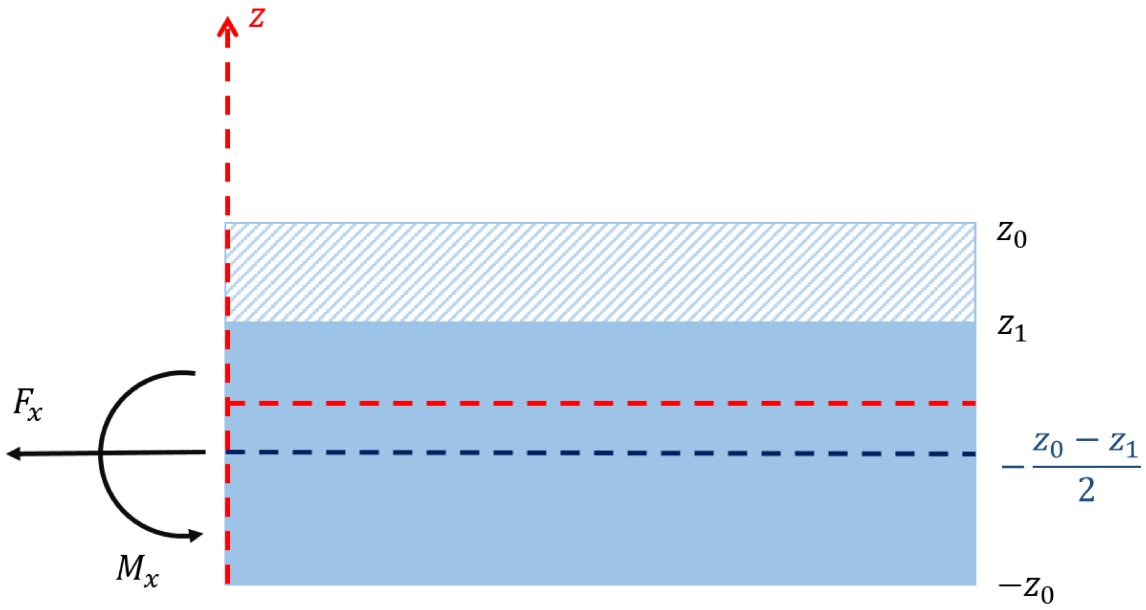

Fig. 2.9: Cross-section of a sample with residual stresses in x-y plane after removal of a layer (Treuting and Read, 1951).

$$\sigma_x(z) = \frac{-E}{6(1-v^2)}\left\{(z_0 - z_1)^2\left[\frac{d\varphi_x(z_1)}{dz_1} + v\frac{d\varphi_y(z_1)}{dz_1}\right]\right. \qquad (2.1)$$
$$\left. + 4(z_0 - z_1)[\varphi_x(z_1) + v\varphi_x(z_1)] - 2\int_{z_1}^{z_0}[\varphi_x(z) + v\varphi_y(z)]dz\right\}$$

In this equation E and v are the elastic modulus and the Poisson's ratio, z_0 and z_1 are the distance between mid-plane and original surface and mid-plane and newly generated

surface as illustrated in Fig. 2.9 and ϕ_x and ϕ_y are the curvatures measured in x and y direction.

To reduce the experimental work, Eq. (2.1) can be simplified for two special cases (Treuting and Read, 1951). For the first one the strain in one direction is considered negligible, which means $\sigma_y = \nu\,\sigma_x$ and $\phi_y = 0$. This assumption results in Eq. (2.2).

$$\sigma_x(z) = \frac{\sigma_y(z)}{v} = \frac{-E}{6(1-v^2)}\left\{(z_0+z_1)^2\frac{d\varphi_x(z_1)}{dz_1} + 4(z_0+z_1)\varphi_x(z_1) - 2\int_{z_1}^{z_0}\varphi_x(z)\,dz\right\} \tag{2.2}$$

In the second case, the stresses are considered to be the same in both direction of the plane. With $\sigma_x = \sigma_y$ and $\phi_x = \phi_y$ the equation can be transformed into Eq. (2.3).

$$\sigma_x(z) = \sigma_y(z) = \frac{-E}{6(1-v)}\left\{(z_0+z_1)^2\frac{d\varphi_x(z_1)}{dz_1} + 4(z_0+z_1)\varphi_x(z_1) - 2\int_{z_1}^{z_0}\varphi_x(z)\,dz\right\} \tag{2.3}$$

According to (Treuting and Read, 1951) the above described calculations are applicable, when three conditions are satisfied: the sample has to behave linear elastic in pure bending, the stresses should be constant in the plane and the removal of the layers must not have an influence on the stress level. Furthermore, the material is assumed to be isotropic in the elastic range and the elastic modulus is assumed to be constant over the thickness.

For the curvature measurement several methods are available, which were examined by (Akay and Ozden, 1994). (Treuting and Read, 1951)and (So and Broutman, 1976) used the dial gauge method, which is often applied for metals, but may cause errors when used for polymers (Akay and Ozden, 1994). An optical method that derives the curvature from a laser beam, which is reflected by mirrors attached to the specimen was used by (Haworth et al., 1982) and (White, 1984). This method was found to result in high experimental work to obtain proper results (Akay and Ozden, 1994). (Akay and Ozden, 1994) also proposed three set-ups for measuring the curvature with a coordinate machine, which is, as almost all described methods, based on the contact between the specimen and a measuring

device. The laser beam scan method, which does not require contact with the specimen was found to be the most accurate curvature measurement method. In general, the stress calculation based on the bending curvature assumes constant elastic properties in the different layers, which is not necessarily the case as for example reported by (Siegmann et al., 1981). Therefore, they conducted measurements, where the bending moment needed to straighten a curved specimens was used to calculate the stresses. The results were found to differ from the ones obtained by curvature measurement. This was believed to be due to the consideration of a non-constant Young's modulus.

The time between the layer removal process and the commencement of the measurements as well as the time, which is given to establish a new equilibrium has to be considered in the analysis. (Turnbull et al., 1998) stated that the time between milling and the beginning of the measurements should be less than 15 min. For the determination of the curvature, no specific elapsed time is given in the literature. (Siegmann et al., 1982a) chose an elapsed time of five days for the determination of the curvature of quenched Poly (p-phenylene oxide). The same time frame was chosen in (Siegmann and Kenig, 1986) for a residual stress study on quenched POM using the layer removal technique.

2.3.2 X-Ray diffraction

X-ray measurements are widely used in polymer science to determine morphological parameters such as long period, lamellar thickness, crystalline structures and crystalline content in a specimen. A coherent X-ray beam is scattered and diffracted by the structure of the sample, which gives rise to characteristic scattering and diffraction patterns. Depending on the sample to detector distance, different deflection angles can be detected, which yield information on different structural dimensions. At larger distances, small angle X-ray scattering is conducted. Here, long period and lamellar thicknesses can be derived from the electron density differences of different phases. For the specimens used in this study, the corresponding measurements were already made previously and hence, are not part of the present work.

For residual stress measurements, wide angle X-ray diffraction can be used, which requires a shorter sample to detector distance. X-ray diffraction is based on the wave nature of light. When a coherent beam meets a crystal, part of it can pass through but part of it is reflected

by different lattice planes (Fig. 2.10). This results in a path difference of the X-rays, which are reflected at parallel lattice planes and as a consequence negative or positive interference occurs. This interference pattern is then detected at the WAXD detector. Positive interference can only occur, when the wavelength is an integral multiple of the path difference δ (Alexander, 1971). This is described by the so-called Bragg's law (Eq. (2.4)). Information on the crystal lattices and the unit cells in the material can be obtained by WAXD. It is usually applied to metals and ceramics, as this materials show clear lattice structures, but it can be also used to examine semi crystalline polymers.

$$n * \lambda = 2 * d * \sin(\theta) \qquad (2.4)$$

Here n is the interference order, λ is the wavelength of the incident beam, d is the distance between the parallel lattice planes and θ is the angle of incidence.

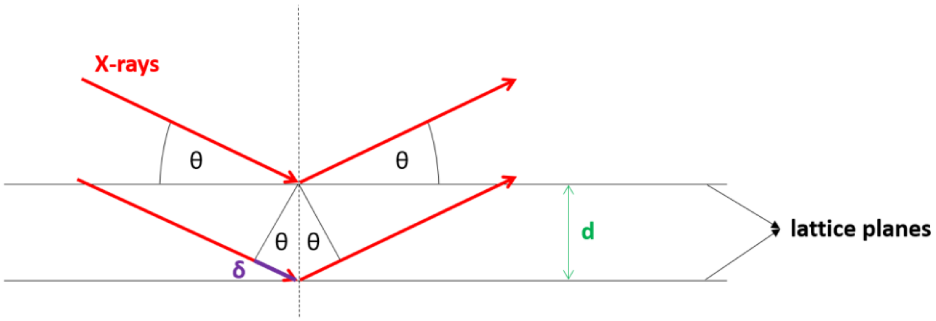

Fig. 2.10: Diffraction of X-rays on parallel lattice planes.

With this method, stresses in a specimen can be determined by measuring the strain distributions of the lattices (Cullity and Stock, 2001). First, a stress free sample has to be analyzed to obtain the position of the diffraction peaks of the different crystal planes in the unstressed state (radially integrated diffraction pattern). When measuring a specimen, which contains stresses, a shift of the peaks on the 2-θ scale can be observed. A shift towards smaller angles is associated with tensile stresses, a shift towards higher angles with compressive stresses (Fig. 2.11).

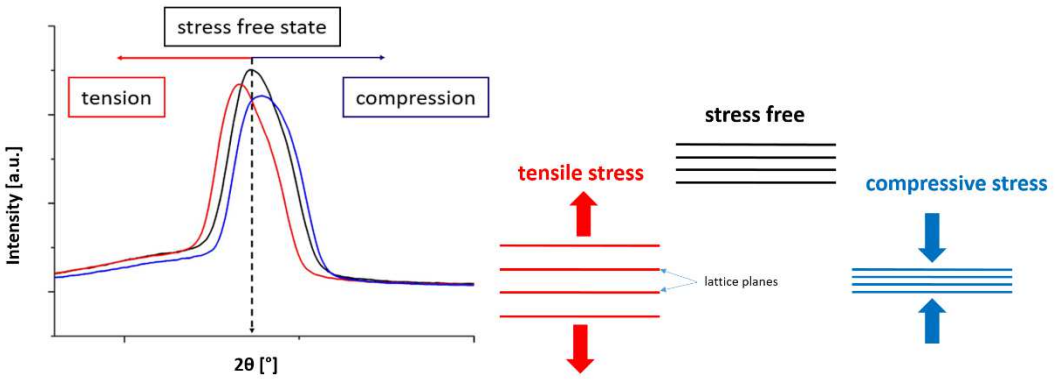

Fig. 2.11: Effect of stresses on the peak position in the intensity profiles obtained from WAXD.

These peak positions and the d-spacing between the parallel lattice planes are linked by Bragg's law according to (Eq. (2.5)). The d-spacing of the stressed specimens is then used along with that of the unstressed state (d_0) to calculate the strains between these planes (Eq. (2.6)), from which stresses can be deduced (Eq. (2.7)). E_{hkl} in the latter equation denotes an elastic constant, which is specific for each group of lattice planes. This value can be determined for example by X-ray measurements during tensile tests as done by (Feuchter 2011).

$$d_{hkl}(X) = \frac{\lambda}{2 * \sin(\theta)} \tag{2.5}$$

$$\varepsilon_{hkl}(X) = \frac{d_{hkl}(X) - d_0}{d_0} \tag{2.6}$$

$$\sigma_{hkl}(X) = \varepsilon_{hkl}(X) * E_{hkl} \tag{2.7}$$

There are also other approaches proposed in literature to determine stresses by WAXD. The "sin²Ψ-method", where mainly line detectors are used requires at least two measurements at different sample orientations to calculate the stress state in the plane (Noyan and Cohen, 1987). The "cosα-method" was developed by (Taira et al., 1978) and enables stress determination from 2-dimensional measurements. Nevertheless, both approaches require the measurement of a specimen at different rotation angles, which yields high experimental effort.

2.3.3 Nanoindentation

The use of nanoindentation to examine mechanical properties such as Young's Modulus, yield strength, hardness, creep stress exponent, fracture toughness and others is rising. It is possible to determine a variety of properties from the load-depth curves without the need to analyze the hardness impression under a microscope (Jang, 2009). When it comes to stresses, it was observed that hardness changes when a load is applied. (Sine and Carlson, 1952) conducted hardness tests on steel, which was loaded alternatingly with compressive and tensile stresses. They found that the material appeared softer when tensile stresses were present and harder, when compressive stresses were present. It was observed that the relationship between the change in hardness and the applied stress was not linear over the whole compressive and tensile regions (Fig. 2.12): hardness is less affected by compressive than by tensile stresses.

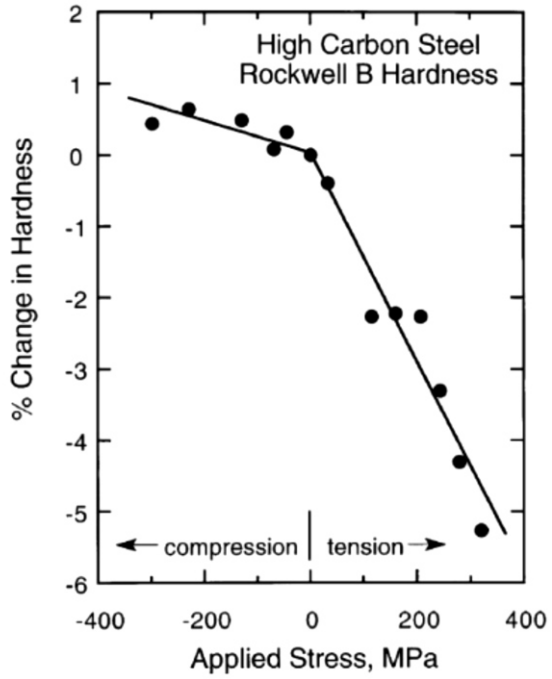

Fig. 2.12: Relative change in the hardness of steel in relation to the applied stress in steel (Sine and Carlson, 1952).

(Bolshakov et al., 1996) found that the loading curve in instrumented indentation of a stressed specimen deviates from the shape of the curve of an unstressed specimen (Fig. 2.13). When compressive stresses are present in the indentation area, a higher force is

needed to indent to the same depth as in a stress free sample. When tensile stresses are present, less force is required. This led to further investigation on the determination of residual stresses. It was found that parameters obtained from the instrumented indentation curves are dependent on the presence of stresses. The hardness obtained by the method proposed by (Oliver and Pharr, 1992), where hardness is derived from a tangent to the unloading curve, for example depends on the stress state. Furthermore, the contact area that is developing between the indenter tip and the sample is dependent on the stress level. Different models were developed for the determination of stresses from instrumented indentation curves. Two of them will be presented in the following. It has to be mentioned, that this models were developed for metals, so the viscoelastic behavior of polymers is not taken into account.

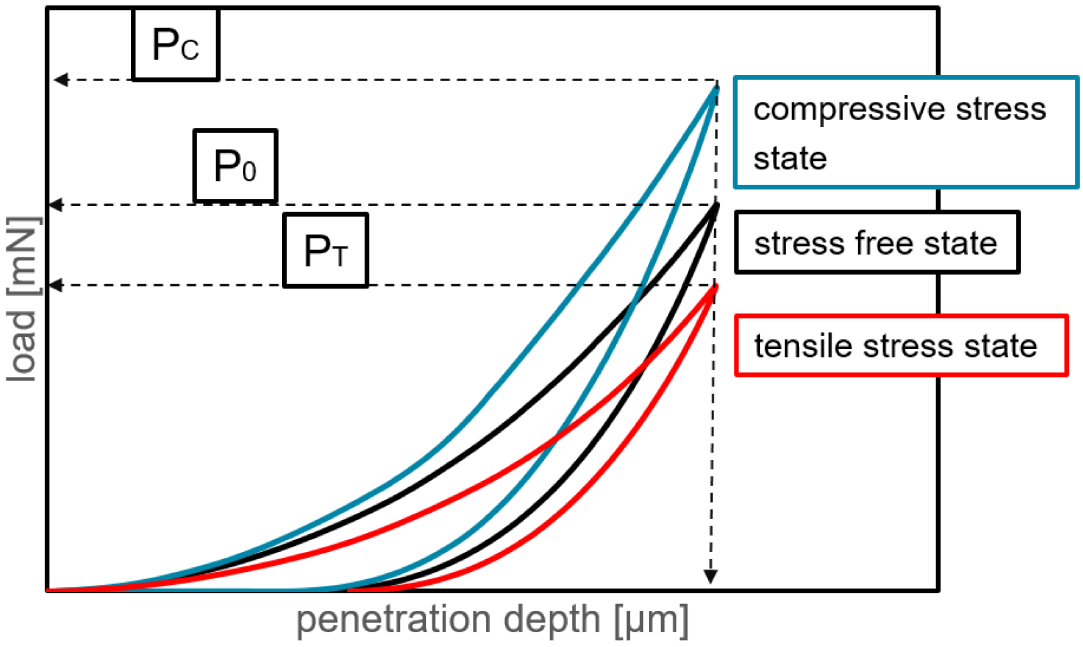

Fig. 2.13: Effect of applied stresses on instrumented indentations curves.

Suresh model

The model by (Suresh and Giannakopoulos, 1998) is based on the assumptions that an equi-biaxial stress is uniform over the indentation depth and an equi-biaxial stress state can be divided into a hydrostatic and uniaxial component. As mentioned above, the presence of

residual stresses affects the indentation contact area. The Suresh model determines the stresses as a function of the ratio between the contact areas of unstressed and stressed sample and the hardness. Furthermore, they took into account the different relationship between hardness change and stress increase for compression and tension as shown before in Fig. 2.12. Therefore, they suggested two equations: with Eq. (2.8) tensile residual stresses can be calculated and Eq. (2.9) is used for compressive residual stresses. Which equation should be used depends on the stress state expected (tensile or compressive) and can be deduced from load-depth curves as shown above in Fig. 2.13.

$$\sigma_{R,t} = \left(1 - \frac{A_0}{A_R}\right) * H \tag{2.8}$$

$$\sigma_{R,c} = \left(\frac{A_0}{A_R} - 1\right) * \frac{H}{\sin(\alpha)} \tag{2.9}$$

In this equations σ_R is the residual stress (tensile or compressive), A_0 and A_R are the contact areas without and with residual stresses, H is the indentation hardness and α is the inclination of the indenter to the surface.

(Jang, 2009) stated that as the contact area is not strongly influenced by the stresses, this model may only be valid when stresses near the yield strength are present and when so-called pile-up is pronounced. Moreover, for quantitatively accurate stress values, the presence of the previously mentioned equi-biaxial stress state is required.

Lee model

(Lee and Kwon, 2004) suggested a model for the determination of non equi-biaxial surface stresses. They introduced a stress ratio $k=\sigma_{R,y}/\sigma_{R,x}$ and applied uniaxial stress (k=0), equi-biaxial stress (k=1), biaxial stress (k=0,66) and pure shear stress (k=-1). As biaxial stress can be divided into equi-biaxial and pure shear stress, where the shear stress does not influence the indentation load, they stated that biaxial stress can be measured simplified as equi-biaxial and calculated by Eq. (2.10).

$$\sigma_{R,x} = \frac{3(P_0 - P_R)}{(1+k)A_R} \tag{2.10}$$

P_0 and P_R are the maximum indentation loads for an unstressed and a stressed specimen and A_R is the contact area of a specimen with residual stresses.

Unlike the Suresh model, the Lee model does not take into account the non-linear relationship shown earlier in this section (Fig. 2.12). The advantage is that non equi-biaxial stress states are considered in the formula.

3 EXPERIMENTAL DETAILS

3.1 Materials, processing and sample preparation

For the measurements, a POM homopolymer of the type Delrin 111PF manufactured by DuPont (E. I. du Pont de Nemours and Company, Wilmington, United States) was used. This resin has an approximate weight average molecular weight of 149.000 g/mol and a polydispersity index of around 2,6. Both values were obtained by gel permeation chromatography and published in (Berer et al., 2018).

Within the project PENELOPE, tensile specimens were injection molded from this material. Both their morphology and their mechanical properties were already examined previously. However, for a complete characterization, the residual stress distributions were still missing. Hence, these specimens were analyzed for their residual stresses in this thesis. Additionally, compression molded (CM) plates and annealed specimens were examined as reference samples. The processing of the IM and CM samples is displayed in the following. Subsequently, the sample preparation for each method is described.

3.1.1 Injection molded tensile specimens

The injection molded tensile specimens made of Delrin 111PF were the main samples used in this thesis. They were analyzed for their residual stress levels and distributions. During processing, the tensile specimens were injection molded with eight different conditions in a mold with two cavities. A design of experiments (DOE) was carried out to study the influence of the processing parameters holding pressure, melt temperature profile and mold temperature on the morphology and the mechanical properties of the samples. The DOE is displayed in Table 3.1. T_P refers to the temperature profile of the band heaters along the barrel of the injection unit. The explanation for the terminus “-1” and “+1” is given in Fig. 3.1. Before injection molding, the material was dried for 2 h at 80 °C in a granulate dryer.

Table 3.1: DOE for injection molding of the tensile specimens (p_{hold} is the holding pressure, T_P the temperature profile along the injection unit and T_{mold} the mold temperature.

Processing Condition	p_{hold} [MPa]	T_P	T_{mold} [°C]
C1	60	-1	50
C2	110	-1	50
C3	60	+1	50
C4	110	+1	50
C5	60	-1	110
C6	110	-1	110
C7	60	+1	110
C8	110	+1	110

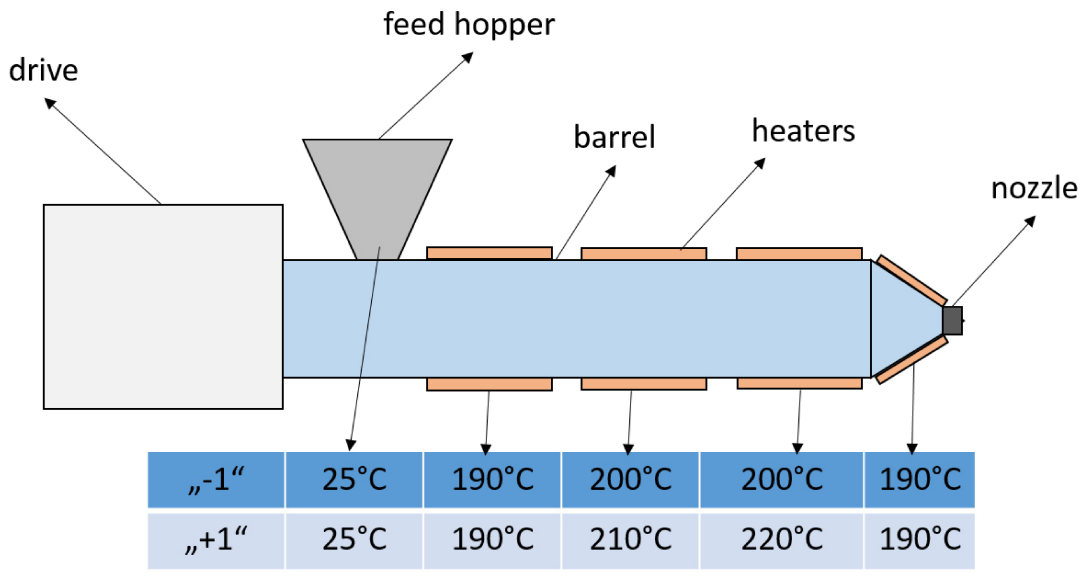

Fig. 3.1: Temperature profiles "-1" and "+1" along the barrel of the injection molding unit.

The values of the processing parameters taken from the injection molding machine are displayed in Table 3.2. Cycle time and filling time were the same for all conditions. It has to be noted that for condition 8, the dosing volume was change from 62 cm^3 to 50 cm^3 due to

the rather high value of cushion. The processing of the tensile specimens was not part of the present thesis. It was carried out by Bruno Ramoa (former researcher at the Polymer Competence Center Leoben) in March 2017.

Table 3.2: Processing parameters measured during injection molding of the tensile specimens.

	$p_{hold,\ measured}$ [MPa]	$T_{mold,\ measured}$ [°C]	Injection pressure [MPa]	melt cushion [cm³]
C1	60,4	46,3	138,9	11,9
C2	110,6	-	140,2	6,7
C3	60,5	-	126,3	11,7
C4	111,0	-	126,8	7,2
C5	60,6	-	128,0	12,5
C6	111,1	-	129,2	8,1
C7	60,6	-	116,1	11,3
C8	111,5	97,1	116,4	15,4
	Cycle time [s]	**Filling time [s]**	**Flow rate [cm³/s]**	**Dosing volume [cm³]**
all conditions	52,7	2,7	15	62 (50)

3.1.2 Compression molded specimens

Compression molded specimens were included in this thesis, because they were originally intended as “stress free” reference samples for the WAXD and nanoindentation measurements. Moreover, they were also part of the annealing study conducted in this thesis (for details please refere to the following section). Compression molded plates of Delrin 111PF were processed within the diploma thesis of Marita Halb (Halb, 2016) and used in this thesis. Their characterization of morphological and fracture mechanical properties is documented in the corresponding diploma thesis and published in (Berer et

al., 2018). Table 3.3 gives the most important processing parameters for the plate used in this work, for further details please refere to (Halb, 2016; Berer et al., 2018).

Table 3.3: Processing parameters for the compression molded plate used in this study (150x150x4mm) referring to (Halb, 2016).

	Temperature [°C]	**Pressure [bar]**	**Time [min]**
Heating	210	1	16
Compression	210	100	15
Cooling	30	100	18

One single compression molded plate was used for all analysis techniques. From this CM plate, the samples needed for the LRT, WAXD and nanoindentation were cut with a circular saw according to Fig. 3.2. During the cutting, the plate was cooled with water mist to avoid changes in the material due to heat development. No bars were taken from the very edges of the plate. For LRT, four bars with a geometry of 150x10x4 mm were cut following the procedure described above. These dimensions were selected to create samples with a similar geometry to the IM tensile specimens (denomination P1-P4 in the following). The same specimens were also used for the WAXD measurements on CM samples. The samples termed N1-N4 in Fig. 3.2 were used for nanoindentation.

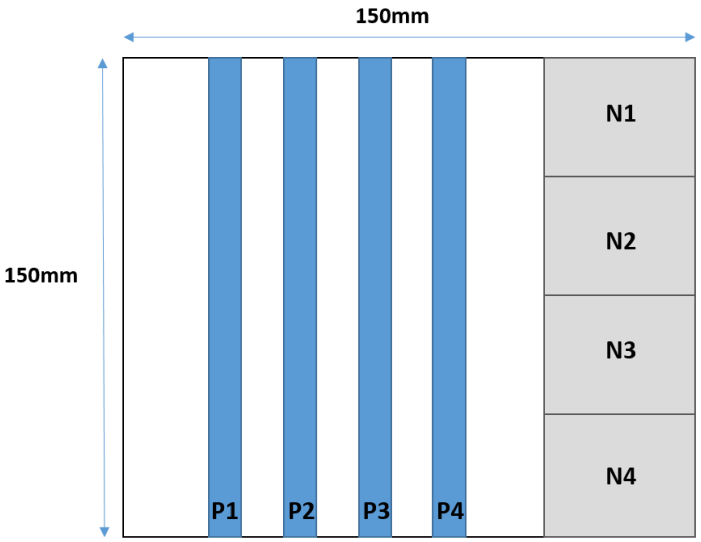

Fig. 3.2: Illustration of sample preparation from the compression molded plate for LRT and WAXD (P1-P4) and nanoindentation (N1-N4).

3.1.3 Annealing procedure

As mentioned in section 2.3, the determination of residual stresses via WAXD and indentation requires a reference sample that is free of stress. Since all IM specimens were considered to contain a significant level of inner stresses, it was tried to release these stresses by thermal treatment. Three different annealing conditions were chosen based on (DuPont 2019). There, 30 min plus 5 min per mm of wall thickness at 160 °C are suggested to accelerate stress relaxation and 24 h at 90 °C are suggested to stabilize parts for continuous high temperature use. With a thickness of 4 mm for all tensile test specimens and the CM specimens a time of 50 min at 160 °C was chosen for stress relaxation. In addition, other samples were annealed at 160 °C for 2 h and at 90 °C for 24 h. Tensile specimens processed with condition 2 from the injection cavity 2 and the compression molded specimens P1-P3 (Fig. 3.2) were annealed. An overview of the combination of specimens and annealing conditions is given in Table 3.4. The CM specimen P4 was not annealed.

Table 3.4: Overview of the annealed injection and compression molded specimens.

Annealing condition [time/temperature]	**Injection molded specimens [condition/cavity]**	**Compression molded specimens**
50 min/160 °C	C2/2	P1
2 h/160 °C	C2/2	P2
24 h/90 °C	C2/2	P3

3.1.4 Sample preparation for nanoindentation

For nanoindentation, a very specific sample geometry was required. In addition, a very parallel and smooth surface was needed to conduct reproducible measurements. Three tensile specimens of processing condition 2 and from injection cavity 2 were cut according to Fig. 3.3 by a circular saw. Two samples were examined at the original, injection molded surface: one along the 4 mm of thickness and one along the 10 mm of width. The details of

the procedure used here will be described later in section 4.3 (Fig. 3.14). The third sample was examined over the cross-section. For this, it was cut with a microtome (Reichert Jung, Heidelberg, Germany) from both sides to obtain a sample with a smooth and parallel surface and a height of 10 mm (Fig. 3.4).

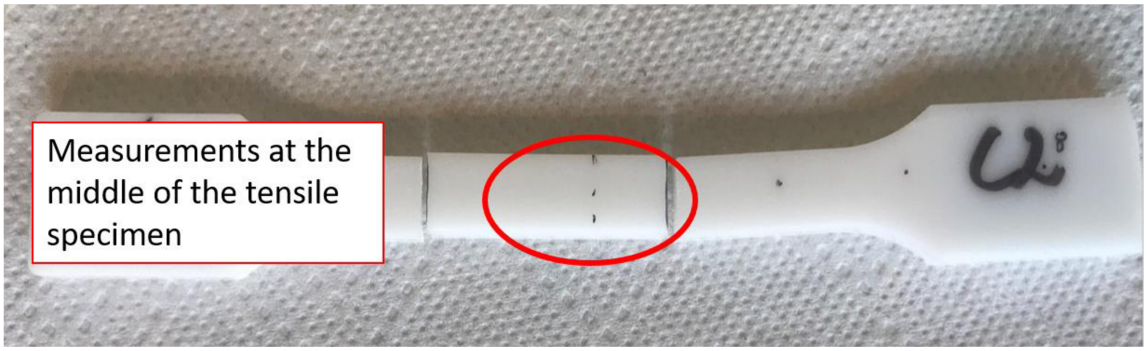

Fig. 3.3: Illustration of the sample positioning for the nanoindentation.

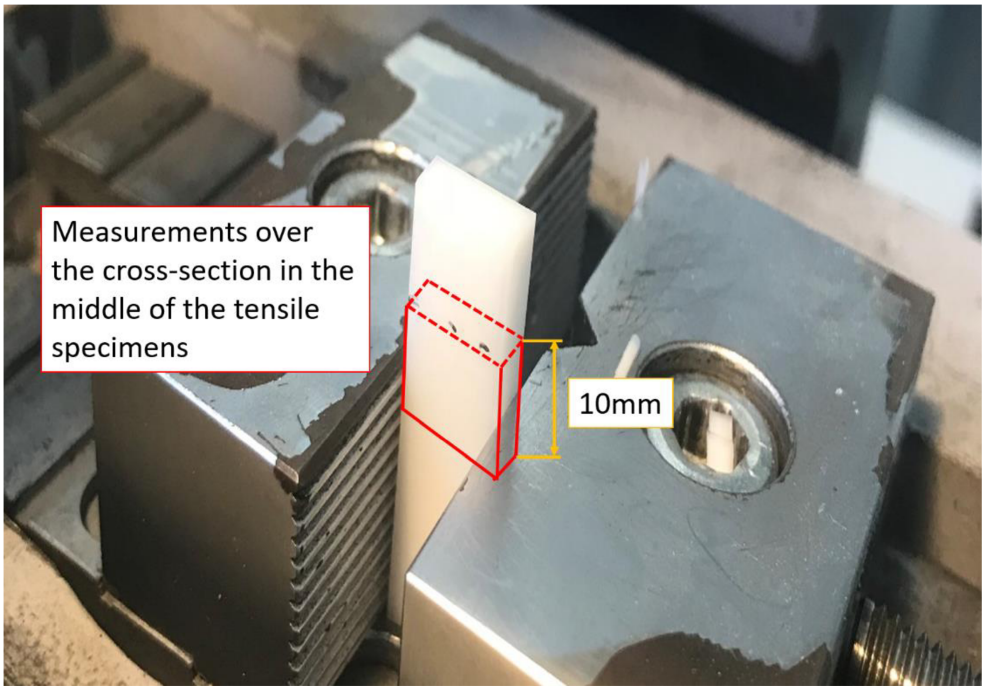

Fig. 3.4: Sample preparation for cross-section measurements by nanoindentation.

The compression molded specimens N1-N4 were cut from the CM plate according to Fig. 3.2. Two of them were annealed before nanoindentation: one at 160 °C for 50 min and one at 90 °C for 24 h. They were examined on their original compression molded surface five times.

3.2 Methods

In Table 3.5 and Table 3.6, all IM and CM samples used for LRT, WAXD and nanoindentation are displayed. The annealed injection molded and all compression molded specimens were measured with WAXD in their original state before the LRT was conducted.

Table 3.5: Overview of the IM samples used in this work for LRT, WAXD and nanoindentation.

INJECTION MOLDING				
Processing condition	**Annealing condition [time/temperature]**	**LRT [samples/milling profile]**	**WAXD [samples/milling profile]**	**Nanoindentation [samples/surface analyzed]**
C1	-	3/profile 1	-	-
C2	-	3/profile 1	3/profile 2	1/thickness 1/width 1/cross-section
C2	50 min/160 °C	1/profile 1 1/profile 2	1/not milled	-
C2	2 h/160 °C	1/profile 1 1/profile 2	1/not milled	-
C2	24 h/90 °C	1/profile 1 1/profile 2	1/not milled	-
C3	-	3/profile 1	-	-
C4	-	3/profile 1	-	-
C5	-	3/profile 1	-	-
C6	-	3/profile 1	-	-
C7	-	3/profile 1	-	-
C8	-	3/profile 1	-	-

Table 3.6: Overview of the CM samples used in this work for LRT, WAXD and nanoindentation.

COMPRESSION MOLDING				
Processing condition	**Annealing condition [time/temperature]**	**LRT [samples/milling profile]**	**WAXD [samples/milling profile]**	**Nanoindentation [samples/surface analyzed]**
CM plate	-	1/profile 1	1/not milled	1/CM surface
CM plate	50 min/160 °C	1/profile 1	1/not milled	1/CM surface
CM plate	2 h/160 °C	1/profile 1	1/not milled	-
CM plate	24 h/90 °C	1/profile 1 (failed)	1/not milled	1/CM surface

3.2.1 Layer removal technique

Injection molded tensile specimens

For the layer removal technique, three IM tensile specimens of each procession condition from injection cavity 1 were used (Table 3.5). Selected tensile specimens were annealed at the three conditions described above. Marks with a diameter of about 1 mm were drawn on the observed part of the specimens with a permanent marker (Fig. 3.5). This marks enabled the evaluation of the specimen curvature by “digital image correlation”.

Since the samples had to be fixed on a vacuum table to conduct the layer removal, it had to be ensured that adhesion to this table was strong enough. Therefore, small defects on the surface had to be removed. In detail, impressions of cavity number and pressure sensors on the injection molded specimens were milled away. Since, they were located on the samples shoulders, which were not monitored during the curvature analysis (Fig. 3.5), no influence on the measurement results was expected.

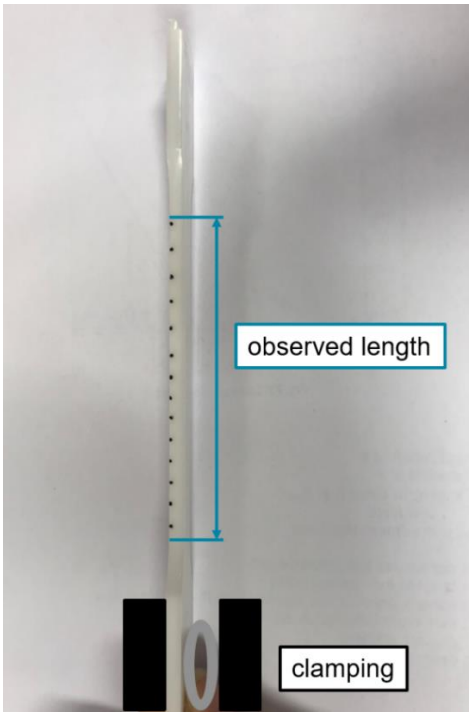

Fig. 3.5: Observed regime of the specimens with the marks for digital image correlation.

The layers were removed with a conventional milling machine (Jih Fong, Taichung, Taiwan). For the fixation of the samples, the above mentioned vacuum table was used. If this was not sufficient, e.g. after several removal cycles, where the specimens already showed some bending, a rubber pad was placed between specimen and vacuum table (Fig. 3.6a). However, this was avoided for the first removal steps with very thin layers, since the use of the rubber pad decreased the accuracy of the layer thickness removed. For the samples, which exhibited a strong bending, especially after several milling steps, mechanical clamping had to be used additionally. This is shown in Fig. 3.6b. The feed rate of the cutter was controlled manually, no automatic feed was available. It was tried to keep a constant milling speed of approximately 1,3 mm/s, because at higher speeds the milled surface became quite rough. The rotational speed of the cutter was approximately 670 rpm. As during the milling process heat was developed, the samples were cooled with compressed air during the layer removal.

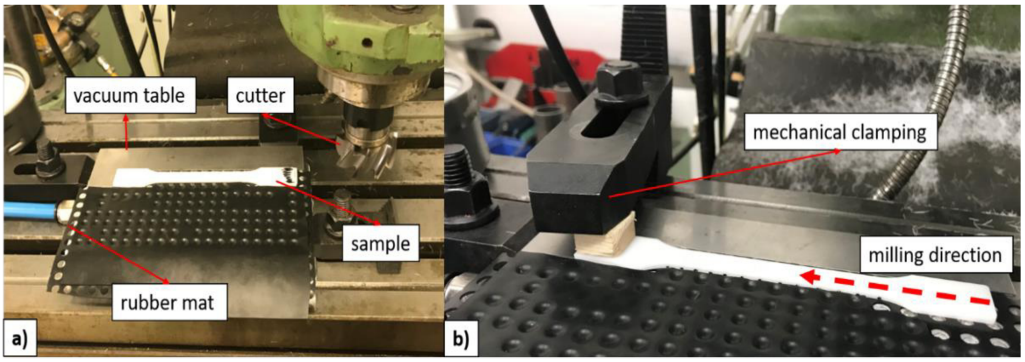

Fig. 3.6: Fixation used for milling of the specimens a) with vaccum only and b) with vacuum and additional mechanical clamping.

Two different milling profiles were carried out. Profile 1 consisted of ten milling steps from the surface to the midplane of the specimens. In Profile 2 five milling steps were conducted. Profile 1 was used for precise measurements, whereas profile 2 was used as a fast scanning technique. The details of thetwo milling profiles are displayed in Table 3.7.

Table 3.7: Thicknesses of the removed layers in each milling step for milling profiles 1 and 2.

Milling step	**Thickness of removed layer**	
	Profile 1 [µm]	**Profile 2 [µm]**
S1	50 *)	50 *)
S2	50 *)	150
S3	100 *)	600
S4	200	600
S5	200	600
S6	200	
S7	200	
S8	200	
S9	400	
S10	400	

*) No use of the rubber pad on the vacuum table to increase the accuracy of the removed layer thickness

For the determination of the specimen curvature, an optical method using a camera system was chosen. The experiments were carried out on a self-made test set-up, which is shown in Fig. 3.7. After each milling step, the specimens were clamped at one edge with a rubber tube and their bending deformation was tracked with a movable camera. Care was taken that the specimens were clamped and aligned exactly at the edge of the sample holder. With the test set-up used, it was possible to track 19 samples simultaneously.

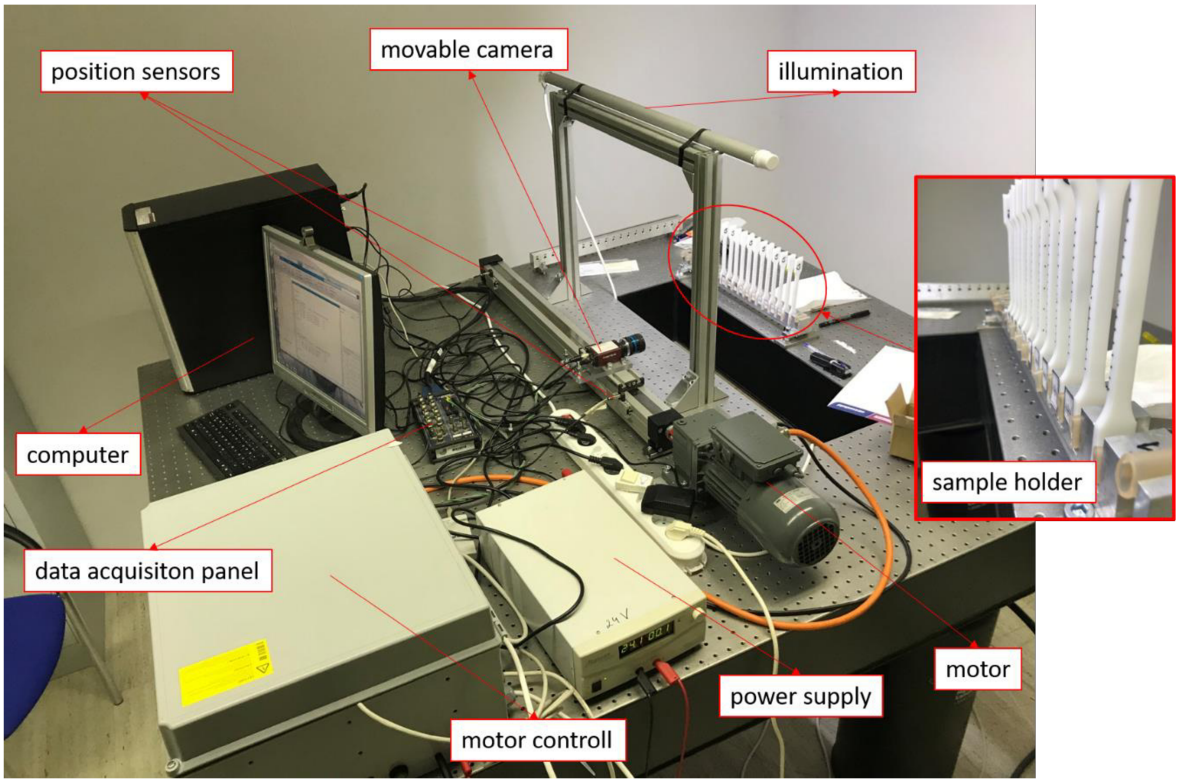

Fig. 3.7: Self-made strain recovery test set-up used in this thesis for the determination of the specimens' curvature development.

Over a time period of 48 h, pictures were recorded according to a specific pre-defined time profile. From these pictures, the curvature of the specimens was obtained by analyzing the positions of the tracking points using the digital image correlation software Mercury RT (Sobriety, Kurim, Czech Republic). In the software, it was tried to align the tracking areas always with the sample edge, but especially for bended specimens, this was sometimes difficult. As illustrated in Fig. 3.8, the positions of all marks on the pictures were tracked. To these mark positions, which were subsequently exported, a circle was fitted by a Matlab (MathWorks Inc., Natick, Massachusetts, USA) tool, which uses a Newton based Pratt-fit

(Pratt, 1987) (Fig. 3.8). The tool was developed by Nikolai Chernov (Department of Mathematics, University of Alabama at Birmingham, USA) and edited by Bruno Ramoa (former researcher at the Polymer Competence Center Leoben). The curvature, which was the inverse of the radius of this circle, was plotted over time and the curvature value at 48 h (2880 min) was taken to calculate the residual stresses. This time period was selected at the beginning of the work, since it was claimed in literature (Maxwell and Turnbull, 2003) that there is a significant change of curvature with time. It has to be mentioned that for the layer removal technique, the initial curvature of an unmilled specimen is supposed to be zero, which was not the case in this study. Therefore, the initial specimen curvature was subtracted from all subsequent values (Turnbull et al., 1998), since the model from (Treuting and Read, 1951) requires an initial value equal to zero.

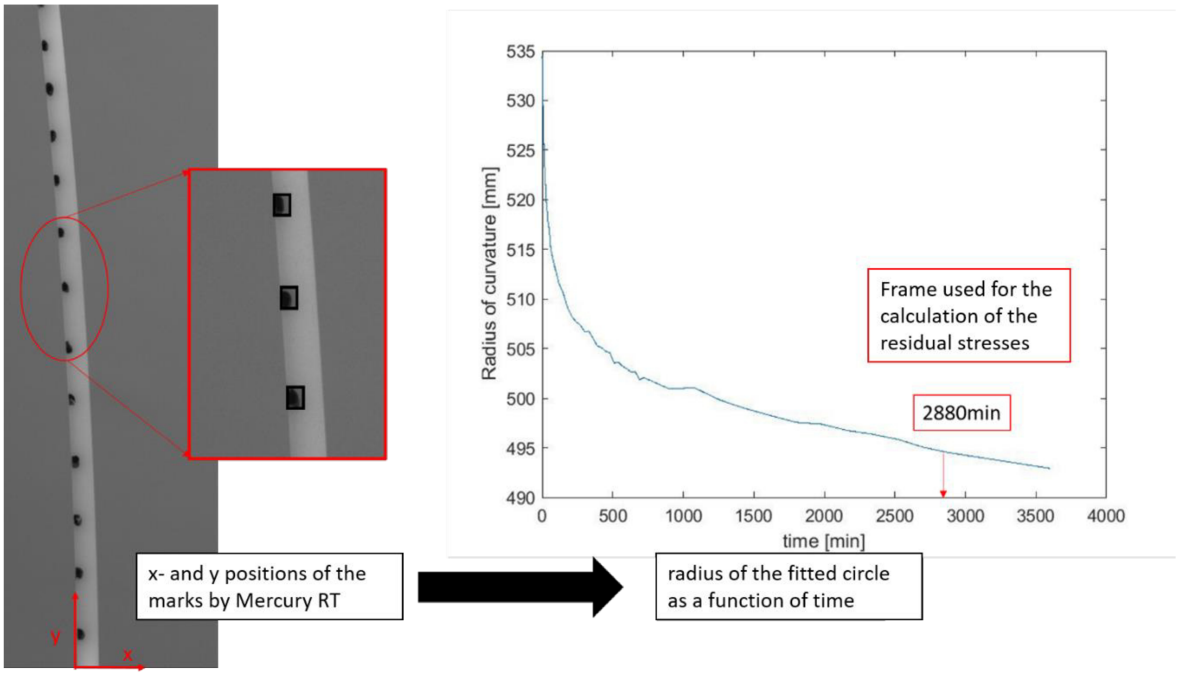

Fig. 3.8: Tracking of the marks with the digital image correlation software Mercury RT and evaluation of the circle radius using a Matlab tool.

IM tensile specimens that were annealed in order to obtain a rather stress free sample were also examined by the layer removal technique. For each annealing condition investigated, first one specimen was tested using the milling profile 1. In order to check the symmetry of the specimens, a second measurement was made using profile 2 and milling from the back side. For further details, please refere to Table 3.5.

Compression molded specimens

All compression molded specimens (annealed and not annealed) were examined with milling profile 2. The milling of the compression molded specimens was more complicated than that of the tensile specimen. First, the thickness of the specimens differed over the length in a range of nearly 200 µm (compared to an overall thickness of approximately 4 mm), which did not allow the removal of a uniformly thick layer. To compensate this issue, it was decided to first mill the backside of the specimen in order to generate a uniform thickness (Fig. 3.9). After this step, the resulting bending deflection was tracked with the camera for 48 h and then the "normal" layer removal process was started.

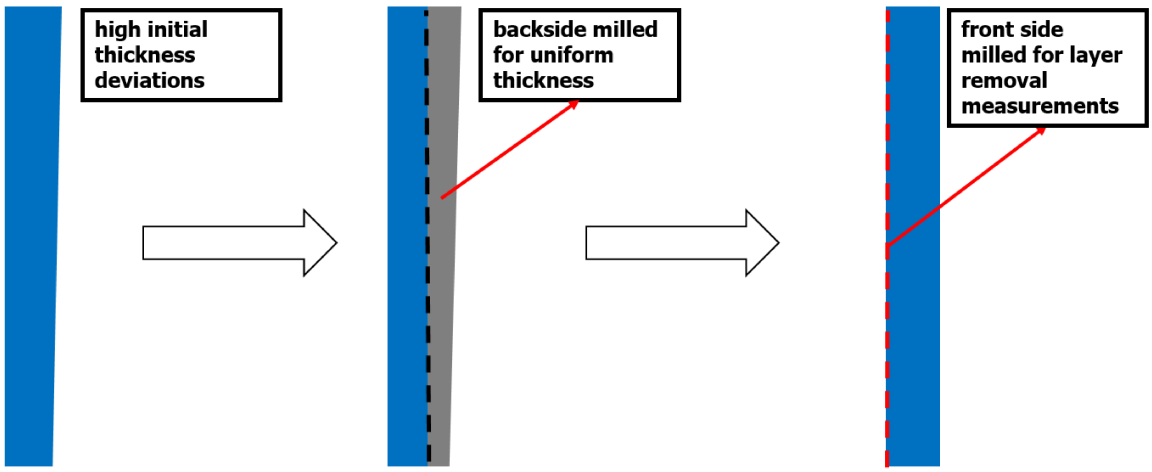

Fig. 3.9: Illustration of the thickness corrections made for the compression molded specimens.

Another issue was the very strong initial bending of the bars. Because of that, it was neither possible to fix them to the table by vacuum nor by mechanical clamping at one side. Therefore, the vacuum table was adapted in order to fix the bars mechanically on both sides (Fig. 3.10). This adaption included, that the specimen could no longer be cut from right to left, but the cutter had to enter the sample from the side. Furthermore, it was observed that although the samples were fixed on the edges, they were not sucked properly by the vacuum in the middle. This led to oscillation of the specimens during the milling process and caused severe surface marks after milling. The curvature measurements and their evaluation was conducted as described above for the injection molded specimens.

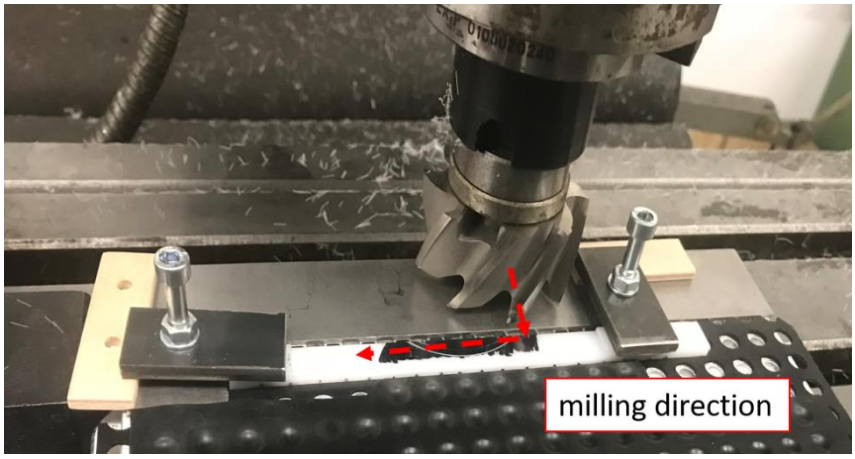

Fig. 3.10: Additional clamping and changed milling conditions for the compression molded specimens.

Experimental limitations of the LRT process

Regarding all LRT measurements, it has to be mentioned that the three assumptions made by (Treuting and Read, 1951) cannot be fully guaranteed in our case. The first assumption that the sample is linear in pure bending, is believed to be satisfied. The second one, requiring constant residual stresses within each plane, is expected to not be fulfilled. This is because processing parameters such as melt temperature and holding pressure for example vary over the flow path in the mold. This was examined in more detail by (Siegmann et al., 1982b) for injection molded plates. Introduction of additional stresses by the layer removal process can also not be fully excluded, although during the milling process the specimens were cooled in order to avoid stress changes due to elevated temperatures. The assumption that the material is isotropic and the elastic modulus is constant over the thickness will at least for the injection molded specimens not be satisfied. Orientations developing during the processing result in an anisotropic material behavior and the elastic modulus is assumed to vary with the varying degree of crystallinity and the morphology in the layers.

The time between milling and the commencement of the measurements was never more than 30 min. This was not according to the suggestion in (Turnbull et al., 1999), which was 15 min. However, compared to a time period of 48 h for the curvature determination, the influence should be quite small. The measurement time of two days (48 h) was chosen,

because it was a good compromise of an experimentally reasonable time duration and the time required for the samples to achieve their equilibrium shape (which was unknown at the beginning of this thesis).

3.2.2 Wide angle X-ray diffraction

Experimental set-up

For the WAXD and SAXS measurements, three IM tensile specimens processed with condition 2 and from injection cavity 2 were used. They were first measured in their original states and then milled following profile 2. After each milling step, WAXD patterns were recorded. Additionally, the CM bars P1-P4 and the annealed IM tensile specimens were examined by WAXD but for them, this was only done before conducting the LRT. Therefore, no residual stress profiles could be determined for the latter specimens. As an additional measurement, SAXS was also conducted for every specimen.

The WAXD and SAXS measurements were conducted on a "Brucker NANOStar" (Brucker Corporation, Massachusetts, USA) with a Iμ X-ray source (incoatec GmbH, Geesthach, Germany) (Fig. 3.11). The X-rays with a wavelength of 1,5418 Å were cut by a circular slit to a beam with a diameter of 300 µm. For the detection of the two-dimensionally diffracted pattern (WAXD) an image plate with a distance of 40 mm from the specimen was used. The calibration was done with Al_2O_3. The SAXS measurements were recorded with a VÅNTEC-2000 2D MicroGap Detector (Bruker Corporation, Massachusetts, USA). Here, the calibration was done by measuring a silver behenate standard. All measurements were conducted in an evacuated measuring chamber.

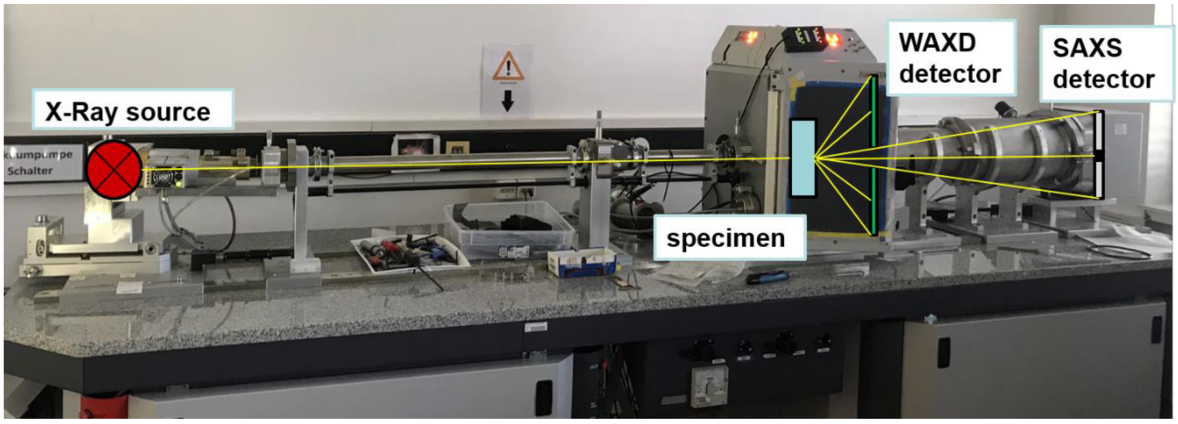

Fig. 3.11: Illustration of the Brucker NANOStar used for the X-ray diffraction measurements.

The tensile specimens were irradiated in total six times (initially and each time after removal of in total five layers). After every WAXD measurement a further layer of material was removed by milling until the mid-plane was reached. The thicknesses of the layers removed are shown in Table 3.8. The removal sequence is identical to profile 2, which was used as fast scanning procedure in the layer removal technique. It was tried to irradiate the samples in a similar area in the middle part for each measurement, but not in exactly the same spot to avoid possible changes of the material due to the energy of the X-ray beam. As in the layer removal technique, the elapsed time between milling and the start of the measurements was protocolled. It was found to lie between 25 and 30 minutes for all measurements. The compression molded bars and the annealed injection molded specimens were only measured in their original state without any layer removal. Each sample was irradiated for 1200 s.

Table 3.8: Thicknesses of the layers removed for the X-ray measurements of the IM tensile specimens.

Milling step	**Thickness of removed layer**
	Profile 2 [µm]
S1	50
S2	150
S3	600
S4	600
S5	600

Evaluation

The sample to detector distance and the coordinates of the beam center were calibrated using the pattern measured for the Al_2O_3. Before the integration of the specimen patterns, two corrections were made. First, the sample to detector distance obtained from the calibration with Al_2O_3 was not exactly the same as the one between sample surface and detector, because the samples were much thicker than the calibration substance.

Additionally, the thickness of the specimens changed after each layer removal. Therefore, the corresponding distance was adapted manually and individually for each specimen thickness. The second correction was made to compensate the fact that the image plate was rotated by 90° when inserted in the testing chamber. As a result, the pattern was also rotated by 90° and additionally, it was mirrored, when digitalized by the reader.

After the different correction steps, radial integration over the azimuthal angle X was done to obtain the intensity profiles (Fig. 3.12). The two dimensional patterns were splitted in different "cakes" to obtain intensity profiles in the X-directions 0°, 90°, 180° and 270°. For this, an X-range of ±5° was chosen for each cake. For example, the profile in 0°-direction was obtained by integrating the pattern from an azimuthal angle of -5° to 5°. The split of the patterns in different cakes enables the calculation of peak shifts and thus lattice strains in the different directions. The diffraction patterns were integrated using the software Fit2d (ESRF, Grenoble, France).

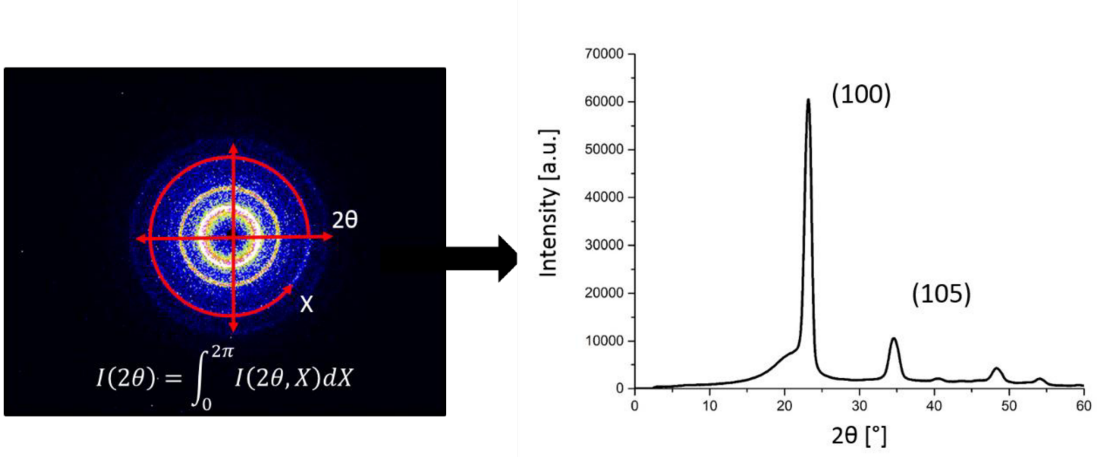

Fig. 3.12: Radial integration of a WAXD pattern to obtain the one-dimensional intensity profile.

As shown in Fig. 3.12, five peaks are present in the intensity profiles. The first peak was related to the lattice planes with the Miller index (100), the second peak to the (105) planes. The further peaks were not evaluated, because of their rather low intensity. The two main peaks were fitted with a self-written Python script using the Pseudo-Voigt peak shape function (Eq. (3.1)) in order to determine the peak positions.

$$I(2\theta) = I_{hkl}[\eta L(2\theta - 2\theta_0) + (1-\eta)G(2\theta - 2\theta_0)] \quad (3.1)$$

This function is a combination of a Lorentz fraction $L(2\theta-2\theta_0)$ and a Gauss fraction $G(2\theta-2\theta_0)$. The mixing factor η specifies the fraction of each peak shape used. The Pseudo-Voigt peak is considered as a combination of the best features of Lorentz and Gauss peaks and is widely used for fitting diffraction peaks.

After fitting the peaks, the d-spacing of the peaks was calculated using Bragg's law (Eq. 2.5). This was done for the intensity profiles in all four directions in order to obtain the d-spacing in dependence of the azimuthal angle X. For the d-spacing calculation, only the first order of the diffraction was used (n was 1 in Eq. 2.5).

Based on the d-spacing, the lattice strain $\varepsilon_{hkl}(X)$ was calculated (Eq. 2.6). For this, the d-spacing of a stress free sample was required. As it was indicated by the results from LRT that neither annealed nor compression molded specimens were free of stress, a value proposed in literature was used: the calculated peak positions for isotropic, hexagonal POM of $2\theta_{0,\,(100)}$=22,9° and $2\theta_{0,\,(105)}$=34,6° were taken from (Lüftl et al. 2013). It has to be mentioned that aside from stresses, crystalline structure also affects the position of the diffraction peaks. POM has for example an alternative polymorphic crystal structure, "orthorhombic" POM (Lüftl et al., 2013), which is considered as "metastable" at room temperature and low pressure. "Orthorhombic" POM shows diffraction peaks at different 2θ-positions.

Using the lattice strains ε_{hkl}, the corresponding stresses σ_{hkl} were determined (Eq. 2.7). In this thesis, the macroscopic modulus obtained by tensile testing instead of "plane-specific elastic constants" was used to estimate the stress levels. Of course in practice, each group of lattice planes has a specific X-ray elastic constant (XEC) that differs from the macroscopic modulus. In general, this XEC is higher than the macroscopic modulus (Feuchter, 2011; Taisei et al., 2015). However, no such plane-specific elastic constants were available for Polyoxymethylene and their determination would have gone beyond of the scope of this thesis. Hence, it has to be kept in mind that the stress profiles obtained can only qualitatively be compared to the outcomes of the other methods (layer removal technique and nanoindentation).

When it comes to stress profiles over the specimen's depth, one has to emphasize that the d-spacing obtained from the pattern of an unmilled specimen is an average d-spacing of a

plane group (hkl) throughout the whole specimen. When now a layer is removed and again a measurement is conducted, part of these planes is "milled away" and the so obtained d-spacing is an average distance over the remaining sample. Therefore, stresses in the milled layer are actually milled away. Since the specimens were not allowed to reach a new equilibrium and bending was constrained by the sample holder, the "milled away" residual stresses are considered to be the difference in stresses before and after each layer removal.

3.2.3 Nanoindentation

The measurements were carried out with a Berkovich tip on an Ultra Nanoindentation Tester UNHT³ (Anton Paar, Graz, Austria). The samples were glued to a microscope slide, which itself was glued to a metal cylinder. This metal cylinder was clamped into the indenter's specimen holder (Fig. 3.13). To remove the specimens from the sample holder, they had to be stored at temperatures above 130°C for at least 1 h (decomposition of the glue). This basically eliminated the rather non-destructive character of this method.

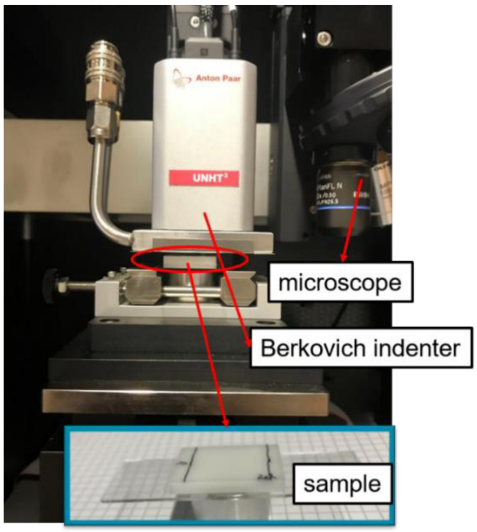

Fig. 3.13: Illustration of the experimental set-up used for the nanoindentation measurements.

The details of the sample preparation for nanoindentation were discussed in section 3.1.4. As described there, three different tensile specimens were used to produce the samples (one per specimen). Two samples (and thus tensile specimens) were examined at the original, injection molded surface: one along the 4 mm thick side (Fig. 3.14a) and one along the 10 mm thick (Fig. 3.14b). For the third sample, the cross-section was prepared as

described in section 3.1.4 and also indented (Fig. 3.14c). The CM samples were measured on their compression molded surface (Fig. 3.14d). Specific indentation profiles from the edges to the middle of the surfaces were chosen (Table 3.9) and repeated six times with a gap of 100 µm between each profile. An indentation depth of 3 µm was used together with with a loading rate of 2,5 µm/min for both loading and unloading. The indenter was paused at the maximum depth for 2 s. Any viscoelastic effects in the material during the measurements were not covered by the two models applied. It was taken care that the measurement parameters were kept constant to enable a comparison between the indentation curves and obtained values.

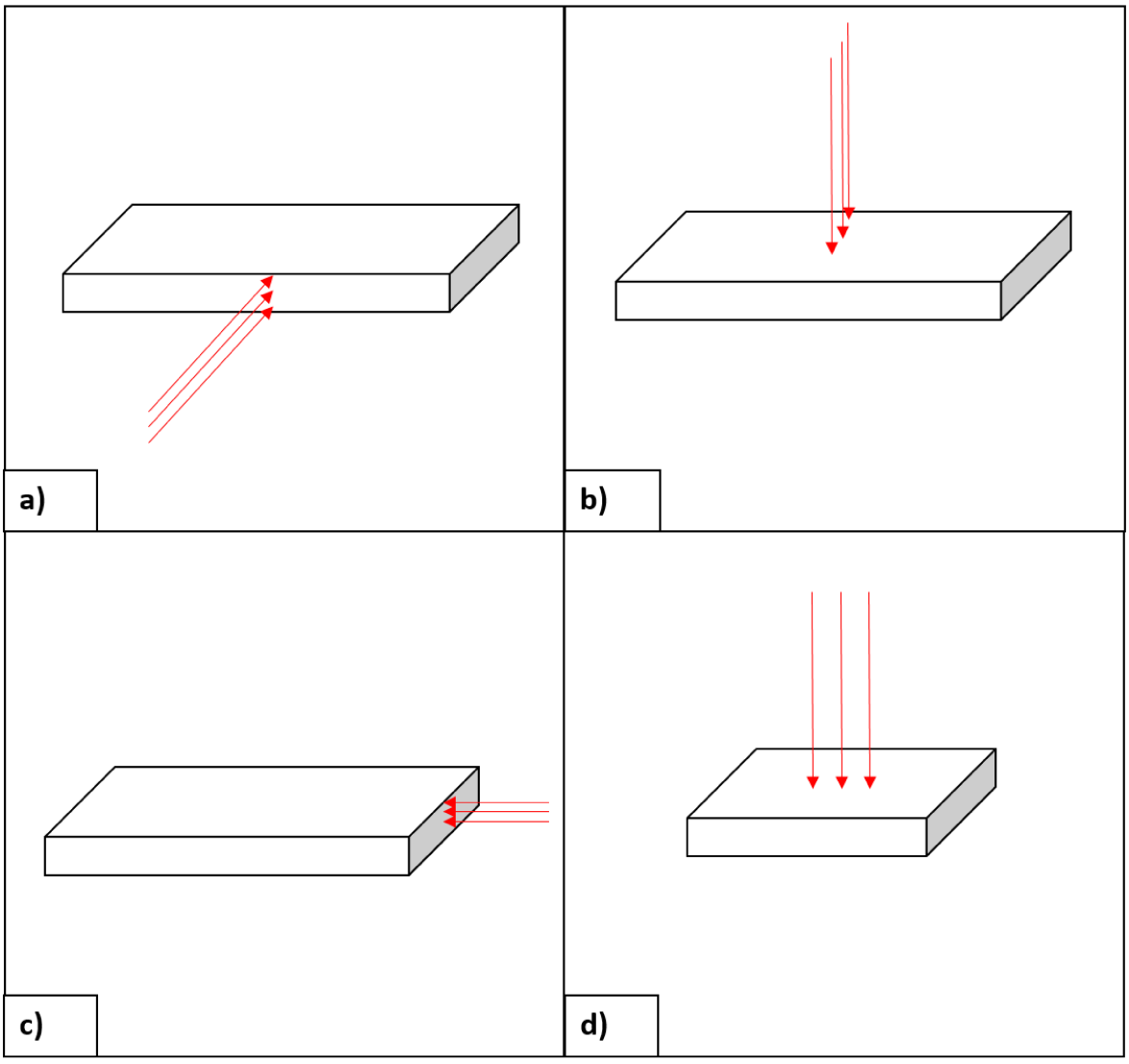

Fig. 3.14: Measurement directions for nanoindentation a)-b) on the IM surfaces of the tensile specimens, c) on the cross-section of the tensile specimens and d) on the CM plate.

Table 3.9: Measurement positions on the different surfaces of the IM samples which were examined by nanoindentation (starting at the edge and moving towards the center of the specimen).

Position Nr.	Along the thickness [µm]	Along the width [µm]	Over the cross-section [µm]
1	0	0	0
2	50	50	50
3	100	100	100
4	150	150	150
5	200	200	250
6	400	400	400
7	600	600	600
8	1000	800	800
9	1400	1000	1000
10	2000	1400	1200
11		1800	1600
12		2200	2000
13		2400	
14		2600	
15		3000	
16		3500	
17		4000	
18		4500	
19		5000	

The evaluation of the indentation curves was conducted in the software of the indenter ("Indentation 8.0.19", Anton Paar, Graz, Austria). All values that were needed for the stress calculation, such as maximum force, indentation area and hardness, were determined from the load-depth curves (Fig. 3.15). For this, the contact area as a function of the contact depth h_c was calibrated with a diamond calibrant. h_c was the vertical distance along the indenter tip with contact to the specimen. A schematic illustration of an indentation cross-section is displayed in Fig. 3.16. There, the difference between the penetration depth h, the contact depth h_c and the permanent indentation depth h_p is shown. The indentation hardness was determined by the Oliver & Pharr tangent method between 98% and 40% of the maximum force (Fig. 3.15). A part of the values obtained through the analysis are displayed in Table 3.10. For the residual stress determination this technique requires, just like the residual stress determination with WAXD, a stress free sample. For this, a not annealed, compression molded specimen was chosen. This was a compromise, because in the layer removal technique it was observed that this sample was not completely free of internal stresses. However, at least the stresses on the surface appeared to be rather low.

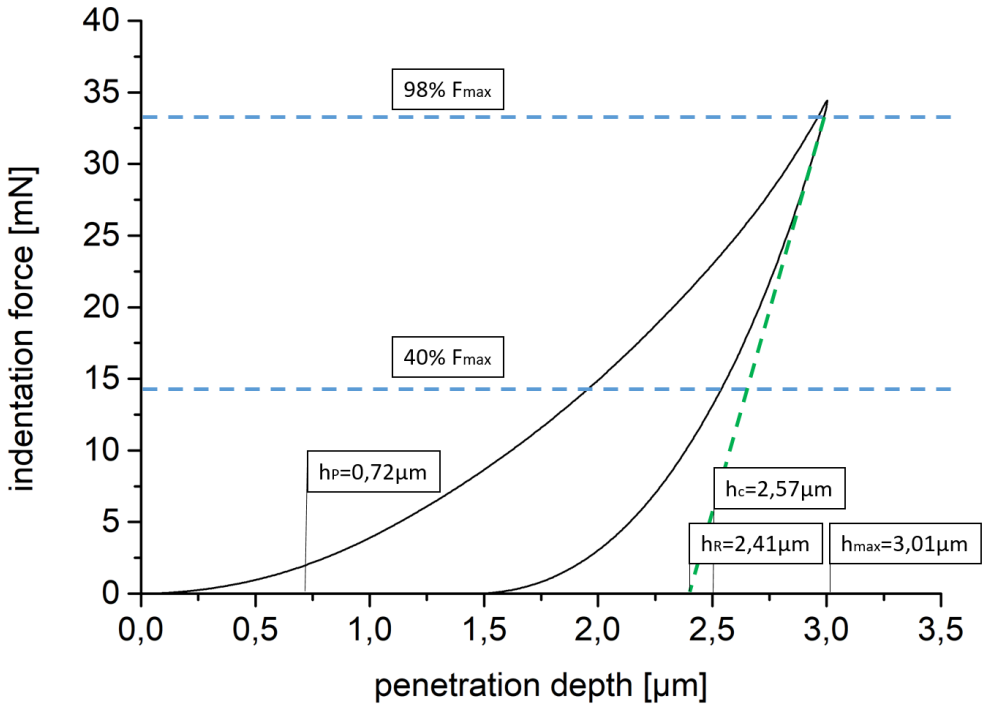

Fig. 3.15: Evaluation of instrumented nanoindentation measurements.

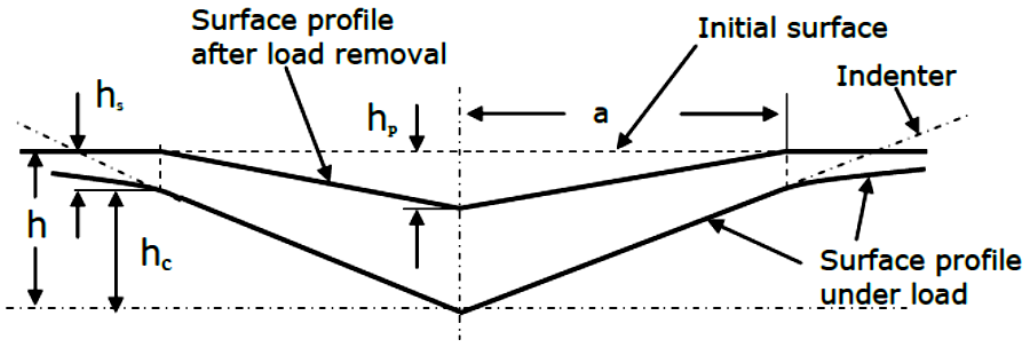

Fig. 3.16: Schematic cross-section of an indented area (Oliver and Pharr 1992).

Table 3.10: Results of the instrumented nanoindentation measurements obtained from the nanoindentation software.

Indentation hardness (H_{IT})	209,3 MPa
Indentation modulus (E_{IT})	3,15 GPa
Vickers hardness (HV_{IT})	19,4 Vickers
Maximum force (F_{max})	34,1 mN
Maximum depth (h_{max})	3005 nm
Contact depth (h_C)	2569 nm
Tangent indentation depth (h_R)	2405 nm
Permanent indentation depth (h_P)	720 nm
Projected contact area (A_P)	$1{,}63*10^8$ nm²

4 RESULTS AND DISCUSSION

4.1 Layer removal technique

4.1.1 Injection molded tensile specimens

In the following, the residual stress profiles for the IM tensile specimens processed with conditions 1-8 will be displayed and discussed. In Table 4.1, the injection molded samples examined by this technique are shown again.

Table 4.1: Overview of the IM samples examined by the layer removal technique.

Processing condition	Samples/milling profile
C1	3/profile 1
C2	3/profile 1
C3	3/profile 1
C4	3/profile 1
C5	3/profile 1
C6	3/profile 1
C7	3/profile 1
C8	3/profile 1

For the layer removal technique, the calculated stresses of three samples per injection molding condition were averaged. These results are presented as a function of the specimen depth. In the following, the influence of the different processing conditions is discussed and compared with literature. In general, a DOE is evaluated by statistical methods such as analysis of variances (ANOVA). This is easily applicable, when only single point data such as part weight or cycle time is measured, but becomes highly sophisticated for multi-point data such as stress distributions. Therefore, interactions between the different processing parameters are not quantified in this work.

The bending of the specimens, which is associated with the residual stresses in the removed layer, is illustrated in Fig. 4.1. After the first two milling steps (“1” and “2”), the bending deflection was rather low, which resulted in very small curvatures. In general, after the first and the second milling step, the samples bended towards the milled surface. These outer layers were compressed by the rest of the specimen. Therefore, when these layers were removed, they no longer constrained this compression mechanically and the specimen bended towards the milled surface. Since these layers were thin, the curvature changes were small, but resulted in rather high compressive residual stresses. When the area containing tensile residual stresses was entered, the samples started to bend in the opposite direction. This started with the third milling step and is shown in Fig. 4.1. The remaining layers with tensile residual stresses, which wanted to contract, produced a bending momentum in the opposite direction and the specimen started to bend away from the milled surface.

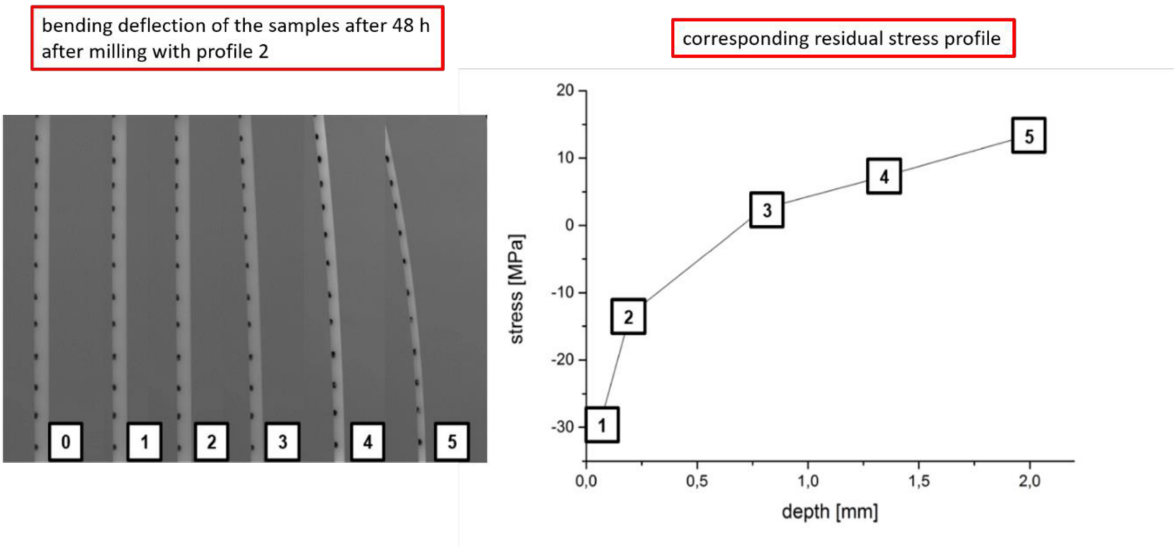

Fig. 4.1: Bending deflections during layer removal and corresponding residual stress profile of the IM specimen.

For all tensile specimens examined, compressive residual stresses were found in the near surface region. These stresses decreased with the depth and at a depth of about 0,5 mm the stress level turned into tension. The residual stresses remained in the tensile region until the midplane of the specimen was reached. Locally, maximum compressive residual stresses of about 15-20 MPa were found for the first and second measurement points. The

maximum tensile residual stresses were found either at a depth of 1 mm or 2 mm and they were always below 10 MPa. The build-up of compressive stresses in the outer layers and tensile stresses in the core is typical for quenched specimens but was also found for injection molded specimens (Siegmann et al., 1982a, 1982b). The injection molded specimens used in this thesis were cooled fast. Also slight sink marks on the surfaces of all specimens were observed. This indicates a rather low holding pressure level, which also results in compression in the near surface region and tension in the middle of the specimens (Fig. 2.4).

In Fig. 4.2, the residual stress distributions for tensile specimens processed at a mold temperature of 50 °C are shown. What is notable here are the very high standard deviations at the first milling steps in the surface region. Hence, it is difficult to make a clear statement in these areas. The high deviations are interpreted to arise from the milling process: after each milling process, the thickness of the samples was measured at six points along the specimens. It was observed that they did not show a 100 % uniform thickness over their length, which was an effect of the fixation by the vacuum. Over their length, the samples are not sucked uniformly to the table. In the first three milling steps without the rubber pad, the thickness deviation along the length of the specimens was less than 20 µm, with the rubber pad it increased to 30-40 µm. Hence, the rubber pad introduced additional height differences because of its softness. Since the first removed layers were very thin (50-100 µm), even the rather small thickness deviations (without rubber pad less than 20 µm) were assumed to have a significant influence on the calculated stress results. A second aspect was that for the first surface layers milled away, the resulting bending deflections were rather small. This resulted in rather big radii obtained by the circle fit. As a consequence a small change in the fitting conditions had a big influence on the radius values obtained from the fit. Since the radius was then converted into curvature and stresses, this directly influenced the data scatter. Moreover, the stresses in the outer layers were changing very strongly within a small increase in depth, whereas in the core region, the removed layers were comparatively thick and the stress values rather constant. When looking at the processing conditions C1 and C3, which were processed at lower holding pressure but with different temperature profiles, it is observed that the lower temperature profile (“-1“) rises the residual stresses in the core, but barely affects the stresses in the

outer layers, at least what is indicated here by these averaged curves. The same behavior in the core was observed for the conditions C2 and C4, which were processed at the higher holding pressure of 110 MPa and with different temperature profiles. Here differences in the surface layers are visible, but due to the high scatter is it difficult to make plausible interpretations. The different temperature profiles represent different melt temperatures and in general higher melt temperatures reduce the tensile residual stresses in the core and the compressive residual stresses near the surface (Siegmann et al., 1982b). Between a depth of 0,5 mm and 1,2 mm all curves show rather similar stress levels. From 1,6 mm to 2 mm, the lower temperature profile leads to residual stresses that are about 1,6 MPa higher than the ones at the higher temperature profile.

When comparing curves with the same temperature profile and different holding pressures (C1 to C2 and C3 to C4, respectively), the lower holding pressure results in higher tensile residual stresses in the core. In general, this is in good accordance with literature, since at low holding pressure, under-compression leads to a contraction of the inner layers, which gives rise to tensile stresses in the core and compressive stresses at the surface. High holding pressure compresses the inner layers and rises tensile stresses at the surface. At 1,6 mm depth, a p_{hold} of 60 MPa results in tensile stresses that are about 1,5 MPa higher than those for a p_{hold} of 110 MPa. At the center of the specimens, the tensile stresses developing at lower holding pressure are about 2,6 MPa higher. The reason for this higher influence in the center lies in the fact that this region is the last to solidify during the injection molding process and therefore, holding pressure is acting longer in this region. The influence of the holding pressure is expected to decrease along the specimens and it is limited by the sealing time.

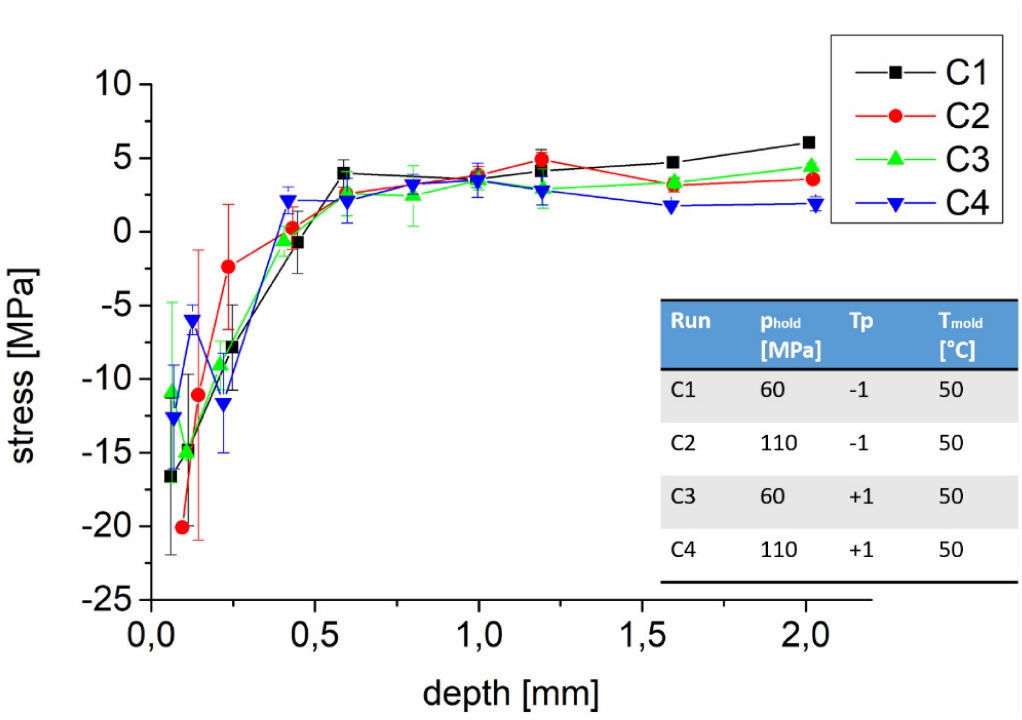

Fig. 4.2: Residual stress distribution in the injection molded specimens produced with low mold temperature.

The results for the tensile specimens produced at the higher mold temperature level of 110 °C are displayed in Fig. 4.3. As already observed before, the scatter in the near surface layers are again very high. In the core, for the lower holding pressure, no influence of the temperature profile can be seen (C5 and C7). For the higher holding pressure (C6 and C8), the lower temperature profile indicates higher tensile stresses in the core, but compared to the other curves, C6 shows rather high scatter in the inner layers. When comparing C5 and C6, which were processed at the lower temperature profile and with different holding pressure levels, it seems that here, higher holding pressure rises higher tensile stresses in the middle of the specimen. This is not according to literature and also differs from the results found for the low mold temperature (Fig. 4.2). Therefore, it is assumed that this effect is an artefact of the high scatter in these data points and hence, is interpreted as issues during the milling and the measurement procedure. Aside from the deviations of condition C6, the tensile specimens processed at high mold temperatures show rather similar residual stress distributions. This indicates that at a T_{mold} of 110 °C the influence of temperature profile and holding pressure on the developing stresses vanishes. (Siegmann et al., 1982b) stated that high mold temperatures may even overrule the influence of other injection molding parameters. An interesting information at this point is that also for the

mechanical and morphological parameters the mold temperature was the dominating processing influence, while holding pressure and melt temperature profile had only minor or even no influence.

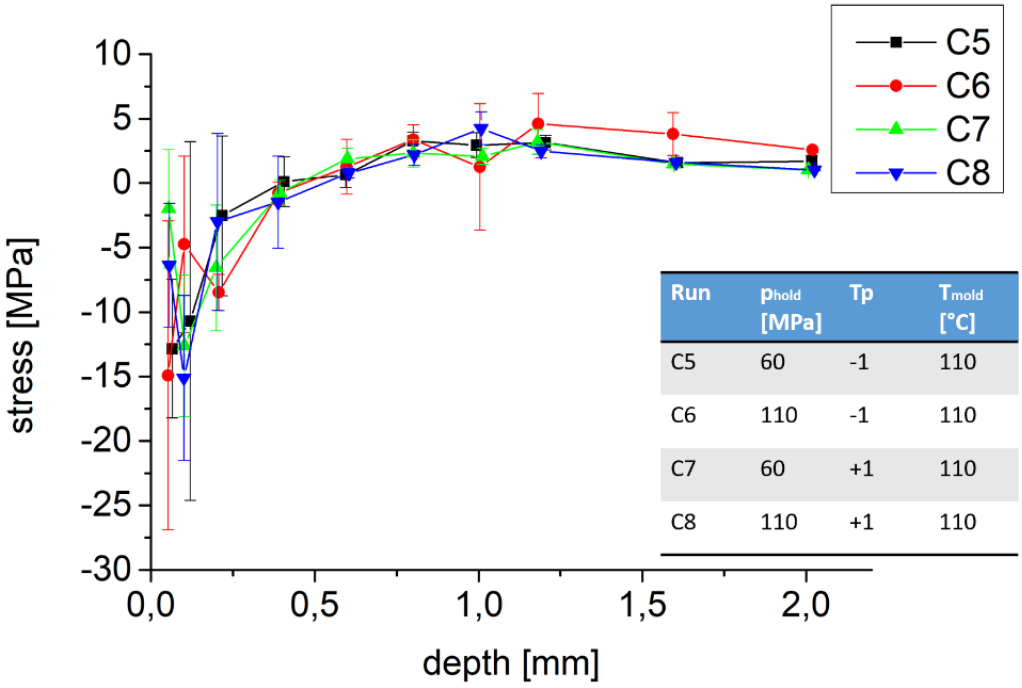

Run	p_{hold} [MPa]	Tp	T_{mold} [°C]
C5	60	-1	110
C6	110	-1	110
C7	60	+1	110
C8	110	+1	110

Fig. 4.3: Residual stress distribution in the injection molded specimens produced with high mold temperature.

In Fig. 4.4, the specimens processed at a holding pressure of 60 MPa are compared. Higher mold temperatures in general result in lower residual stresses (C5 and C7). (Siegmann et al., 1981) found that for injection molded PPO, residual surface stresses keep rather constant up to a mold temperature of 60 °C and then decrease with increasing mold temperature. In Fig. 4.4, it is again illustrated that the influence of the temperature profile on the residual stresses between 1,2 mm and 2 mm in depth is more pronounced for the lower mold temperature (C1 and C3) than for the higher one (C5 and C7).

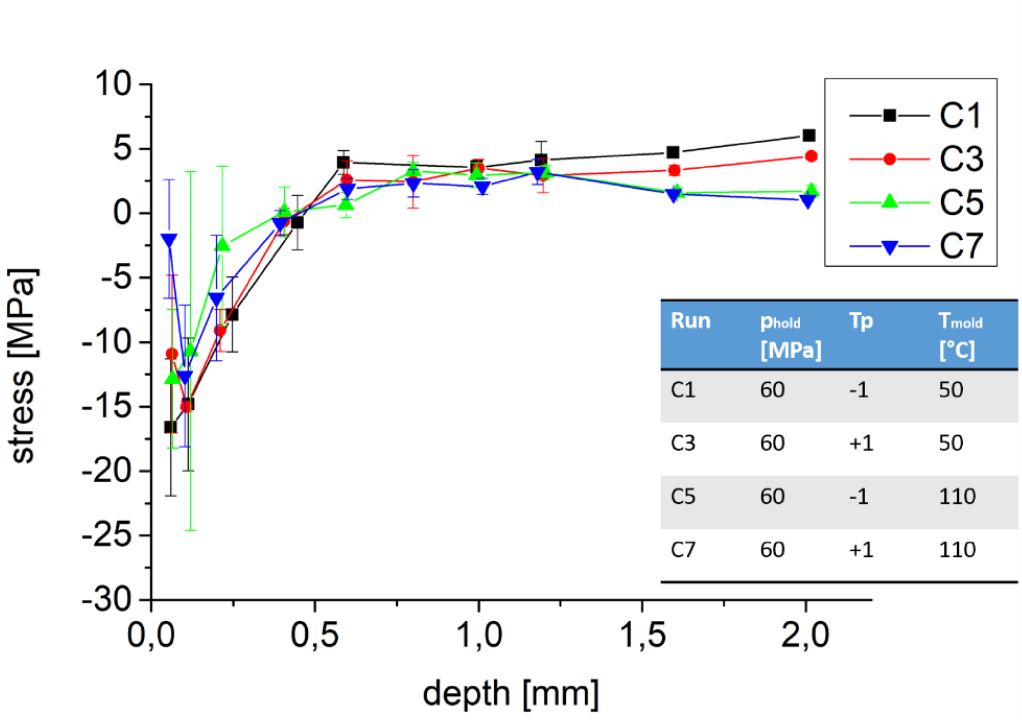

Run	p_{hold} [MPa]	Tp	T_{mold} [°C]
C1	60	-1	50
C3	60	+1	50
C5	60	-1	110
C7	60	+1	110

Fig. 4.4: Residual stress distribution in the injection molded specimens produced with low holding pressure.

In Fig. 4.5, the specimens with high holding pressure are displayed. Slightly lower values in the middle of the specimens are visible for a T_{mold} of 110 °C (except for condition C6, for which the deviation was attributed to the rather high scatter in its data points). When comparing C4 to C2 (different temperature profile) and C4 to C8 (different mold temperature), it is indicated that higher mold temperatures also lead to lower compressive stresses in the near surface area. It seems that at the higher holding pressures, the temperature profile has a higher influence on the residual stresses in the core than the mold temperature. It is assumed that the holding pressure can act on the melt for a longer time due to the higher melt temperature.

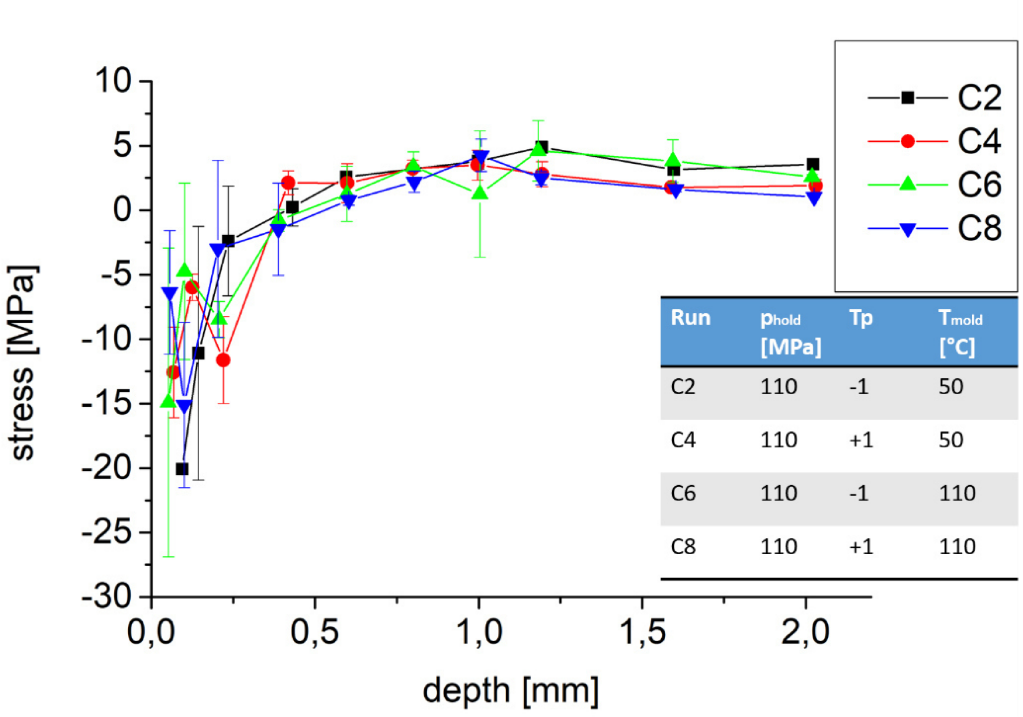

Fig. 4.5: Residual stress distribution in the injection molded specimens produced with high holding pressure.

Based on the observations discussed above, the following conclusions are drawn for our processing conditions. Lower holding pressure, lower temperature profile and lower mold temperature result in higher residual stresses in the core. Moreover, the influence of the holding pressure and the temperature profile is less pronounced at higher mold temperatures. This supports the assumptions made by (Siegmann et al., 1982b). Furthermore, it indicates that the biggest difference in the residual stresses (at least in the center of the specimens) has to be expected for the conditions C1 and C8 (Fig. 4.6). The corresponding stress difference in the center was about 5 MPa. In general, stress levels were higher for C1 than for C8. It is also indicated in Fig. 4.6 that the position of the maximum compressive residual stress value occurred closer to the surface for processing condition 1. Closer to the surface, it is believed that for C1 the residual compressive stresses will also decrease, but unfortunately this area was not accessible by the method.

It was a general drawback of the results and thus of the method used in this thesis that the stresses in the surface layers exhibited very strong scatter. Because all three processing parameters discussed above are known to affect these near surface stresses. Their

examination would have been highly interesting. Additionally, the highest residual stress values occurred in this area. According to (Siegmann et al., 1981), ultimate tensile stress and elongation at break show a minimum at the location of the maximum stress, which makes it important to determine the stresses in the surface regions accurately.

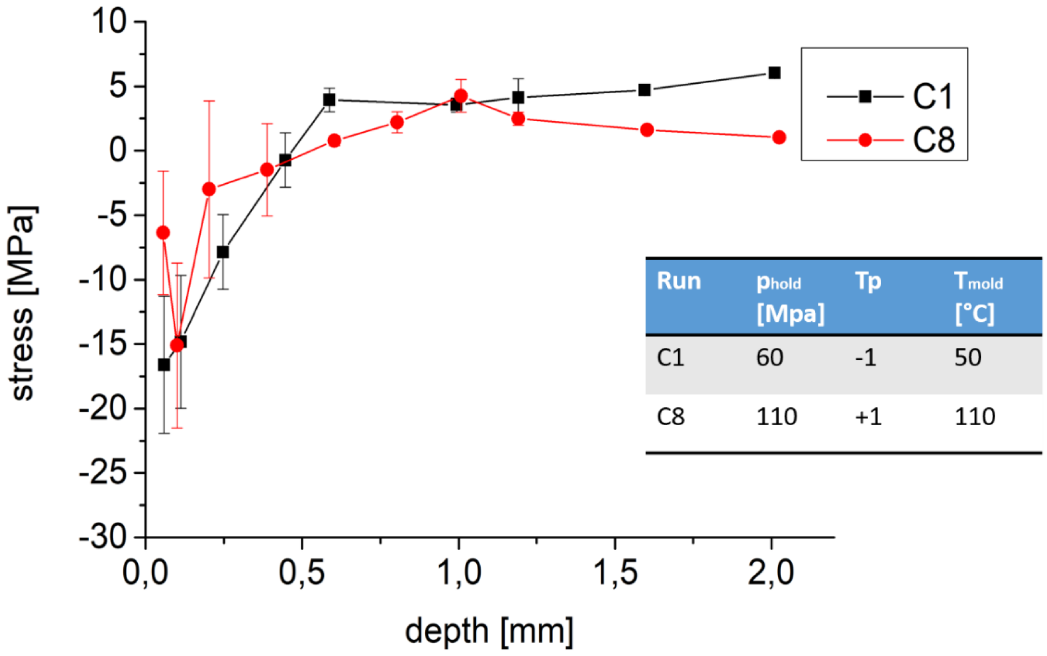

Run	p_{hold} [Mpa]	Tp	T_{mold} [°C]
C1	60	-1	50
C8	110	+1	110

Fig. 4.6: Residual stress distribution in the injection molded specimens produced with only the low (C1) and only the high (C8) levels of the varied processing parameters.

4.2 Wide angel X-ray diffraction

In this section, residual stress profiles obtained by wide angle X-ray diffraction are displayed and compared to the results of the layer removal technique. Three injection molded specimens produced with processing condition 2 in cavity 2 were examined using milling profile 2. It has to be kept in mind that due to the assumptions made for the calculation of the stresses from the WAXD profiles (d-spacing of the stress free sample d_0 was used from the literature and elastic modulus from tensile test was used instead of plane-specific X-ray elastic constants), only the shape of the profiles but not the quantitative values can be compared. For a better understanding, Fig. 4.7a shows the directions, in which the stresses were calculated. The specimen alignment and thus the flow direction corresponds to the

0°/180° direction. The d-spacing in 0° and 180° was calculated separately and both values were then averaged. The same was done for the 90° and 270° directions. In Fig. 4.7b the two rings that were chosen for the evaluations are emphasized.

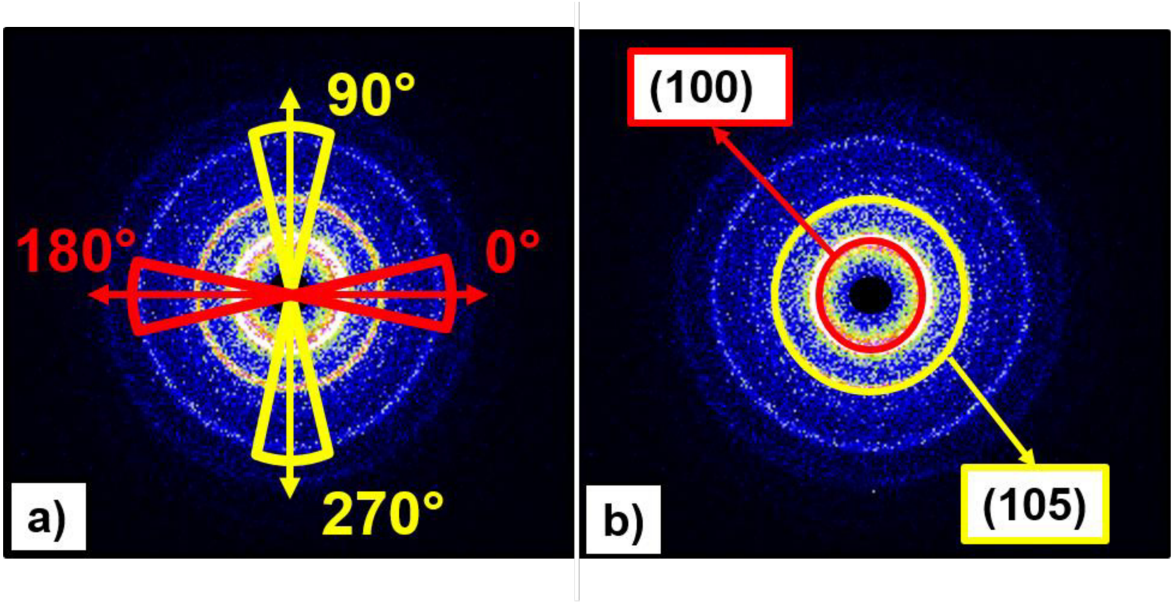

Fig. 4.7: Illustration of a) the evaluation directions and b) the WAXD rings used for the residual stress determination.

4.2.1 Calibration and thickness correction

In order to get correct peak positions both in WAXD and in SAXS, the so-called beam-center and the sample to detector distance in the machine have to be calibrated before the measurements. For this, specific calibration substances with known peak positions are used. In our case, this was Al_2O_3 for WAXD and silver behenate for SAXS. In this thesis, the calibration for WAXD was done in Fit2d by fitting a circle to manually chosen graphical coordinates of the first diffraction ring of Al_2O_3. The calibration was repeated five times and mean values for the beam center coordinates and the sample to detector distance were calculated. An integration of the calibration substance in the four chosen directions showed a standard deviation of 0,0225 for an average peak position of 25,58° for the first ring of Al_2O_3. The small deviation in the peak positions in the different directions was attributed to the manual selection of the fitting points during the calibration process (Fig. 4.8). This can result in a small shift in the beam-center (center of the concentric rings) and / or the sample to detector distance.

The sample to detector distance has a direct influence on the peak positions: an incorrect distance leads to an additional peak shift. While this has no effect, when only crystallinities are calculated from WAXD patterns, it is especially important for this thesis. The correct peak positions are the basis for the residual stress determination by WAXD. Any deviation here highly affects the stress values obtained and thus introduces a systematic error to the results. In order to get a precise sample to detector distance, it was not only necessary to calibrate this distance as described above, but to carry out an additional "thickness correction". This thickness correction takes into account the different thickness of calibration substance and samples. Figure 4.9 exemplary shows the influence of the sample thickness (and thus the sample to detector distance) on the WAXD profile. For illustration purposes, the WAXD profile is shown for a sample with and without thickness correction (the corresponding thickness correction was always conducted within this thesis). After the correction, the peak shifts to higher angles. In this example, the different diffraction angles also results in a different d-spacing and hence, in a different lattice strain and stress. Therefore, it was necessary to calibrate the sample to detector distance precisely with a calibration substance and to include additionally the thickness of the samples in the analysis.

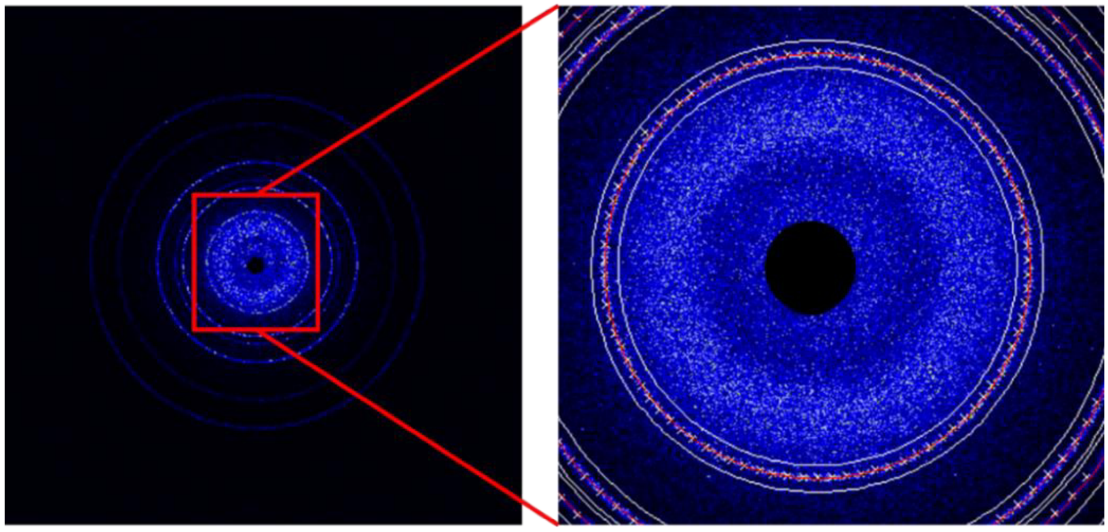

Fig. 4.8: Diffraction pattern of the WAXD calibration substance (Al_2O_3) and the circle fit used for calibration.

It is possible that there is some small shift in the so called beam-center (center of the concentric rings). Secondly, the sample to detector distance can be negatively affected. The sample to detector distance has an influence on the peak positions. An incorrect distance

leads to an additional peak shift, which has no effect when crystallinities are calculated from WAXD patterns. However, it highly affects the residual stress determination and introduces a systematic error to the results. Fig. 4.9 exemplary shows the influence of the sample to detector distance on the WAXD profile. For illustration purposes, the WAXD profile is shown for a sample with and without thickness correction (the corresponding thickness correction was always conducted during the analysis). After the correction the peak shifts to higher angles. In this example, the different diffraction angle also result in a different d-spacing and hence, in a different lattice strain and stress. Therefore, it is necessary to calibrate sample to detector distance precisely with a calibration substance and to include the thickness of the samples in the analysis.

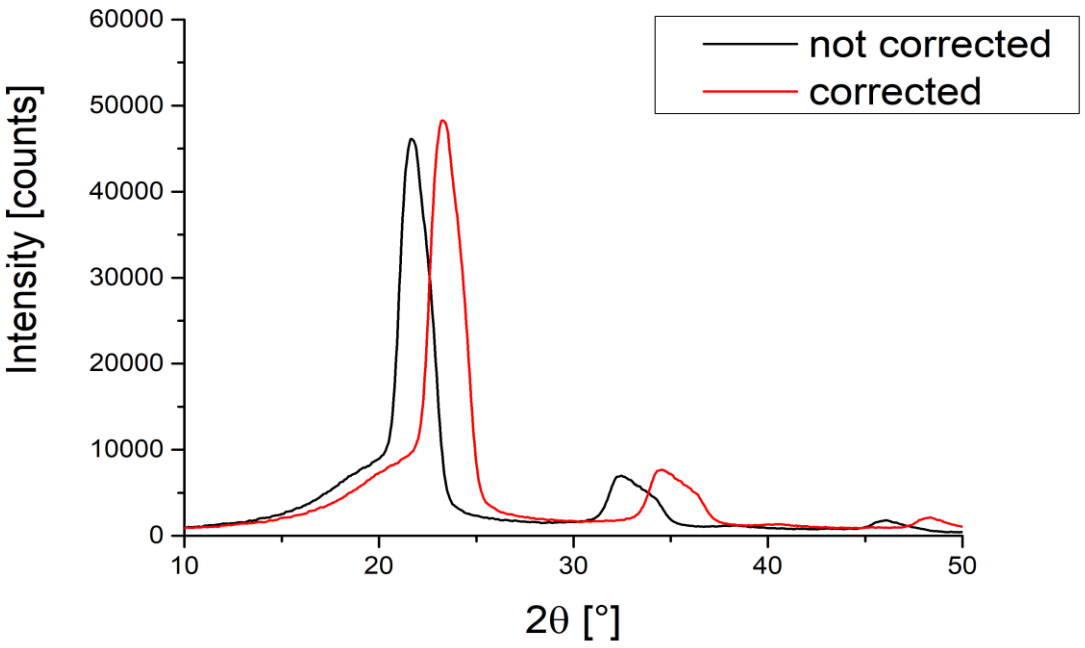

Fig. 4.9: Effect of the correction of the sample to detector distance with the sample thickness.

4.2.2 Injection molded tensile specimens

In the following, the results of the residual stress measurements with WAXD in both directions (0°/180° and 90°/270°) for the (100) (Fig. 4.10) and the (105) planes (Fig. 4.11) are shown. The calculated stress values obtained from the three tensile specimens examined with milling profile 2 were averaged. For both planes, compressive surface

stresses and tensile stresses in the core were found. Especially for the (100) plane, the stress profile in the outer layers seems to follow the trend found by LRT. In the tensile core region, where stresses were found to be rather constant in layer removal technique the WAXD stress profiles show an increase of the stresses. This is expected to arise from the fact that in the first few milling steps the bending of the specimen was quite small and was restricted during the measurements by the sample holder in the Nanostar. During subsequent layer removal, the bending of the specimen got stronger and could no longer be prevented completely during the measurement. The change in the macroscopic shape will also cause deformation on micro- and nanoscale. This effect is interpreted to cause the apparently increasing stresses in the core region. The (100) planes show different stress profiles in the two directions examined, whereas the (105)-stresses appeared to be quite similar.

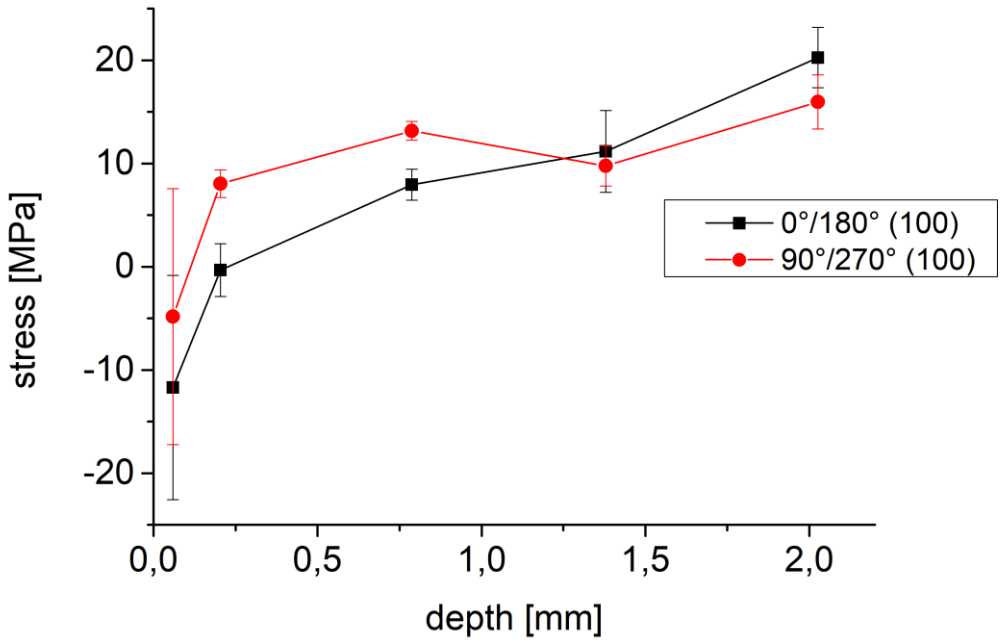

Fig. 4.10: Residual stress profiles for the injection molded specimens (condition 2) analyzed using the (100) peaks in the WAXD intensity profile.

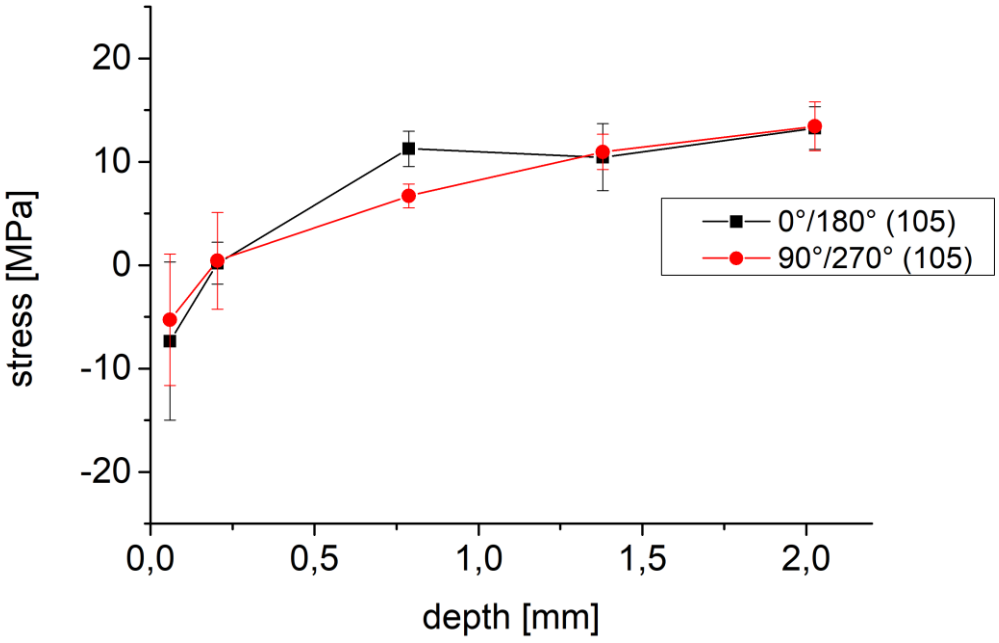

Fig. 4.11: Residual stress profiles for the injection molded specimens (condition 2) analyzed using the (105) peaks in the WAXD intensity profile.

4.3 Nanoindentation

In this section, the residual stress profiles along the different examined surfaces evaluated by both the Suresh and the Lee model are presented. An overview on the measured samples is given in Table 4.2. Only tensile specimens from processing condition 2 and cavity 2 were investigated using the nanoindentation technique. For illustration purposes, the measured surfaces and the indentation directions on the IM tensile specimens are displayed in Fig. 4.12. Additionally, reference measurements on a CM specimen were carried out.

Table 4.2: Overview of the samples examined by nanoindentation (for details on the indentation profiles please refere to Table 3.8).

Samples	**Indentations**
IM tensile specimen processed with condition 2 in cavity 2 (1 sample per direction)	6x profile along the thickness 6x profile along the width 6x profile along the cross-section

CM plate (1 sample, not annealed)	5x reference measurement

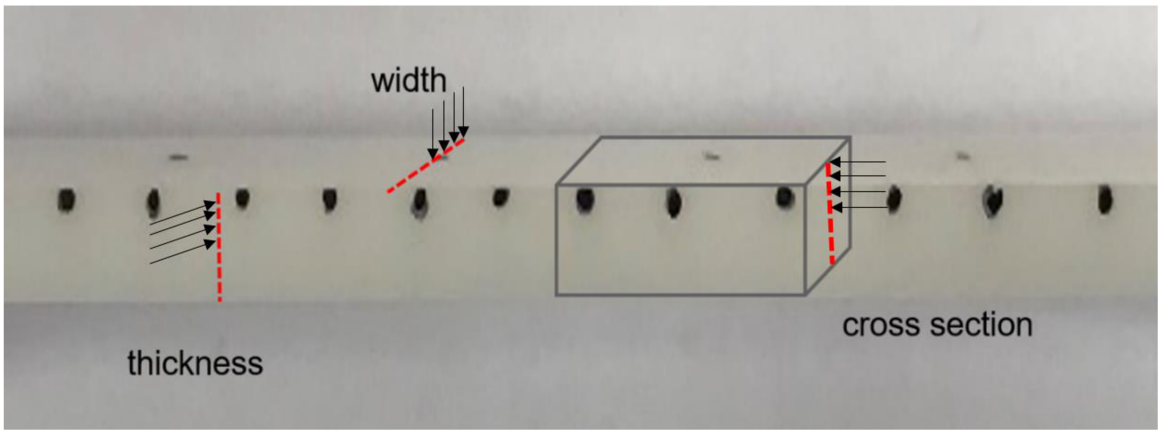

Fig. 4.12: Illustration of the tensile specimen surfaces examined by nanoindentation.

The residual stress profiles obtained by the two different models along the specimen's thickness, along the width and over cross-section are displayed in Fig. 4.13, Fig. 4.14 and Fig. 4.15, respectively. The two models gave different stress values and profiles. The Suresh model indicates a rather constant stress value along all three surfaces, but the Lee model led to a rather random stress distribution. The data points for this model also show very high standard deviations. Especially along the thickness and the width, both models show a kind of oscillation behavior at the positions near the edges, probably a result of the high data scatter in these regions.

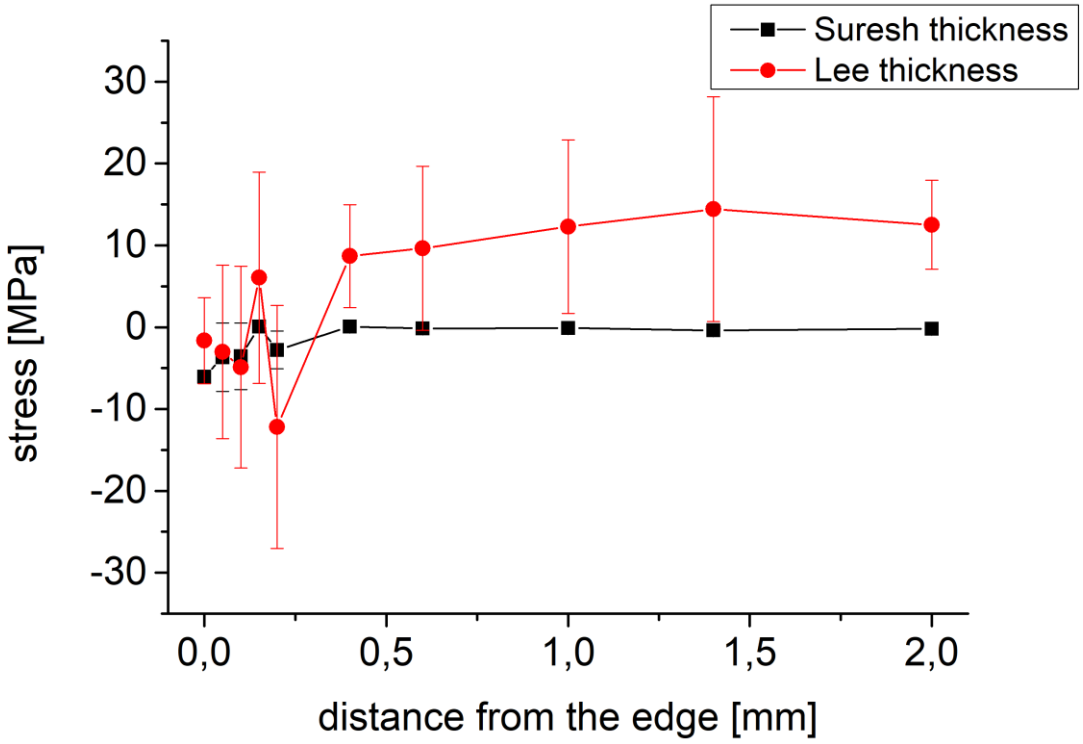

Fig. 4.13: Residual surface stresses along the thickness of the injection molded tensile specimen according to the Suresh and the Lee model.

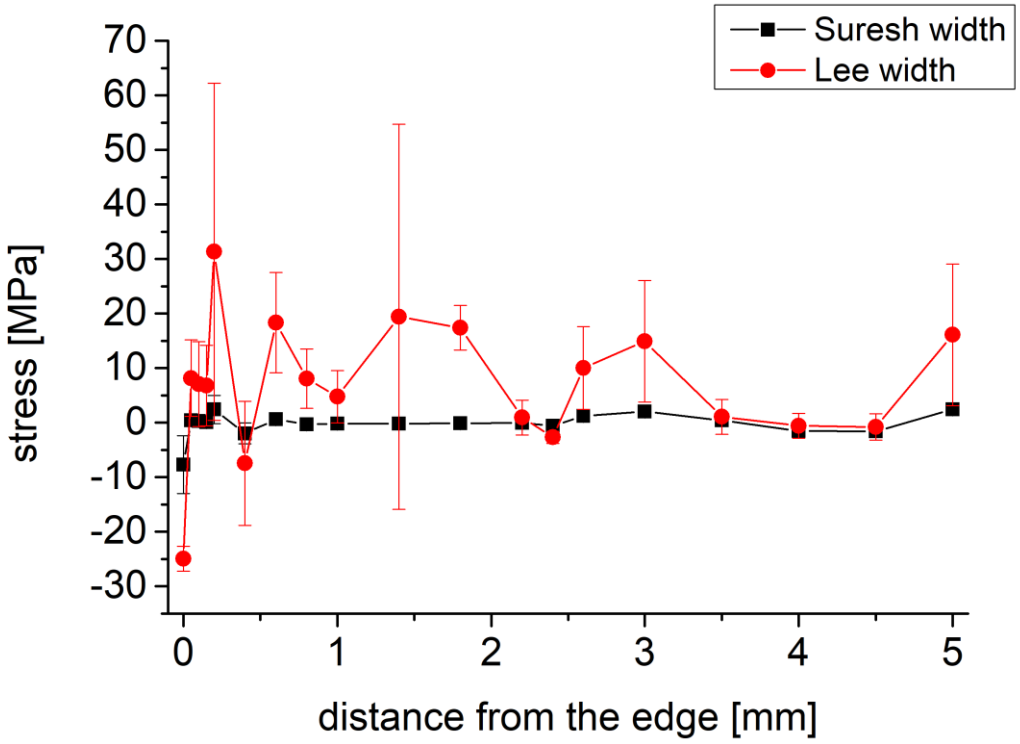

Fig. 4.14: Residual surface stresses along the width of the injection molded tensile specimen according to the Suresh and the Lee model.

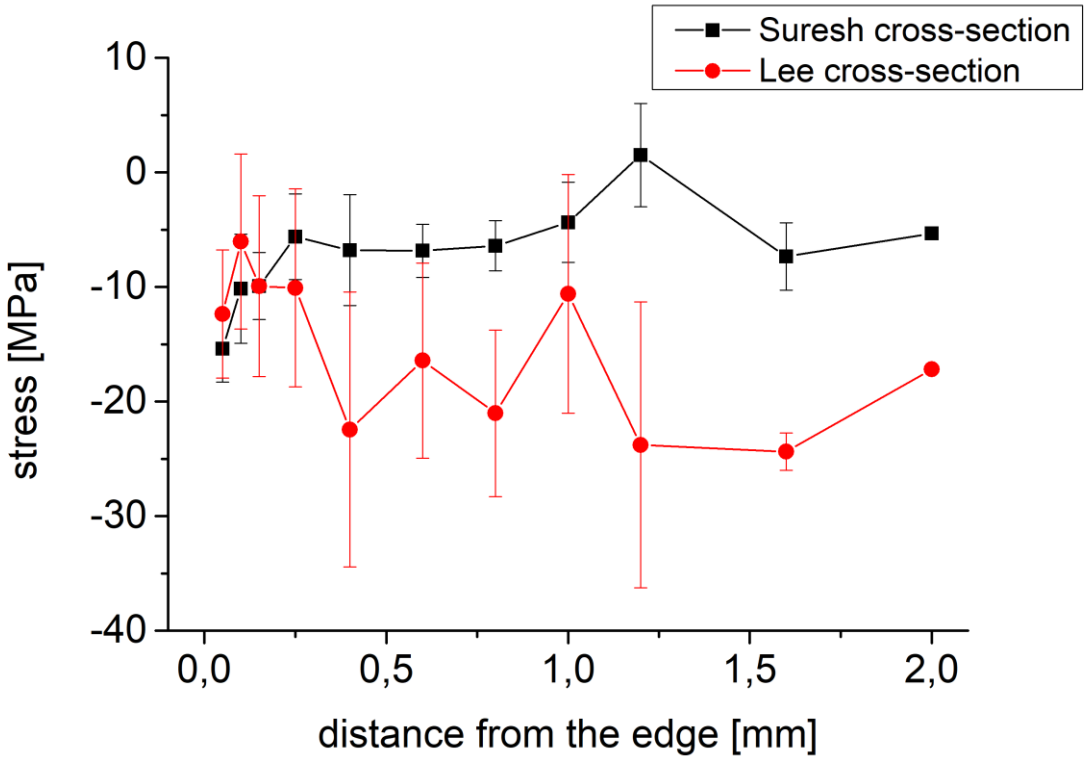

Fig. 4.15: Residual surface stresses over the cross-section of the injection molded tensile specimen according to the Suresh and the Lee model.

The reasons for the oscillating profile at the edges and the high standard deviations in Lee's model are assumed to arise from surface and geometry issues. First of all, the samples used did not show uniform thicknesses along their different dimensions (Fig. 4.16). As a result, the indenter tip did not reach the surface uniformly and therefore, no valid indentation measurements could be performed, especially at the edges. Another issue was that for the measurements along the thickness and width, the edges of the surfaces were not sharp edges but a little rounded. This led to quite high height differences and gave rise to the oscillating stress profiles in these areas.

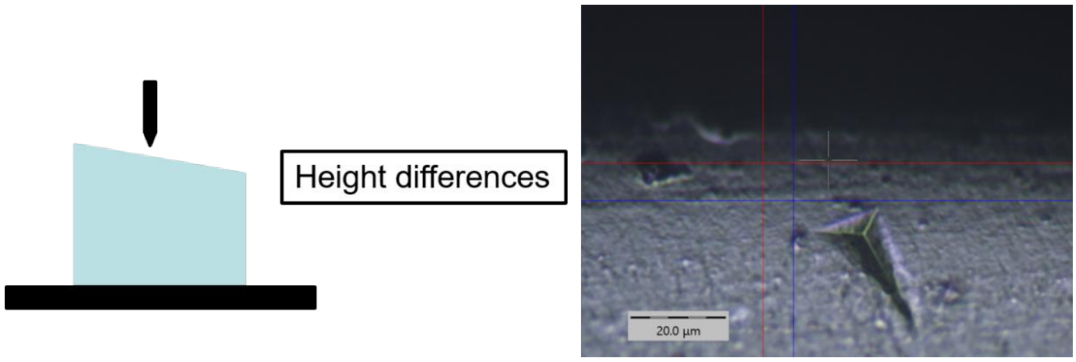

Fig. 4.16: Schematic illustration of height differences and the effect of the rounded edges on the tensile specimens.

Moreover, the injection molded surfaces that are considered to be quite smooth after the process, are still too rough for precise indentation measurements (Fig. 4.17). This led to significant errors in the indentation force. Since Lee's model takes the difference in the indentations forces of unstressed and stressed state into account, very high standard deviations were obtained for this model.

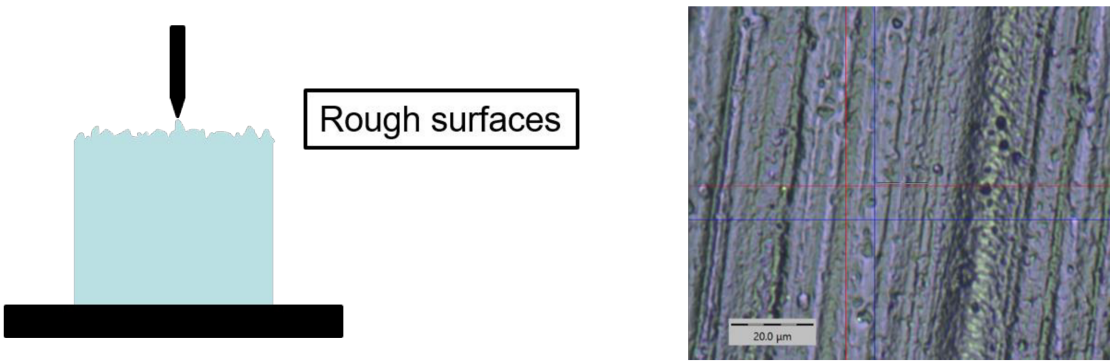

Fig. 4.17: Injection molded surfaces of the tensile specimens, which were found to be quite rough for the nanoindentation technique.

As a general conclusion, no satisfying results were obtained by nanoindentation. The method is yet not well examined for polymers and geometrical issues caused major problems in the measurements. Aside from that, viscoelasticity is not taken into account by the two models applied. It is assumed that the Suresh model works better in our case. It is less affected by the scatter in the indentation force and a constant stress value along the thickness and width seems plausible. Lee's model gave stress values along the width, for which the standard deviation even reached up to 65 MPa. This is in the range of the tensile strength of POM, which is around 70 MPa. Therefore, these data points are practically useless. Also the measurements on the compression molded plate showed very high scatter. Moreover, as indicated by the layer removal technique, they cannot be considered as stress free and hence, they are no proper reference for nanoindentation.

4.4 Comparison of the methods

Aim of this thesis was the conduction of residual stress measurements for a series of injection molded specimens and the comparison of three different measurement techniques. Since for nanoindentation no proper stress distributions were obtained, only LRT and WAXD will be compared in this section. In Fig. 4.18, the stress profiles obtained by layer removal technique and WAXD (in flow direction) are shown for the injection molding condition C2. In order to ease the comparison, the WAXD profiles were shifted by -5 MPa along the y-axis (the original curves are represented by the dashed lines). Layer removal technique was interpreted to be the most reliable method. It gave plausible results throughout the whole measurement series. The stress profiles and their changes due to the different processing parameters were in good accordance with literature. WAXD also yielded plausible stress profiles, although the absolute stress values could not be determined accurately due to the unavoidable assumptions on d_0 and the elastic constants. Nevertheless, in Fig. 4.18 the WAXD-profiles match the LRT profiles quite well except for the last data point, which is believed to correlate with bending during the WAXD measurements (please refere to section 4.2.2 for more details). Both methods show high standard deviations in the surface region, which is assumed to arise from the milling process and the small bending curvature measured for these layers. For WAXD also a higher standard deviation in the core region was observed. Both models are interpreted to be

suitable for residual stress determination in injection molded parts. They both yield advantages and disadvantages. The layer removal technique is very time consuming both in measurements and evaluation However, it resulted in the most plausible results, although the requirements defined by (Treuting and Read, 1951) were not completely satisfied. WAXD is significantly faster, but additional information on the stress free state and elastic constants is needed. Another advantage of WAXD is that this method also yields additional morphological information and that it can easily be combined with SAXS measurements.

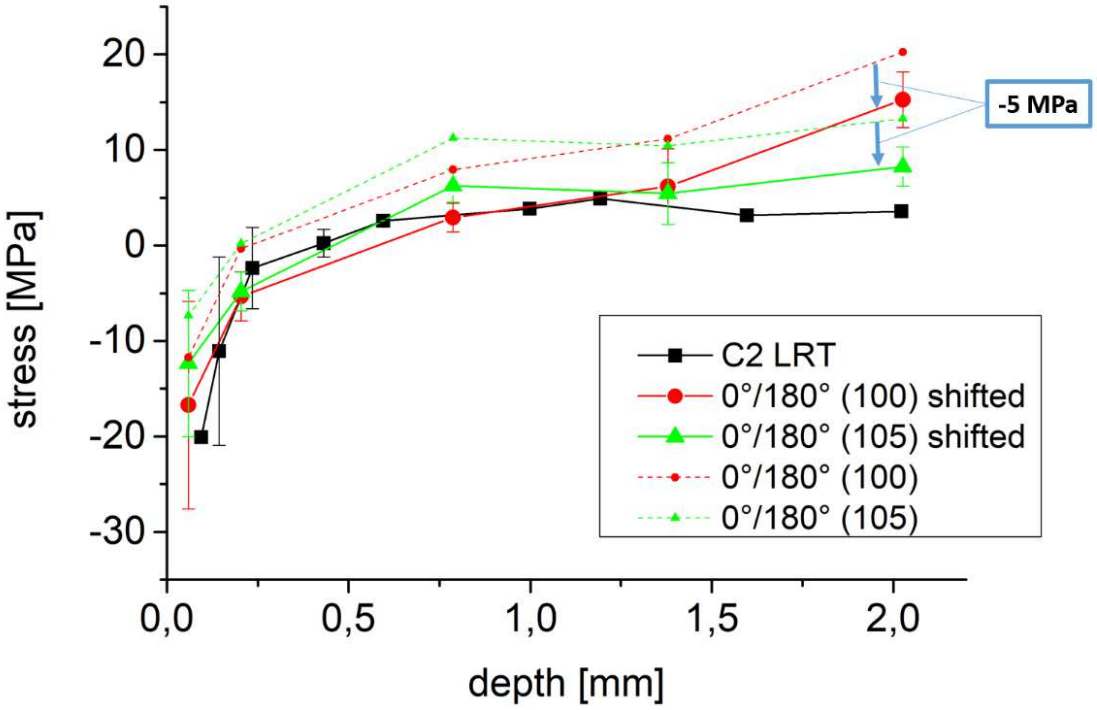

Fig. 4.18: Comparison of the residual stress profiles measured using the layer removal technique and WAXD (residual stress profiles of WAXD are shifted by a value of -5 MPa).

4.5 The effect of annealing on the injection molded and compression molded specimens

In the following, the effect of annealing on the injection molded and compression molded specimens will be described. Before conducting the layer removal technique, the annealed samples were examined by both, WAXD and SAXS in their original state (no milling had

been carried out). In Table 4.3, an overview of the specimens and the measurements conducted is given. IM samples processed with condition 2 in cavity 2 were used. The not annealed injection and compression molded samples were used as references.

Table 4.3: Overview of the samples used to study the effect of annealing.

ANNEALED SPECIMENS			
Processing condition	**Annealing condition [time/temperature]**	**WAXD [samples/milling profile]**	**LRT [samples/milling profile]**
C2	-	3/profile 1	3/profile 1
C2	50min/160°C	1/not milled	1/profile 1 1/profile 2
C2	2h/160°C	1/not milled	1/profile 1 1/profile 2
C2	24h/90°C	1/not milled	1/profile 1 1/profile 2
CM plate	-	1/not milled	1/profile 2
CM plate	50min/160°C	1/not milled	1/profile 2
CM plate	2h/160°C	1/not milled	1/profile 2
CM plate	24h/90°C	1/not milled	1/profile 2 (failed)

4.5.1 Effects of annealing on WAXD measurements

As mentioned above, the annealed tensile specimens and all compression molded specimens were examined by both, WAXD and SAXS before they were milled and analyzed using the layer removal technique. The WAXD and SAXS measurements were conducted only one time and therefore, no stress profiles can be displayed here. The WAXD- and SAXS-patterns for the annealed and not annealed tensile specimens are shown in Fig. 4.19a and Fig. 4.20a. From the WAXD patterns, no significant difference can be seen for the different

thermal histories. The inner ring, corresponding to the (100) plane shows an intensity concentration at 90° and 270° for the injection molded specimens (Fig. 4.19a), which indicates an orientation of these planes in flow direction. This cannot be found for the compression molded specimens (Fig. 4.19b). Only little intensity changes can be observed for the different annealing conditions. Hence, the crystalline lattice structure is not expected to be significantly affected by annealing. When looking at the SAXS patterns of the injection molded (Fig. 4.20a) and the compression molded specimens (Fig. 4.20b), an influence of annealing is pretty obvious. From SAXS measurements of POM, information on long period and lamellar thickness of the folded chain crystals (FCC) as well as the extended chain crystals (ECC) can be obtained. No detailed analysis of the SAXS patterns was conducted, since this would have gone beyond the scope of this work. However, the interpretation of some of these SAXS patterns indicates that thickening of the lamellae in both flow and perpendicular direction happened during annealing especially at the highest temperature. It is expected that also the orientation is affected during annealing but this has to be proofed in further research. Concerning the intensity in the patterns, the CM specimens have a much higher one than the IM specimens. The CM samples do not show intensity concentrations in the 0°- and 180°-directions. This is not surprising, since they are considered to have almost no orientations in their morphology. The IM samples on the other hand, have strong intensity concentrations in 0° and 180° direction, indicating orientation of the amorphous layers perpendicular to the flow direction. This seems surprising at the first view, but was already observed previously for this tensile specimens. From this previous study, it is known that the perpendicular orientation is a combined effect of the holding pressure and this very fast crystallizing POM resin. The effect can also be observed in visible light, e.g. when polarized light microscopy of microtomed cuts is carried out (Fig. 4.24). What is surprising is that the intensity concentration (and thus the orientation) becomes even more pronounced with annealing. The opposite would be expected.

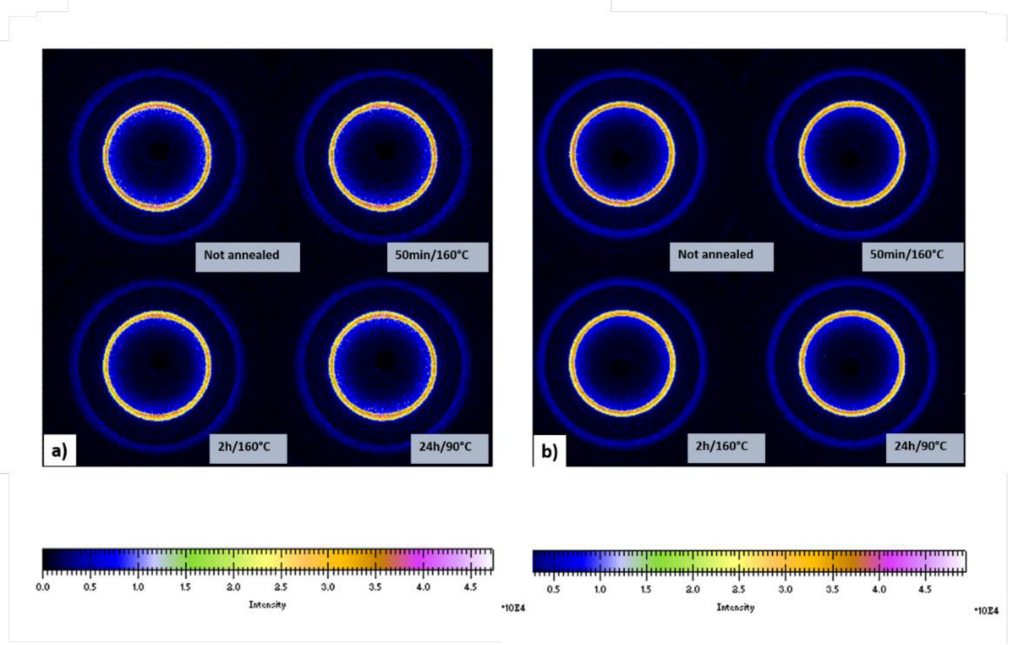

Fig. 4.19: WAXD patterns for a) not annealed and annealed injection molded and b) not annealed and annealed compression molded specimens.

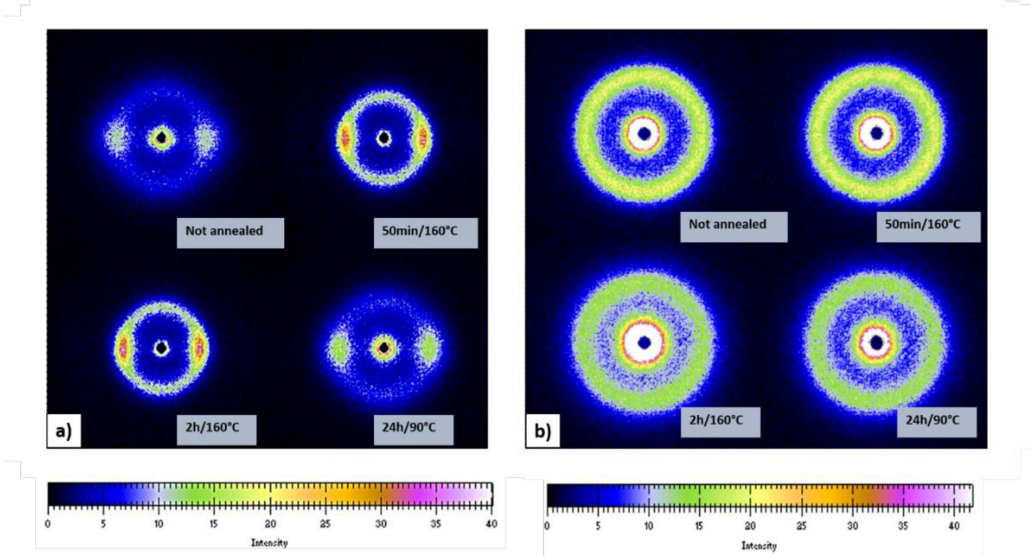

Fig. 4.20: SAXS patterns for a) not annealed and annealed injection molded and b) not annealed and annealed compression molded specimens.

As mentioned earlier in this section, no milling profile was carried out for the WAXD measurements of the compression molded and annealed tensile specimens. In Fig. 4.21, the calculated d-spacings for the (100) planes of the tensile specimens processed with IM condition 2 (C2) are shown. The d-spacing decreases with increasing annealing

temperature. The same behavior is found for the compression molded specimens (Fig. 4.18). The stress free lattice distance d_0 from literature is 3,88 Å (Lüftl et al., 2013). Therefore, the tensile specimens apparently show higher compressive stresses in these planes than the compression molded samples. It is surprising that annealing seems to have a greater influence on the lattice distances of the compression molded specimens. Moreover, it is surprising that annealing leads to lattice distances in the (100) planes, which indicates stronger compressive stresses than before annealing. However, it is expected that this is compensated by simultaneous changes in the other crystal planes, but further research will be necessary to clarify these details.

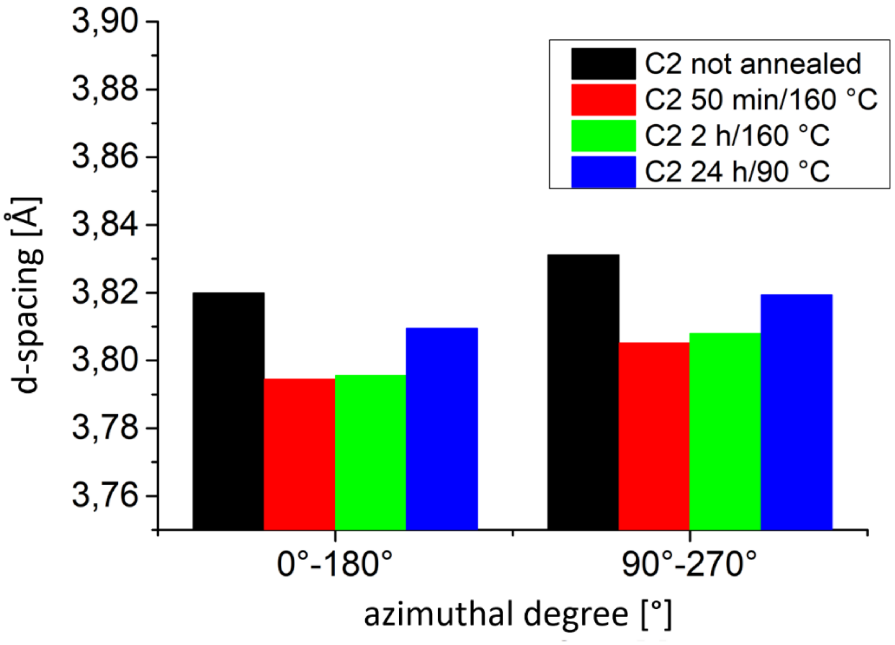

Fig. 4.21: Changes in the d-spacing of the (100) planes of the IM tensile specimens after annealing.

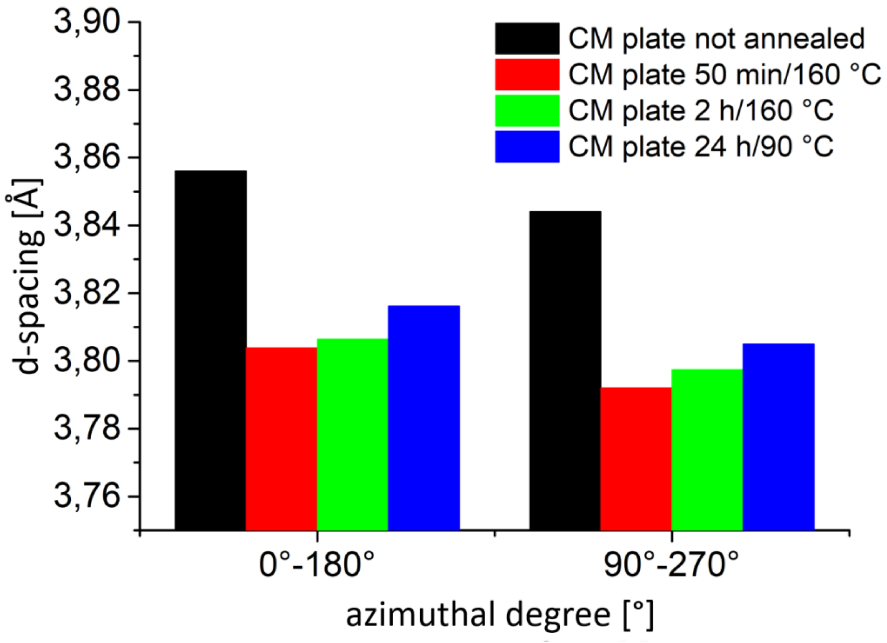

Fig. 4.22: Changes in the d-spacing of the (100) planes of the CM specimens after annealing.

4.5.2 Effects of annealing in the layer removal technique

Injection molded tensile specimens

Selected injection molded specimens processed by condition 2 were annealed as described in the experimental section 3.1.3. They were expected to show a significantly lower level of residual stresses after annealing. As presented in Fig. 4.23 this was not the case. Obviously, no stress relaxation occurred and there was even an increase of tensile stresses in the core. The level of increase depended on the annealing temperature. For annealing at 90 °C for 24 h, an increase of the stress in the midplane of 4 MPa was found. When annealing at 160 °C, stresses increased by 11 MPa. Here the time of annealing had apparently no influence on the stresses in the core. Moreover, the regime with compressive stresses broadened under annealing. However, for the interpretation, it has to be kept in mind that only one measurement with layer removal scheme “profile 1” was performed per annealing condition. Since all the previous results showed rather high scatter in the surface region, some uncertainty remains here. In the core region on the other hand, a single specimen measurement is expected to be representative.

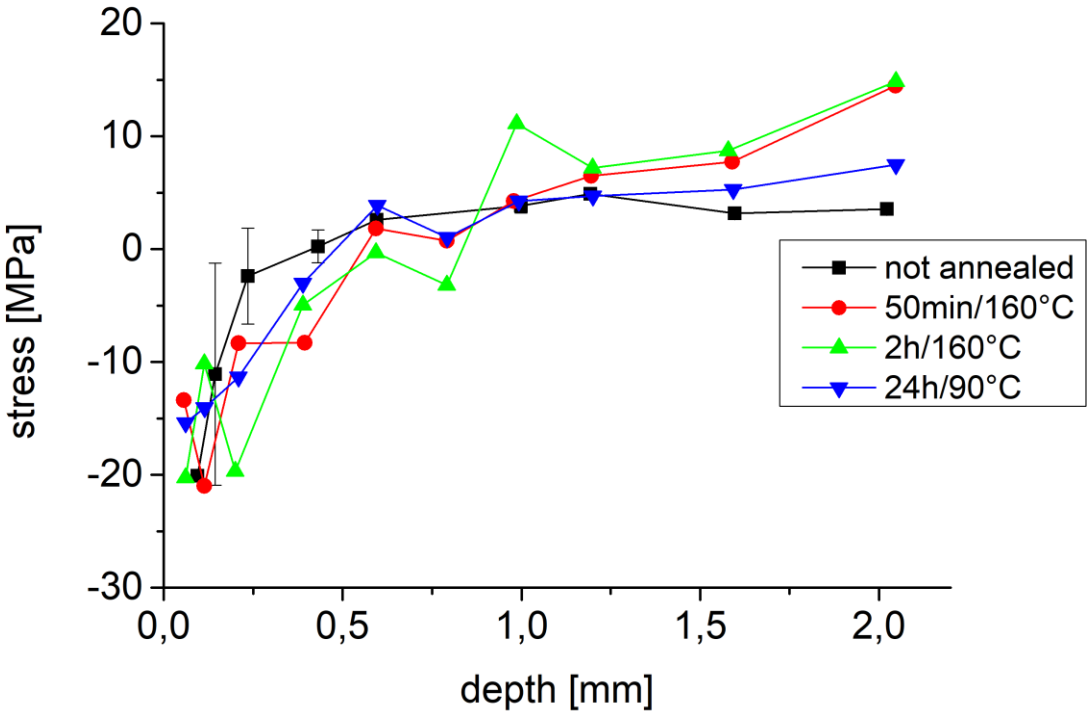

Fig. 4.23: Residual stress distribution in injection molded tensile specimens produced with processing condition 2 after different annealing conditions.

The results again indicate rather unexpected behavior of the POM specimens during annealing, as it was already discussed for the WAXD results in the previous section. Interestingly, the results discussed above correspond to the residual stress changes found by (Siegmann and Kenig, 1986) for quenched POM upon aging. There, this was linked to secondary crystallization processes during annealing at room temperature. Further crystallization was actually not expected, since this POM type crystallizes very fast (the material is highly nucleated). Nevertheless, previous DSC measurements for these specimens showed a degree of crystallinity of about 60%-65%. The crystallinity obtained by WAXD was slightly higher around 68%. This is rather low for POM, which is known for being highly crystalline. Therefore, crystallization during annealing especially in the surface layers appears plausible. To support the interpretation, polarized light microscopy was conducted for a limited number of microtomed cuts to detect differences for example in the spherulite structure, shear layers and in highly oriented areas (Fig. 4.24) before and after annealing, but no significant differences were found.

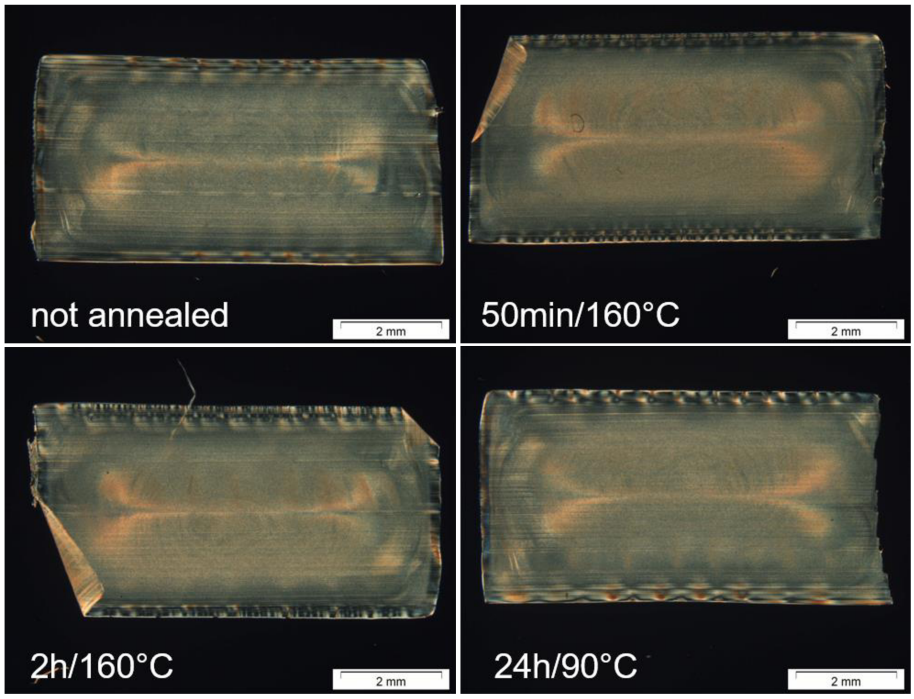

Fig. 4.24: Polarized light microscopy for not annealed and annealed tensile specimens (microtomed).

In order to check for the symmetrical distribution of the residual stresses over the thickness of the specimens, a second measurement run was started. Again tensile specimens processed with condition 2 in cavity 2 were annealed using the annealing conditions described in section 3.1.3. This time the specimens were milled from the back side and examined by LRT to proof the symmetrical distribution of the residual stresses. Profile 2 was used to reduce the measurement time. As illustrated in Fig. 4.25, the same annealing effects as in Fig. 4.23 were found. Based on these results, the specimens can be considered to be roughly symmetrical concerning their residual stress distribution. What is notable is that the stresses in the near surface region are higher for the measurements with milling profile 2. This is supposed to originate from the scatter, which was found in this region for the not annealed specimens (section 4.1.1). An influence of the milling profile on the residual stress profiles is not expected, but cannot be fully excluded either.

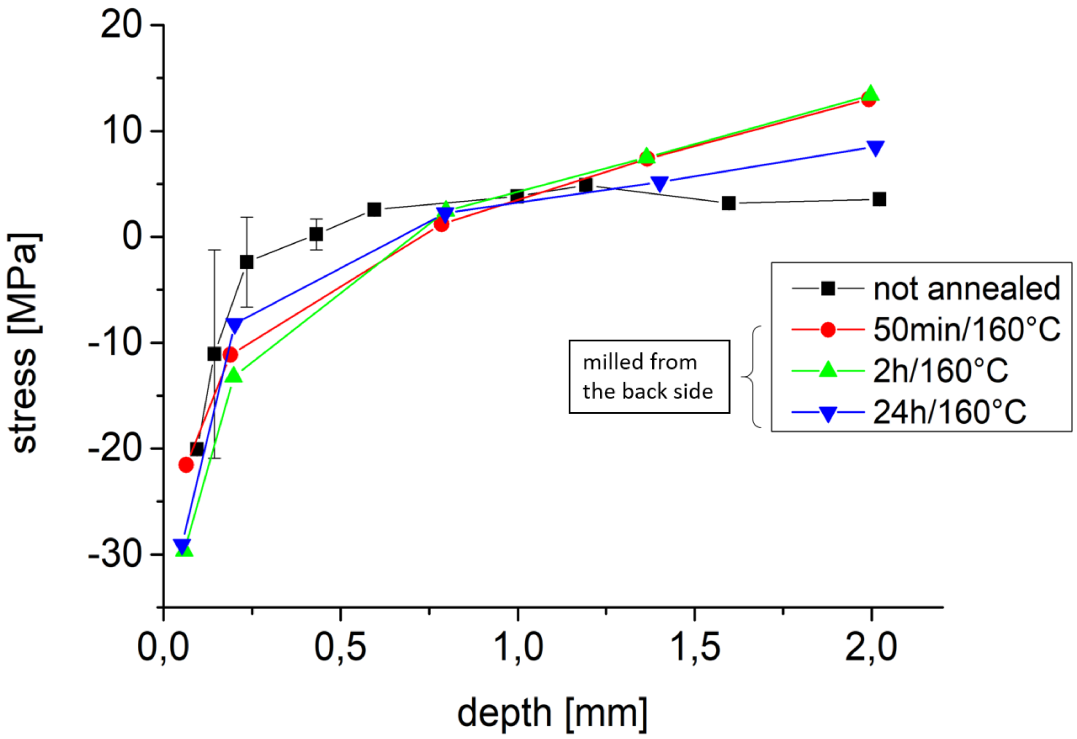

Fig. 4.25: Backside measurements of annealed tensile specimens analyzed using milling profile 2 and comparison to the results of the not annealed specimens shown in Fig. 4.23.

Compression molded specimens

The effect of annealing on compression molded specimens was also investigated by layer removal technique. For these samples, the milling process was very difficult. Due to a rather strong initial bending deflection, the milling set-up was adapted for the compression molded specimens as described in section 3.3.2. The specimen annealed at 90°C for 24h was even destroyed during milling and hence, is not displayed here. The residual stress distributions of the remaining samples are shown in Fig. 4.26. It has to be kept in mind that only one measurement was conducted per annealing condition. The not annealed compression molded sample shows tensile stresses in the outer layers followed by compressive stresses in the core. Since in compression molding the plate was slowly cooled from 210 °C to 30 °C, compressive stresses at the surface and tensile stresses in the core were expected. Hence, the residual stress distribution in Fig. 4.26 was rather unexpected. The compression molded plate was produced within a diploma thesis (Halb, 2016) and since then stored at room temperature. It is expected that the unexpected curves in Fig. 4.26 are

a result of ageing and stress relaxation effects. As for the tensile specimens, it was found that annealing shifts the stresses in the core in tensile direction. In the surface regions, the tensile stresses were also found to increase. Based on these results, none of the compression molded specimens can be considered as stress free. The not annealed sample indicates rather low surface stresses. Thus it was decided to be the best choice for the reference sample for nanoindentation.

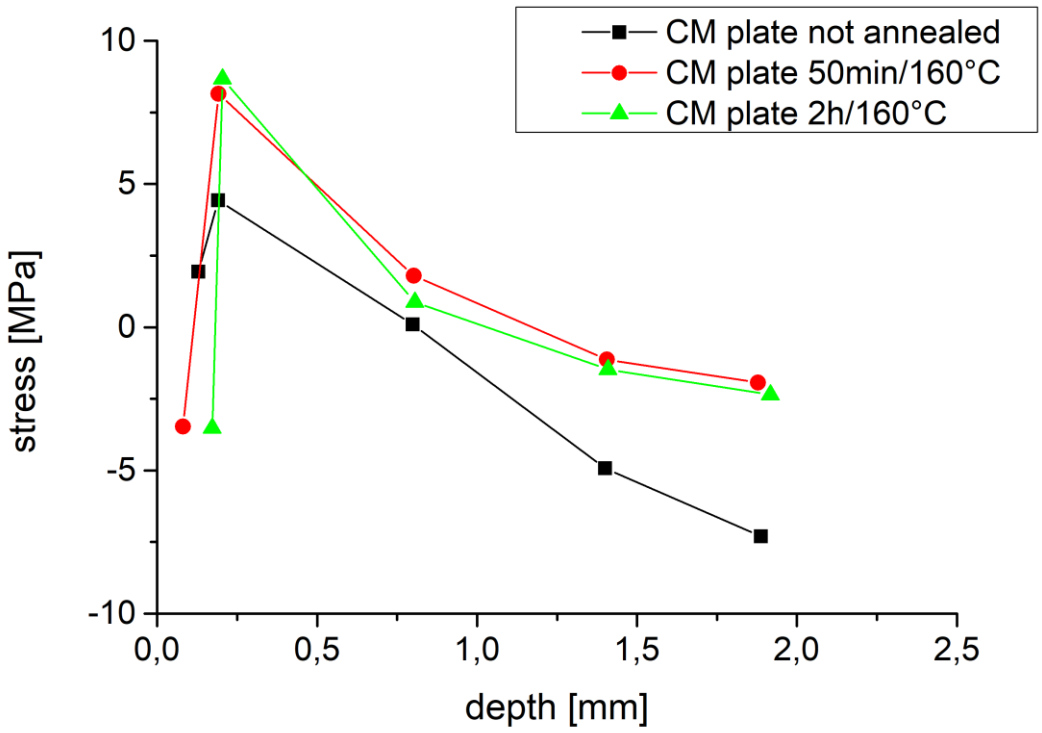

Fig. 4.26: Residual stress distributions for not annealed and annealed compression molded specimens.

5 SUMMARY, CONCLUSIONS & OUTLOOK

POM is a highly crystalline engineering thermoplastic, which is frequently used in structural parts. It is often processed by injection molding. Injection molding conditions are known to highly influence the morphology of the material, which itself influences the material properties of the part. Additionally, residual stresses and stress distributions develop during processing and also affect the mechanical properties. Therefore, the correlation of morphology, mechanical properties and residual stresses is of interest both on scientific and engineering level.

Injection molded tensile specimens produced with eight different processing conditions were subject of this thesis. During processing, holding pressure, temperature profile along the barrel and mold temperature were varied within a design of experiments. Aim of this work was to measure the residual stresses in these specimens and to compare three different methods for residual stress determination (layer removal technique, wide angle X-ray diffraction and nanoindentation). Layer removal technique (LRT) is widely used for the determination of residual stress profiles of metals and polymers. The approach proposed by (Treuting and Read, 1951) was used in this thesis. Wide angle X-ray diffraction (WAXD) is also often applied for crystalline and semi-crystalline materials. Here the residual stresses are determined by analyzing peak shifts in the intensity profiles. For nanoindentation, the Suresh and the Lee models were used to determine residual stresses from the load-depth curves. Nanoindentation is not yet well examined for polymers.

For the layer removal technique, plausible residual stress profiles were obtained. Three specimens of each injection molding condition as well as annealed and compression molded specimens were examined. The results were in good accordance with literature. Very high scatter of the stress values in the outer layers were found. This is believed to arise from the milling process and the small bending deflection obtained in these areas. A big disadvantage of this method is that the measurements and the evaluation are very time consuming.

For WAXD, three specimens of processing condition 2 were analyzed. Here several assumptions had to be made to calculate the stresses. The d-spacing of an unstressed

specimen was taken from literature and the elastic constants for each (hkl)-plane group were replaced by the elastic modulus from tensile tests. Therefore, the quantitative comparison to the other methods is difficult. It was found that the stresses obtained by this method qualitatively match the results from layer removal technique, except for a deviation in the center of the specimens. The latter was believed to arise from bending after the milling process, which it was tried to restrict by the sample holder. WAXD measurements have the advantage that additional information on morphology can be taken from the patterns, especially when combined with SAXS measurements.

Nanoindentation was carried out along the thickness, the width and over the cross-section of a specimen injection molded with processing condition 2. The two models applied were proposed by (Suresh and Giannakopoulos, 1998) and (Lee and Kwon, 2004) and both required a stress free reference sample. For this, a compression molded plate was used. However, stress profiles obtained from the layer removal technique indicated that the plate was not completely stress free. This introduced an error in the stress values measured by nanoindentation. Additionally, geometrical and surface issues occurred, which made it difficult to conduct valid measurements. Generally, one advantage of nanoindentation is that additional information on mechanical properties can be obtained. A general issue in this work was the annealing of the specimens. It was expected that stress free samples can be obtained by applying a thermal treatment recommended in literature for stress relaxation (DuPont, 2019). This, unfortunately, was not successful and led to problems in the stress calculations for WAXD and nanoindentation.

To sum it up, it was possible to determine plausible stress profiles by layer removal technique and WAXD. In case of the layer removal technique, even the absolute stress values are in good correlation with the literature (Siegmann and Kenig, 1986). Nevertheless, for the absolute values it has to be kept in mind that they were calculated using the bending images at 48 h after milling. Further research on this topic showed that even after eight weeks, continuous bending occurred without any sign for a plateau indicated in the curvature-time plots. Hence, also for the layer removal technique, the absolute stress values have to be treated with care. Nanoindentation did not give plausible results.

For LRT, it would be necessary to improve the milling process to minimize the scatter, especially in the outer layers. Also for the fitting procedure, there is potential for improvement, which is assumed to further reduce the scatter in the outer layers. For the WAXD measurements, it is important to obtain a proper stress free sample and the values of the elastic constants. In literature, there are also several approaches described to alternatively calculate residual stresses from WAXD measurements on rotated samples. For this however, the test set-up would have to be modified and adapted. Nanoindentation was found to be the method least applicable at the present. To minimize geometrical and surface issues in the future, it is suggested to embed and polish the samples before the measurements. Care has to be taken that no heat is introduced in this process, in order to avoid any influence on morphology and residual stresses. Additionally, the two models used in this thesis should be validated by measuring samples with known stresses. They were developed for metals and therefore their suitability for polymeric materials has to be cross-checked.

An issue that occurred during the conduction of the experiments was that it was not possible to obtain stress free samples by annealing. Annealing even introduced higher stress levels in both, injection and compression molded specimens. Further investigations, beginning with a detailed evaluation of the SAXS measurements conducted, has to be made on annealed specimens in order to determine the morphological changes during their thermal treatment.

6 REFERENCES

Akay, M.; Ozden, S. (1994): Measurement of Residual Stresses in Injection Moulded Thermoplastics. In *Polym. Test.* (13), pp. 323–354.

Alexander, L. (1971): X-ray diffraction methods in polymer science. In *J. Mater. Sci.* 6 (1), p. 93. DOI: 10.1007/BF00550300.

Berer, M.; Halb, M.; Feuchter, M.; Pacher, G.; Pinter, G. (2018): Fatigue fracture properties and morphology of Polyoxymethylene (POM) plates produced under moderate processing conditions. In *Int. J. Pol. Sci. 2018, pp. 1-18.* DOI: 10.1155/2018/7410925.

Berer, M.; Major, Z. (2010): Characterization of the global deformation behaviour of engineering plastics rolls. In *Int. J. Mech. Mater. Des.* 6 (1), pp. 1–9. DOI: 10.1007/s10999-010-9111-9.

Berer, M.; Major, Z. (2012): Characterisation of the Local Deformation Behaviour of Engineering Plastics Rolls. In *Strain* 48 (3), pp. 225–234. DOI: 10.1111/j.1475-1305.2011.00816.x.

Berer, M.; Pinter, G.; Feuchter, M. (2014): Fracture mechanical analysis of two commercial polyoxymethylene homopolymer resins. In *J. Appl. Polym. Sci.* 131 (19), pp. 1–15. DOI: 10.1002/app.40831.

Bolshakov, A.; Oliver, W. C.; Pharr, G. M. (1996): Influences of stress on the measurement of mechanical properties using nanoindentation: Part II. Finite element simulations. In *J. Mater. Res.* 11 (03), pp. 760–768. DOI: 10.1557/JMR.1996.0092.

Chen, R.; Tyler, D. R. (2004): Origin of Tensile Stress-Induced Rate Increases in the Photochemical Degradation of Polymers. In *Macromolecules* 37 (14), pp. 5430–5436. DOI: 10.1021/ma0496302.

Cullity, B. D.; Stock, S. R. (2001): Elements of X-ray diffraction. 3. ed., internat. ed. Upper Saddle River, NJ: Pearson/Prentice Hall.

DuPont (2019): Design Guide - Module III. Delrin acetal resin. Available online at http://www.dupont.com/content/dam/dupont/products-and-services/plastics-polymers-and-resins/thermoplastics/documents/Delrin/Delrin%20Design%20Guide%20Mod%203.pdf , checked on 2/15/2019.

Feuchter, M. (2011): Microstructure optimization and structure-property relationships of thermoplastic nanocomposites. Dissertation. Montanuniversitaet Leoben, Austria. Chair of Materials Science and Testing of Plastics.

Guevara-Morales, A.; Figueroa-López, U. (2014): Residual stresses in injection molded products. In *J. Mater. Sci.* 49 (13), pp. 4399–4415. DOI: 10.1007/s10853-014-8170-y.

Halb, M. (2016): Influence of the Processing Conditions on Morphology and Fracture Mechanical Properties of unfilled Polyoxymethylene (POM). Diploma Thesis. Montanuniversitaet Leoben, Austria. Materials Science and Testing of Plastics. Available online at http://www.unileoben.ac.at/images/stories/Bibliothek/edoc/AC13281649n01vt.pdf, checked on 2/26/2019.

Hauk, V.; Behnken, H. (2006): Structural and residual stress analysis by nondestructive methods. Evaluation - application - assessment. Transferred to digital printing. Amsterdam: Elsevier. Available online at http://www.sciencedirect.com/science/book/9780444824769.

Haworth, B.; Hindle, C.; Sandilands, G. J.; White, J. (1982): Assessment of internal stresses in injection moulded thermoplastics. In *Plastics and Rubber Processing and Applications* 2.

Heym, B.; Beitz, W. (1995): Zur Belastbarkeit von Stirnzahnrädern aus dem Hochtemperatur-Thermoplast PEEK. In *Konstruktion* 47, pp. 351–357.

Jang, J.-I (2009): Estimation of residual stress by instrumented indentation: A review. In *Journal of Ceramic Processing Research* 10.

Jansen, K. M. B. (2015): Residual stresses in injection molded products. In. THE SECOND ICRANET CÉSAR LATTES MEETING: Supernovae, Neutron Stars and Black Holes. Rio de Janeiro - Niterói - João Pessoa - Recife - Fortaleza, Brazil, 13–22 April 2015: AIP Publishing LLC (AIP Conference Proceedings), p. 20007.

Kubat, J.; Rigdahl, M. (1976): Reduction of internal stresses in injection molded parts by metallic fillers. In *Polym. Eng. Sci.* 16 (12), pp. 792–798. DOI: 10.1002/pen.760161203.

Lee, Y.-H.; Kwon, D. (2004): Estimation of biaxial surface stress by instrumented indentation with sharp indenters. In *Acta Materialia* 52 (6), pp. 1555–1563. DOI: 10.1016/j.actamat.2003.12.006.

Lüftl, S.; Visakh, P. M.; Chandran, S. (2013): Polyoxymethylene handbook. Structure, properties, applications and its nanocomposites. Hoboken, New Jersey: John Wiley & Sons (Polymer science and plastics engineering).

Maxwell, A. S.; Turnbull, A. (2003): Measurement of residual stress in engineering plastics using the hole-drilling technique. In *Polym. Test.* 2003 (22), pp. 231–233.

Noyan, I. C.; Cohen, J. B. (1987): Determination of Strain and Stress Fields by Diffraction Methods. In Ismail C. Noyan, Jerome B. Cohen (Eds.): Residual Stress. New York, NY: Springer New York, pp. 117–163.

Oliver, W. C.; Pharr, G. M. (1992): An improved technique for determining hardness and elastic modulus using load and displacement sensing indentation experiments. In *J. Mater. Res.* 7 (06), pp. 1564–1583. DOI: 10.1557/JMR.1992.1564.

Pratt, V. (1987): Direct least-squares fitting of algebraic surfaces. In *SIGGRAPH Comput. Graph.* 21 (4), pp. 145–152. DOI: 10.1145/37402.37420.

Rösler, J. (2005): Zur Tragfähigkeitssteigerung thermoplastischer Zahnräder mit Füllstoffen. Dissertation. Technische Universität Berlin, Germany. Fakultät V. Available online at https://depositonce.tu-berlin.de/bitstream/11303/1428/1/Dokument_38.pdf, checked on 8/14/2017.

Siegmann, A.; Buchman, A.; Kenig, S. (1981): Residual stresses in polymers. II. Their effect on mechanical behavior. In *Polym. Eng. Sci.* 21 (15), pp. 997–1002. DOI: 10.1002/pen.760211503.

Siegmann, A.; Buchman, A.; Kenig, S. (1982a): Residual stresses in polymers I. The effect of thermal history. In *Polym. Eng. Sci.* 22 (1), pp. 40–47. DOI: 10.1002/pen.760220107.

Siegmann, A.; Buchman, A.; Kenig, S. (1982b): Residual stresses in polymers III. The influence of injection-molding process conditions. In *Polym. Eng. Sci.* 22 (9), pp. 560–568. DOI: 10.1002/pen.760220908.

Siegmann, A.; Kenig, S. (1986): Simultaneous residual stresses and crystallinity changes during ageing of polyoxymethylene. In *J. Mater. Sci. Lett.* 5 (12), pp. 1213–1215. DOI: 10.1007/BF01729368.

Sine, G.; Carlson, R. (1952): Hardness measurement for determination of residual stresses. In *ASTM Bulletin* 180, pp. 35–37.

So, P.; Broutman, L. J. (1976): Residual stresses in polymers and their effect on mechanical behavior. In *Polym. Eng. Sci.* 16 (12), pp. 785–791. DOI: 10.1002/pen.760161202.

Suresh, S.; Giannakopoulos, A. E. (1998): A new method for estimating residual stresses by instrumented sharp indentation. In *Acta Materialia* 46 (16), pp. 5755–5767. DOI: 10.1016/S1359-6454(98)00226-2.

Taira, S.; Tanaka, K.; Yamasaki, T. (1978): A Method of X-Ray Microbeam Measurement of Local Stress and Its Application to Fatigue Crack Growth Problems. In *Journal of the Society of Materials Science, Japan* 27 (294), pp. 251–256. DOI: 10.2472/jsms.27.251.

Taisei, D.; Nishida, M.; Junichi, O. (2015): Residual Stress Measurement of Industrial Polymers by X-Ray Diffraction. In *AMR* 1110, pp. 100–103. DOI: 10.4028/www.scientific.net/AMR.1110.100.

Treuting, R. G.; Read, W. T. (1951): A Mechanical Determination of Biaxial Residual Stress in Sheet Materials. In *J. Appl. Phys.* 22 (2), p. 130. DOI: 10.1063/1.1699913.

Turnbull, A.; Maxwell, A. S.; Pillai, S. (1999): Residual stress in polymers-evaluation of measurement techniques. In *Journal of Material Science* (34), pp. 451–459.

Turnbull, A.; Maxwell, T.; Pillai, S. (1998): Residual Stress in Polymeric Mouldings.

White, J. R. (1984): Origins and measurements of internal stress in plastics. In *Polymer Testing* 4 (2-4), pp. 165–191. DOI: 10.1016/0142-9418(84)90010-2.

Withers, P. J.; Bhadeshia, H.K.D.H. (2001): Residual stress. Part 1 – Measurement techniques. In *Materials Science and Technology* 17 (4), pp. 355–365. DOI: 10.1179/026708301101509980.